The BioRobotics Institute – Scuola Superiore Sant'Anna

PhD Programme in BioRobotics

Robotic solutions for controlled delivery of therapeutic implant and drug

Ph.D. Candidate   *Tutor*

Izadyar Tamadon   **Dr. Leonardo Ricotti**

Prof. Arianna Menciassi

Supervisor

Prof. Paolo Dario

31st May 2019

XXXI Doctor Cycle

Dedication

This study is dedicated

To my beloved parents, Maryam & Hamid, who continually provide their moral, spiritual, emotional and financial support;

To the memory of my grandmother, Parivash, who passed away during this doctoral period;

To my wife, Roya, who tolerate my mental absence due to these works;

To my brother, Amir, who has been my source of inspiration;

To Prof. A. Menciassi and L. Ricotti who shared their words of advice and encouragement to finish this study;

And lastly, all friends and colleagues, thank you for the guidance, strength, power of mind, protection and skills.

Table of contents

Abstract

Recent advancements in continuous body monitoring have led to control many pathologies, potentially reaching more effective treatment of several life-threatening chronic diseases. Despite significant steps in the past decades both in the field of minimally invasive surgery (MIS) and in pharmacology, with the development of more and more sophisticated instrumentation and drug formulations, there is still room to deliver effective treatment with minimized side effects. Merging competencies derived from mechatronics, robotics and bioengineering can help in moving forward in this research endeavour, aiming at effective treatment by developing technologies, components and designs that are able to treat many pathologies in the human body, even in hard-to-reach areas.

In this framework, an ambitious dream is to develop therapeutic instruments able to treat pathologies that are nowadays in an invasive way and also to improve existing treatments, making them more accurate, fast and easy.

This thesis explores novel robotic systems that aim to overcome some of the limitations featuring current therapeutic paradigms. To this aim, the main focus is on miniature systems, which potentially allow to access human's chest and to be implantable in endoluminal sites. Furthermore, a specific attention has been paid to systems for controllable *one time* delivery of prosthesis (i.e. artificial heart valve) and *daily* delivery of drugs (i.e. insulin). The thesis is organized in five chapters and one Appendix . Chapter three and four deal with the development of a novel miniaturized robot with mechatronics solutions. Each reported system is not an evolution of the one reported in the previous Chapter.

Chapter 1 reports the motivation of the whole thesis and a general background concerning therapeutic strategies and mechatronic systems for medical applications. Also, my contribution to reach the final system is illustrated in Figure 0-1.

Chapter 2 reviews the state of the art in two separate devices. The first part focuses on robots and manipulators for delivering prostheses and the second part

deals with implantable drug delivery systems. It also aims at sketching limitations, open challenges in the mentioned domains and positive features in each system.

Chapters 3 and 4 report the design, fabrication and testing of a manipulator for heart surgery and an implantable pump for insulin delivery, respectively, both devised for targeted therapeutic delivery in the human body.

The system described in Chapter 3 is a MIS manipulator for prosthesis delivery, devised for operation in the human's chest. More in detail, Chapter 3 demonstrates the design, fabrication and performance evaluation (*in vitro*) of the novel robotic system. The robotic manipulator is compatible with the MIS approach and equipped with endoscopic visualization, for aortic heart valve replacement. The robotic manipulator is able to reach the intervention site and place the valve in a safe, effective and fast way. The results show successful implantation of a commercial valve with the aid of endoscopic vision of the aortic root. This paves the way to future applications of these systems in the fields of surgical robotics.

Appendix I adds the mathematical modelling of the manipulator for constant curvature kinematics.

In Chapter 4, an implantable insulin delivery device is illustrated for T1 diabetic patients. It presents the design, miniaturization and fabrication of an advanced prototype of fully implantable artificial pancreas refillable by means of ingestible capsules. Following an existing idea, the system will be miniaturized, enriched with additional components and optimized for future in-vivo implantation and cadaver testing.

In both cases, a never ending struggle has involved to reach reliable solutions for intra-body therapeutic devices/robots by following several stages of prototyping and experiments. Also, multi-disciplinary teamwork among bioengineers and clinical surgeons provide valuable feedback to enhance the system performance on the way to reach the final goal. Both systems described in Chapters 3 and 4 are just the final and experimentally approved ones and the prototypes (failed ideas) are ignored, even if they helped to identify the best option.

Finally, Chapter 5 sketches out the conclusions of this study and highlights future perspectives, by describing possible routes and strategies to address scientific and medical issues still hampering the wide adoption of robots in the clinical practice.

Figure 0-1 Thesis organization and workflow

List of Tables

List of Figures

List of Abbreviations

AP = Artificial Pancreas

AS = Aortic Stenosis

AVR = Aortic Valve Replacement

BAV = Balloon Aortic Valvuloplasty

CA = Cross Axial

CPB = Cardiopulmonary bypass

CSII = Continuous Subcutaneous Insulin Infusion

CT = Cable Tension

DDS = Drug Delivery System

DoF = Degrees of Freedom

EM = Electro Magnetic

FBG = Fiber Bragg Grating

FC = Following Cable

FDA = Food and Drug Administration

GI = gastrointestinal

GUI = Graphic User Interface

HARP = Highly Articulated Robotic Probe

IDDS = Implantable drug delivery systems

IMD = Implantable Medical Devices

IP = intraperitoneal

LC = Leading Cable

LT = Leading Tension

MEMS = Micro Electro Mechanical Systems (MEMS)

MIAVS = Minimally Invasive Aortic Valve Surgery

MIS = Minimally Invasive Surgery

MPS = Model Predictive Control

MRI = Magnetic Resonance Imaging

MSD = Magnetic Switchable Device

PID = Proportional-Integral-Derivative

RMS = Root Mean Square

SAVR = Surgical Aortic Valve Replacement

SC = Subcutaneous

SMBG = Self-Monitoring Blood Glucose

SPA = Single Port Access

TAVR = Transcatheter Aortic Valve Replacement

1. Motivations and Contributions

1.1 Motivations

Medical robotics is changing therapies to a higher level by the rapid growth in technological improvements (actuators, materials, and control engineering), advances in medical imaging (higher resolutions, magnetic resonance imaging, and 3D ultrasound), and an increase in surgeon/patient acceptance. A robot is defined as "a programmable, multi- functional machine capable of carrying out a complex series of actions automatically or semi-automatically." As a result, robots are generally indicated for tasks requiring programmable motions, particularly where those motions should be quick, precise, on time and untiring [1].

For almost 30 years, research in medical robotics has led to many prototypes that have been validated technically and clinically. The most impressive impact of medical robots has been in surgery [2,3]. There are many specialties in this regard: orthopedics, neurosurgery, cardiac, vascular, otolaryngology etc. are a few among others [4]. Medical robotics is a young and relatively unexplored field over the past couple of decades. Yet by looking at the current market and representative research systems, positive guesses can be made about the impacts of robots on near-future medicine [5].

Although still in its infancy, robotic surgery is a cutting-edge development in surgery that will have far-reaching implications. While improving precision and dexterity, this approach allows surgeons to perform operations that were traditionally not feasible to minimal access techniques. As a result, the benefits of minimal access surgery may be applicable to a wider range of procedures with increased safety.

Even though a lot of efforts have been done in robotic systems with tissue ablation [6,7] and biopsy [8,9], specially in abdominal surgery, there are limited numbers of systems that are able to deliver therapeutic care to patients in chronic diseases.

In the following sections, after defining and classifying targeted therapy systems, an overview of surgical systems proposed so far will be provided with a main focus on their controlled therapeutic delivery. Therefore, we exclude the robots which

are used for biopsy/grasping with retractor/forceps. Anyway, advanced robotic systems such as the da Vinci can be used in multiple purposes in surgical room.

1.1.1 Controlled delivery of prosthesis

One of the major focus of recent medical robotics research is on the ergonomic and safety issues related to the introduction of flexible access techniques. Flexible/bendable manipulators can be viewed as being internal segmented backbone comprised of (many very small) rigid-links, such as snakes. Their benefits are the potential to use the backbones in operations with very tight spaces, thus penetrating areas where conventional robots would be unable to enter. Perhaps the most direct approach to bend a flexible structure is using remotely actuated tendons. It is driven externally by the surgeon, either directly in a co-manipulation or from a master workstation in a tele-operation mode.

The route towards the development of the perfect robot able to deliver the target therapeutic care is still long. The miniaturization poses many challenges from a physical and fabrication viewpoint, hampering the maximum force for targeted therapy and efficiently perform the desired therapeutic function.

In Chapter 2, an overview of flexible manipulators will be provided, and in Chapter 3 we particularly focus on artificial heart valve delivery systems.

1.1.2 Controlled delivery of drugs

Numerous drug delivery implants based on micro- or nano-fabrication technologies are being developed. Implantable medical devices (IMDs) are devices implanted within the body to treat a medical condition, monitor the state, or improve the functioning of a body part. Current examples of IMDs include pacemakers and defibrillators (to monitor and treat cardiac conditions), neuro-stimulators (for deep-brain stimulation in cases such as epilepsy or Parkinson's disease), drug delivery systems (DDSs) in the form of infusion pumps, and a variety of biosensors to acquire and process different bio-signals. As noted earlier, we restrict the current discussion only to IMDs designed for drug delivery.

An ideal IMD would protect the drug from the body until needed, allow for continuous or pulsatile delivery of drug formulations, and has to be controllable by the physician or patient. A device meeting these criteria may typically include an array of individually sealed reservoirs that could be opened on command to expose their contents to the body. One or more drug formulations could be sealed in the reservoirs, protecting them from the environment until the reservoir is opened and the drug is released. One of the important advantages of implantable delivery systems with individually addressable drug-containing reservoirs is the ability to totally control drug delivery amount and timing. There is great flexibility in tailoring these systems for specific applications, because the release characteristics can be governed independently by the release mechanism, reservoir geometry, or drug formulation.

Moreover, in Chapter 2, implantable drug delivery systems will be discussed and in Chapter 4, a special focus will be put on diabetic patients to delivery small controlled dosage of insulin at intraperitoneal level.

1.2. Contributions

In this Thesis, novel enabling technologies and designs aiming to overcome some limitations in current treatments were investigated. The focus on "macroworld", where forces and torques (such as weight) are dominating [12]. Their dimensions in the body can reach at the maximum a few centimeters and forces exerted on tissues by the robots/devices range from a few milli-N to several newtons.

First of all I have reviewed the state of the art for two different robotic system (i.e. flexible manipulators and implantable drug delivery systems) to reach unique characterization, needs and missing gaps to step over state of the art.

For each system, I started from mechanical solutions at the mili-centimetric scale and actuator technologies suitable for medical applications. Then I considered the whole system as consisting of several small blocks, novel mechanisms and actuators with pursued electronics. Programming and computing to reach accurate movements which enhance the performance in each block. Then, every block is ready for further investigation and analysis as part of the whole robotic system.

Furthermore, the solutions can be redesigned or completely changed for improving the results (against the initial performance goals and specifications). Finally, the interaction between every small block inside the entire system will be explored to satisfy the proper task.
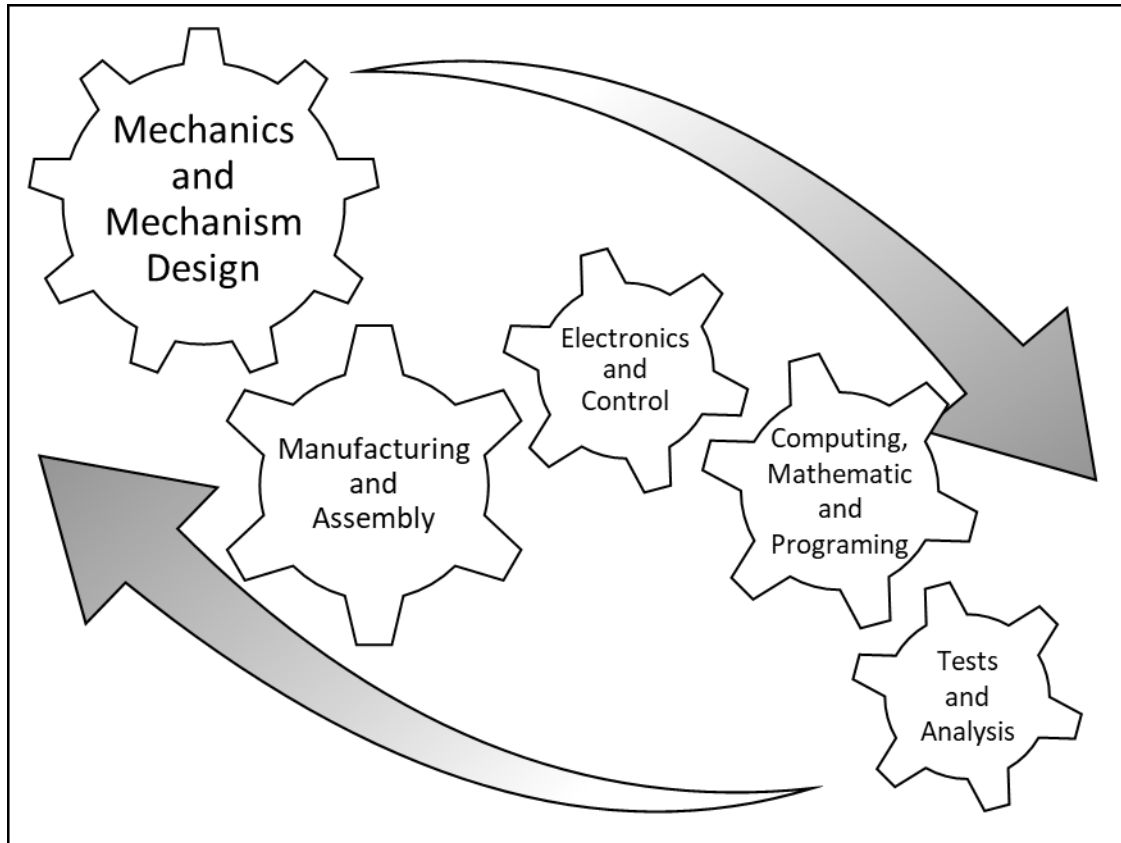
Figure 1-1 Contribution block diagram

The first robot was a flexible manipulator for aortic heart delivery, devised for MIS operation in right anterior minithoracotomy. The robotic manipulator is compatible with MIS approach and is equipped with endoscopic visualization. Proposing three endoscopic visions in tip, are very effective to find the nadir points and proper expansion site. The manipulator was validated *in vitro* and showed great functionality in precise positioning of Sorin prosthesis in aortic root based on patient anatomy. Novel mechanisms and available DoFs in the system makes the delivery in safe, fast and effective way. Introducer with minimum disturbance in manipulator's pose and two stage valve expansion was a privilege of our design in compare with the robotic delivery in state of the art. Also, mathematical modeling of the manipulator for constant curvature kinematics were helping for controlling

the manipulator and finding the tip's positon. Thus, tele-surgery by means of remote joysticks and camera visions on screen is also possible. Moreover, we introduced a simple cable tensioning strategy based on the leading tension concept, and we effectively achieved stiffening by considering a variety of starting poses. The maximum stiffening factor was in between 2 and 9, based on relevant margins from the initial pose to the workspace boundary, and on potential contributions by the structure itself. The robotic manipulator paves the way to future applications of these systems in the fields of surgical robotics.

The second one was an implantable insulin delivery device as substitution of pancreas for T1 diabetic patients. The system is able to be refilled by means of a full ingestible capsules when the reservoir is depleted. The mechanisms for docking and punching the capsule was also designed, fabricated and validated. An advanced prototype of fully implantable artificial pancreas was tested. The prototype was placed in intraperitoneal cavity and injecting insulin with resolution of 3µL on demand were performed. Also, successful refiling of the reservoir was performed by MSD and needle punching mechanisms in capsule. The proposed pumping mechanism resulted extremely efficient and led to drug release also in non-continuous fashion. Furthermore, the aspiration of insulin and variable volume reservoir makes the system to be filled very fast and keep the insulin far from bubbles or air.

References

1. Howe RD, Matsuoka Y. Robotics for Surgery. *Annu Rev Biomed Eng*. 1999;1(1):211-240. doi:10.1146/annurev.bioeng.1.1.211

2. Challacombe B, Stoianovici D. The Basic Science of Robotic Surgery. In: *Urologic Robotic Surgery in Clinical Practice*. London: Springer London; 2008:21-43. doi:10.1007/978-1-84800-243-2_2

3. Davies B. A review of robotics in surgery. *Proc Inst Mech Eng Part H J Eng Med*. 2000;214(1):129-140. doi:10.1243/0954411001535309

4. Moustris GP, Hiridis SC, Deliparaschos KM, Konstantinidis KM. Evolution of autonomous and semi-autonomous robotic surgical systems: a review of the literature. *Int J Med Robot Comput Assist Surg*. 2011;7(4):375-392. doi:10.1002/rcs.408

5. Gomes P. Surgical robotics: Reviewing the past, analysing the present, imagining the future. *Robot Comput Integr Manuf*. 2011;27(2):261-266. doi:10.1016/j.rcim.2010.06.009

6. Lanfranco AR, Castellanos AE, Desai JP, Meyers WC. Robotic Surgery. *Ann Surg*. 2004;239(1):14-21. doi:10.1097/01.sla.0000103020.19595.7d

7. Taylor RH, Menciassi A, Fichtinger G, Dario P. Medical Robotics and Computer-Integrated Surgery. In: *Springer Handbook of Robotics*. Berlin, Heidelberg: Springer Berlin Heidelberg; 2008:1199-1222. doi:10.1007/978-3-540-30301-5_53

8. Badaan SR, Stoianovici D. Robotic Systems: Past, Present, and Future. In: *Robotics in Genitourinary Surgery*. London: Springer London; 2011:655-665. doi:10.1007/978-1-84882-114-9_59

9. Berkelman, Peter, Jocelyne Troccaz and PC. Body-supported medical robots: a survey. *J Robot Mechatronics*. 2004;16:513-519.

10. Altieri MS, Almasry I, Jones T, et al. Implantable cardioverter defibrillators and permanent pacemakers: prevalence and patient outcomes after trauma. *Am J Surg*. 2016;212(5):953-960. doi:10.1016/j.amjsurg.2016.07.013

11. Jonas O, Calligaris D, Methuku KR, et al. First In Vivo Testing of Compounds Targeting Group 3 Medulloblastomas Using an Implantable Microdevice as a New Paradigm for Drug Development. *J Biomed Nanotechnol*. 2016;12(6):1297-1302. doi:10.1166/jbn.2016.2262

12. Gauthier M, Andreff N, Dombre E. *Intracorporeal Robotics*. Hoboken, USA: John Wiley & Sons, Inc.; 2014. doi:10.1002/9781118579107

2. General review in surgical targets

2.1 Flexible manipulators

Medical manipulators are devices providing full (or at least more than 2) mobility to the tool with actuated DoFs located between the entry port in the body and the tool [1]. These devices may be scaled version of conventional robot arms or flexible instruments designed to perform surgery with safe entry point [2,3]. Typically, manipulators have a centimetric size, generating submillimetric to centimetric displacements and can exert forces of the order from 1 N (e.g. to insert a needle into a coronary artery) to several tens of newtons to retract tissue [4].

Different options may be adopted in the design:

– Discrete architectures with embedded actuators [5];

– Discrete architectures with remote actuators (outside the patient) [6];

– Continuum architectures (or snake, elephant trunk like architectures) with remote actuators [7].

Two important principles to be considered in flexible robot design are range of motion (workspace) and stiffness [7]. Workspace and stiffness must both be large enough for the robot to reach the required locations and exert the required tissue forces during the procedure for which the robot is designed. Both of these attributes are primarily a function of a manipulator's structural design—in particular, its backbone cross-sectional geometry and the elastic strain limits of its materials. To achieve a combination of both large workspace and high stiffness, backbone materials with high elastic stress limits (the product of Young's modulus and elastic strain limit) are preferable.

The design space contains many variables that influence the capabilities and characteristics of the flexible robot (e.g., material properties, segment lengths, diameters, and curvatures), and the effect of these variables on workspace, dexterity, and strength is not always intuitive or simple.

For our classifications, we define actuation as the final conversion of power to the mechanical energy domain. Thus, a cable-driven robot may be actuated by

electromagnetic motors translating the base of each cable outside of the robot (extrinsic), or by the shortening of each cable by the shape memory effect (intrinsic). There are various tradeoffs that should be considered in light of the specific application for which an actuation/transmission system is designed. Principles that should be considered when designing a manipulator actuation system include manipulator diameter, operating footprint, output force range, backdrivability, friction and hysteresis, speed and dynamic bandwidth, and compatibility with medical imaging systems such as MRI. Extrinsic actuation can often reduce the required manipulator diameter, thus increasing range of motion and accessibility of confined spaces, but this comes at the potential price of large external footprint, increased friction and hysteresis, and introduction of elastic instabilities (in the case of concentric-tube transmissions). On the other hand, direct intrinsic actuation may reduce footprint and friction while requiring larger manipulator diameters.

The compliance of manipulators is often viewed as a feature that endows safety and adaptability to surgical manipulators that interact with sensitive anatomical structures. The shape of the robot can passively and gently conform to confined anatomical boundaries and objects in its environment. Catheter systems in particular rely on compliance to avoid exerting excessive force on the vascular walls. However, compliance also fundamentally limits the maximum force that a manipulator can apply.

2.1.1 Discrete architectures with intrinsic actuators

The structure of a discrete multibackbone manipulator is typically composed of discrete rigid links connected by joints. The designs of Simaan *et al.,* have used a central primary backbone and three secondary backbones for bending section that are offset from the central backbone using spacer disks and rigidly attached to the last disk of a bending section [8]. Along these same lines, Xu *et al.,* developed a multibackbone design with many backbones and a "dual flexible" actuation mechanism that increases modularity. Moses *et al.,* have also proposed a manipulator structure made of many interlocking fiber "backbones" that run down the length of the manipulator [9]. Recent work has also explored the possibility of

using a parallel multibackbone approach without intermediate constraints, allowing nonconstant-curvature backbone shapes and increased DoFs per section [10,11].

Intrinsic actuation strategies investigated for medical applications include hydraulic chambers [12–14], pneumatic chambers [15,16], the shape memory effect [17–20], embedded micromotors [21], fluidic fiber-reinforced elastomers [22], and McKibben muscles [23,24]. Robotic catheters actuated by magnetic fields generated by a magnetic resonance imaging (MRI) machine [25,26] can be considered intrinsic as power conversion to the mechanical takes place at embedded magnets on the manipulator structure. Intrinsic pneumatic actuation has also been combined with extrinsically actuated (tendon-driven) structures to produce active stiffening of the backbone structure by particle jamming [25].

2.1.2 Discrete architectures with extrinsic actuators

Transmission mechanisms for extrinsic actuation that are currently being developed for flexible robots in surgical applications include tendon/cable driven mechanisms [27,28–31] and multibackbone structures [8,9,32–33,34]. Implementation at cable allows you to control the direction of the manipulator remotely and for this it appears to be one of the most commonly used strategies in this sector. However, there are examples of manipulators having implementation on board, mainly miniaturized actuators on each joint of the articulated portion of the manipulator, as in the case i-Snake robot developed by Yang et al., from the Hamlyn Center for Robotic Surgery [21,35–37]. The use of the actuation system directly to the edge of the distal articulation involves, in most cases, complete occlusion of the central lumen.

Concentric-tube transmissions are driven by axial rotations and translations of the tube bases, which change the shape of the concentric-tube collection. Medical robots with discrete-jointed structures that closely resemble flexible robots include the i-Snake [21,36,38–40] and the Flex System developed by Choset et al., and commercialized by Medrobotics Corporation. The variable neutral-line manipulator from Kim et al. [41] and the arthroscopic tool of Dario et al. [27] are also in the hybrid serial discrete joint category. In the maxillary sinus surgery system of

Yoon et al. [42], one of the manipulators uses both an elastic spring backbone and a serial chain of discrete spherical joints. Recently, elastic and discrete structures have been combined in series (interleaved) by Conrad et al. [43,44] to increase the dynamic bandwidth of tendon-actuated elastomeric catheter robots and in parallel by Xu et al. [45] to increase torsional stiffness in multi-backbone flexible robots.

2.1.3 Continuum architectures

Continuum robots have a fundamentally different structure than conventional manipulators. When a robot has more degrees of freedoms (DOFs) than are necessary to execute a task, (e.g., a 7-DOF arm with 6-DOF task space), it is said to be redundant or in extreme cases, hyper-redundant [46]. In the limit as the number of joints approaches infinity (and the link lengths approach zero), the robot approaches what is known as a continuum robot [47]. The first continuum and hyper-redundant robot prototypes were built in the late 1960s [47,48]. Development of snake inspired robot designs by Hirose's research program [49] was then followed by Chirikjian and Burdick's theoretical advances in hyper-redundant robots based on approximating them as elastic continua [50-52]. The number of researchers has increased significantly since the late 1990s and early 2000s. Several review papers have since been published, e.g., on continuum robots in general [53], snake-inspired hyper redundant robots [54], bioinspired soft robots [55,56], design and modelling of constant-curvature continuum robots [48], concentric-tube continuum robots [57], and modelling continuum structures in robotics and structural biology [58]. This collection of reviews provides an excellent set of resources for many aspects of continuum robots and related topics.

We divide the categories in several fields and will mention every positive benefit of each device in operation room.

2.1.4 Vascular Surgery

Minimally invasive vascular surgery usually involves using catheters and guidewires to perform injections, drain fluids, and insert additional surgical instruments. A catheter is a thin (a few millimeter in diameter), long (of the order of tens centimeter) and hollow tube that allows the passage of functional catheters

of smaller diameter. These may hold various miniature sensors (pressure, ultrasound probe, optical fiber, etc.) or instruments, e.g. for the local administration of a drug, the insertion of a prosthesis (stent, angioplasty balloon, etc.), the endovascular coiling of aneurysms, the puncture/biopsy for diagnostic purposes or tumor destruction (radiofrequency abalation, laser therapy, etc.). The catheter is inserted into a blood vessel and the portion external to the patient is manipulated to move the catheter tip to the surgical site. The main challenge for the operator in using catheters and guidewires is steering [59]. Due to the supporting tissue, catheters only require three degrees of freedom, typically: tip flexion, tip rotation, and insertion depth. It is steered, under radiographic control, by the doctor who rotates it around its longitudinal axis and pushes it to its destination. This is made difficult because of the narrowness of the vessel, the frictions on the wall and the many bifurcations [59]. The difficulty for the surgeon is thus to transmit force and motion to the end effector with little or no relevant kinesthetic feedback. The surgeon operates the catheter under intraoperative medical imaging (fluoroscopy), and correlating the push/pull and rotation of the catheter or guidewire to image-space motion is rather challenging. Steerable, robotic catheters seek to overcome these limitations [60,61]. Possible benefits of robot-steered catheters are shorter procedures, reduced forces exerted on the vasculature by the catheter tip, increased accuracy in catheter positioning, and teleoperation (reducing exposure of the physician to radiation)[62].

- The Sensei X (Hansen Medical, FDA clearance and CE mark 2007) is a commercially available steerable catheter system for electrophysiology interventions (radiofrequency ablation) within the heart. It designed to navigate the peripheral vasculature and provide a conduit for the placement of therapeutic devices. It uses two steerable sheaths, one inside the other, by controlling the tension of tendons routed through channels to create a tight bend radius [63,64]. The sheaths are steered via a remotely operated system of pulleys. IntelliSense force sensing allows constant estimation of the contact forces by gently pulsing the catheter a short distance in and out of the steerable inner sheath and measuring forces at the proximal end of

the catheter. These forces are communicated visually as well as through a vibratory feedback to the surgeon's hand on the "3D joystick". Artisan Control Catheter Extended (Hansen Medical), a swiveling robotic sheath that, when combined with the Sensei X Robotic Catheter System, provides dexterity, stability and high strength during intra-cardiac procedures [65].

- The Niobe (Stereotaxis, CE mark 2008, FDA clearance 2009) is a remote magnetic navigation system, in which a magnetic field is used to guide the catheter tip [66]. The system is composed of two external, focused field permanent magnets mounted on manipulator arms. The surgeon manipulates a joystick to specify the desired orientation of the catheter tip, causing the orientations of the magnets to vary under computer-control, and thereby controlling the magnetic field. By arranging the magnets on either side of the patient's table and changing their orientation and position, a uniform magnetic field is generated to steer a magnetic catheter tip within the patient. Within the magnetic field (i.e., the workspace of the system), the magnetic tool can be moved omni-directionally. In addition, a fluoroscopy unit is used for imaging the patient with the current position and orientation of the catheter inside the body. The workstation includes a visualization of the magnetic field orientation, fluoroscopy images, and additional procedure information. Chun et al. report significant improvements in surgical outcomes due to advances in the design of magnetically guided catheters [67].

- Corindus Vascular Robotics is the CorPath 200 device designed for percutaneous coronary interventions. The CorPath comes with a radiation-shielded "cockpit" for the surgeon. The CorPath 200 is the 1st and only robotic-assisted procedure to allow for controlled placement of coronary guidewires and stent/balloon catheters from an optimized interventional cockpit. In using the system, the surgeon operates CorPath 200 from behind a radiation-shielded "cockpit." Rather than standing over a patient while clad in a lead apron, the operator is seated behind an operating station, manipulating surgical tools with a series of touch-screen and joystick controls. That reduces a physicians exposure

to radiation while also providing a more comfortable and ergonomic experience, especially during long and complex procedures.

- Kesner and Howe [68] have developed robotic catheters for cardiac surgery, which enable motion compensation using 3-D ultrasound images. The drive system consists of a linear coil actuator and a linear slide for translating the catheter's guidewire. The system's controller compensates for friction and backlash of the guidewire and the sheath of the catheter. The system has been used in porcine *in vivo* and demonstrated promising results (RMS errors below 1 mm for position tracking) [68]. A recent addition to the system includes a force sensor integrated to an ablation end-effector in order to control the force on a fast moving target [69].

Figure 2-1 Vascular surgery commercial robots

2.1.5 Orthopedics

The expected benefit of robot assistance in orthopedics is accurate and precise bone resection [70], so robotic systems can improve alignment of implant with bone and increase the contact area between implant and bone, both of which may improve functional outcomes and implant longevity. Orthopedic robots have so far targeted the hip and knee for replacements or resurfacing [71,72].

- RIO robotic arm (MAKO Surgical Corp, FDA approval) is used for implantation of knee components [73]. As part of the trend away from autonomous robot motions, both the RIO and the surgeon simultaneously hold the surgical tool, with which the surgeon moves about the surgical site. The Mako system can be used for partial knee replacements and hip surgeries currently, with the launch of a total knee replacement system slated for some time this year, according to the company.
- iBlock (Praxim Inc.) is an automated cutting guide for total knee replacement [74]. Koulalis et al. report reduced surgical time and increased cut accuracy compared with freehand navigation of cutting blocks [75].
- The Navio PFS (Blue Belt Technologies) does not require a CT scan for unicondylar knee replacement, instead it uses intraoperative planning. A total knee system is scheduled to launch in 2017 for its Journey II implant. Blue Belt's development program for a bi-cruciate-retaining implant will be incorporated into the British company's own bi-cruciate-retaining knee arthroplasty program. Total hip arthroplasty and adjacencies including sports medicine are also on the horizon.
- The Stanmore Sculptor (Stanmore Implants) is a synergistic system similar to the RIO, with active constraints to keep the surgeon in the planned workspace [76].

Figure 2-2 Orthopedics commercial robotics

2.1.6 Neurosurgery (Brain and spinal cord surgery)

Brain surgery involves accessing a concealed target surrounded by delicate tissue, a task that benefits from the ability for robots to make precise and accurate motions based on medical images [77,78,79]. Image guidance is now widely used in operating rooms world-wide [80], helping neurosurgeons to accurately reach targets within the brain.

- The NeuroMate (by Renishaw) in addition to biopsy, the system is marketed for deep brain stimulation, stereotactic electroencephalography, transcranial magnetic stimulation, radiosurgery, and neuro-endoscopy [81]. Li et al. report in-use accuracy as submillimeter accuracy with infrared tracking [82].

- Pathfinder (by Prosurgics), Reported uses of the system include guiding needles for biopsy and guiding drills to make burr holes [83,84].

- Renaissance (by Mazor Robotics, Israel, the first generation system was named SpineAssist) is a robot-assisted spinal surgical system that is minimally-invasive and improves percutaneous degenerative repair, pedicle screw fixation for complex spinal deformity and vertebral augmentation. It provides tool guidance based on planning software for various procedures. Studies show increased implant accuracy and provide evidence that the Renaissance/SpineAssist may allow significantly more implants to be placed percutaneously [85]. To use the Renaissance Guidance System, surgeons create a blueprint of the surgery in a virtual 3D program. They attach the device to the patient to ensure accuracy and take two fluoroscopic images that are matched to their corresponding location on the pre-operative CT. Then the tools are guided using the Renaissance Guidance System to the location with 1.5mm accuracy.

The NeuroMate   Pathfinder

Renaissance
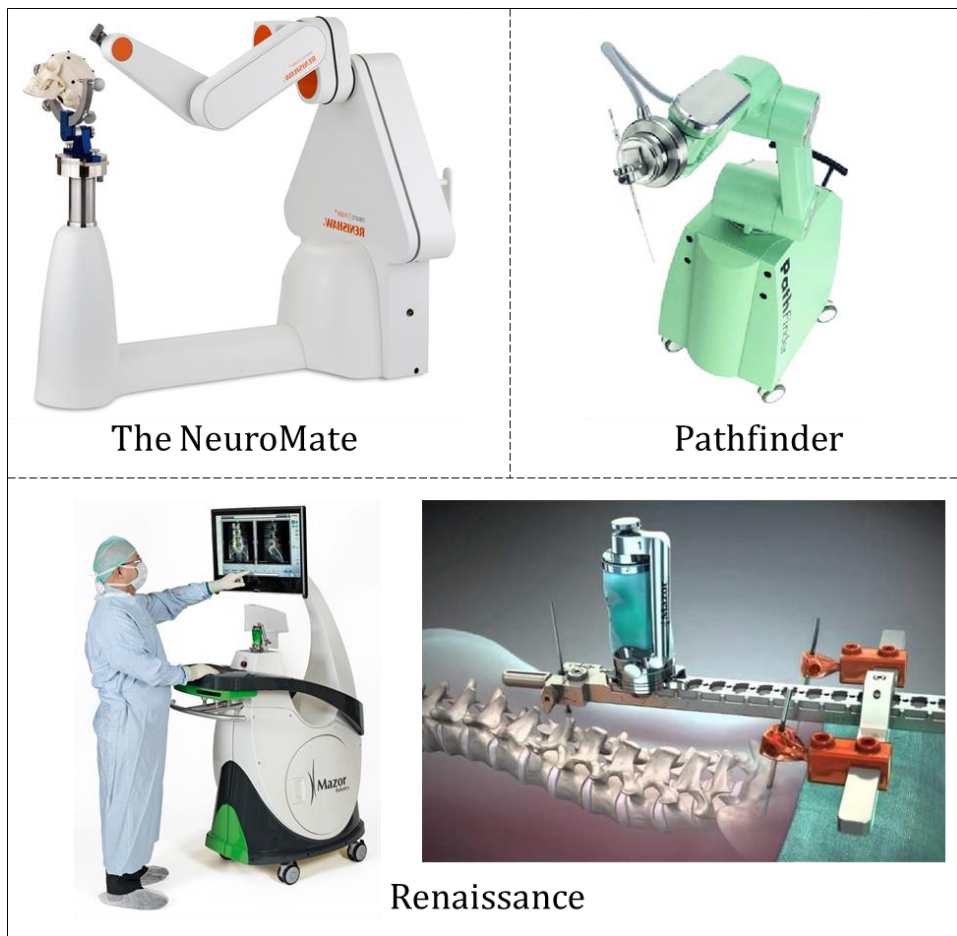
Figure 2-3 Neurosurgery commercial robotics

2.1.7 Otolaryngology

Otolaryngology (the study of diseases of the ear and throat) inherently provides natural orifice access to several regions of interest for a variety of surgical treatments. Surgeons usually use straight or flexible endoscopes and additional instruments entering through the nostril, mouth, or ear canal. For diseases located in those regions, conventional open surgery is performed. Endoscopic sinus surgery is performed with flexible endoscopes in clinical practice [86]. However, dexterity of flexible endoscopes is limited and steering can be challenging, especially in deeper sinus cavities such as the maxillary sinus. Yoon *et al.,* developed a dual master-slave system for maxillary sinus surgery, which comprises two continuum robots: a 4-DOF endoscope (diameter 4 mm) and a 5-DOF biopsy continuum robot (diameter 5 mm) [87]. The design of the endoscope continuum robot is based on a spring backbone. Actuation is achieved by tendons routed through cylinders. A CMOS camera is used as the end-effector. The biopsy robot is similar in principle, but the cylinders are connected with ball joints to increase stiffness and payload capacity, making it a hybrid serial robot. Concentric-tube robots have also been applied for skull base surgery through the nasal cavity [88]. The authors developed a robot system consisting of two manipulators, two 6-DOF input devices, and an EM tracking system. Each manipulator consists of three tubes with the inner lumen being used for integrating the surgical instrument for tissue manipulation, either a curette or a gripper. Visualization of the region of interest is currently enabled using conventional, rigid endoscopes alongside with the continuum robot manipulator arms. The endoscopic view is presented to the surgeon tele-operating the robot with two input devices. EM tracking of the manipulator tip allows for image guidance, which is also used in conventional trans-nasal skull base surgery. Simaan *et al.* [8] presented a telerobotic system for surgery of the throat, clinically motivated by the need for distal instrument mobility and advanced 3-D vision. The system features a bimanual design with two slave robotic arms, both multibackbone continuum robots made from Nitinol rods. Both robot arms are composed of two segments: the proximal one with 23mm and the distal segment with 12 mm length. Each robot arm has an additional DoF, as it

can be rotated about its backbone. The group of Simaan further introduced a system for microsurgical throat surgery through the nose [89].

2.1.8 Cardiac surgery

The heart has long been a target for surgical robots and various systems continue to investigate how best to treat cardiac diseases, particularly while the heart is beating. Structural heart procedures such as valve replacements/repairs or closure of septal defects often require open cardiac surgery. After opening the chest, a cardiopulmonary bypass is used to perform the surgical procedure on a nonbeating heart. Some surgeries can be performed on the beating heart by stabilizing the region of interest. In recent years, catheter based cardiac surgery is enabling minimally invasive surgery in the heart through small incisions. However, difficulties with catheter-based surgery include 1) a limited ability to apply and control forces necessary to perform the surgery and 2) the challenge of positioning of the catheter within the beating heart. This has motivated research on continuum robot manipulators for cardiac surgery.

Gosline *et al.* [90] use the concentric-tube continuum robot design for delivery of metal microelectromechanical systems (MEMS) to intracardiac locations. The robot can apply higher forces since it is stiffer than a catheter. They propose to deliver the robot through the patient's neck to the right atrium of the heart. The robot is teleoperated using a 6-DOF input device. Alternatively, each DOF per tube can be controlled manually using a regular keyboard. A graphical user interface displays the current shape of the robot combined with intraoperative imaging [91].

HeartLander uses suction to crawl around the surface of the heart [92,93,94]. The system is designed for intrapericardial drug delivery, cell transplantation, epicardial atrial ablation, and other such procedures.

The use of navigation systems in cardiac surgery is becoming common for the Catheter ablation of arrhythmias (for which there is a commercial system electro-anatomical mapping CARTO-MERGE). Recent literature studies have also shown the accuracy in vitro or in vivo, on animals, of the navigation systems based on

reality techniques increased and electromagnetic localization for driving the transapical mitral valve repair [95] and aortic aneurysms repair by stent-graft [96].

The robotic application in cardiac surgery also includes another example of a manipulator end-effector swivelling and implemented by cables: the HARP (Highly Articulated Robotic Probe), developed by Degani et al. and capable to reach pericardial regions remotely. Also making a delivery with minimal disruption to organs or surrounding tissues [97,98].

2.2 Implantable drug delivery systems

Implantable drug delivery systems (IDDS) are designed to store and deliver small, precise doses of therapeutic drugs or medicines into the blood stream or to specific tissue sites. They aim to reduce the frequency of dosing, prolong duration of action, increase the patient compliance, and reduce the systemic side effects [99,100]. With today's technology, the components of IDDS can be fabricated on miniature scale, for example, in the eye or spinal cord. IDDS essentially consist of a micropump, reservoir, pump mechanism, valves and catheter to direct the drug to a target site.

The concept of IDDS in may be originated by Deansby and Parkes, in 1938 [101] and pioneered by Folkman and Long, in 1960s, with controlled drug release by a silicon rubber membrane [102]. In certain areas, like interventional cardiology and contraception, IDDSs have revolutionized clinical management practices and proven themselves as Industry standard and/or excellent therapeutics. Progress in other areas, such as oncology has been slower. The advantages of IDDSs have been summarized in **Table 2.1**. IDDSs are very attractive for a number of classes of drugs, particularly those that cannot be delivered via the oral route, irregularly absorbed via the gastrointestinal tract, or that benefit from site-specific dosing. Examples include steroids, chemotherapeutics, antibiotics, analgesics and contraceptives, and biologics such as insulin or heparin [103–109].

Table 2.1 summary of design features of ideal implantable drug delivery systems

Design Feature	Summary of Potential Advantages
Localized delivery	Drug(s) are released in immediate vicinity of implant. Action may be diffusion, limited to the specific location of

	implantation
Improved patient compliance	Patient does not need to comply with repeated and timely intake of medication.
Minimized side effects	Adverse effects away from site of action are minimized
Lower dose	Localized implantation of site specific drugs can avoid first pass hepatic effects
Improved drug stability	Protection of drug undergoing rapid degradation in the gastrointestinal and hepatobiliary system
Suitability over direct administration	Hospital stay or continuous monitoring by healthcare staff may not be required for chronic illnesses

Implant morphology is typically cylindrical, with monolithic devices at the millimeter or centimeter scale, being most commonly employed. Implantation is typically done in subcutaneous or intramuscular tissue, with the aid of special implantation devices, needles, or the use of surgery. Subcutaneous tissue or intramuscular tissue are ideal locations for implantation of drug-depot devices, due to high fat content that facilitates slow drug absorption, minimal innervation, good hemoperfusion, and a lower possibility of localized inflammation (low reactivity to the insertion of foreign materials) [110]. In addition to subcutaneous implantation, various other body regions have also successfully served as implantation sites, particularly for delivery to localized tissue such as intravaginal, intravascular, intraocular [111], intrathecal [112] intracranial, and peritoneal [113].

Implants can be used as delivery systems for either systemic (absorbed into the blood circulation) or local therapeutic effects [114]. Pathology-targeting implants aim to release a drug and limit the therapeutic effect at the site of implantation [115]. An ideal IDDS should be environmentally stable, biocompatible, sterile, and be readily implantable and retrievable by medical personnel to initiate or terminate therapy. Additionally, it must enable rate-controlled drug release at an optimal dose, be easy to manufacture and provide cost-effective therapy over the treatment

duration [116]. Beginning with Gliadel [117] initial progress in commercializing safe and effective implants has been slow, despite considerable effort. Performance issues, such as lack of compatibility between drug and carrier leading to burst release or shutdown, and concerns regarding potential toxicity and carcinogenicity, stability and reproducibility, had to be overcome. Furthermore, acceptance by patients and physicians was initially limited [118–120].

2.2.1 Classification of implantable drug delivery systems

Classification of IDDSs is difficult, given that there are numerous exceptions and hybrids that may be listed under multiple categories. However, drug implants can be broadly subdivided into passive and active systems. Passive systems can be further classified into nondegradable and degradable implants that typically have no moving parts or mechanisms. Active systems employ some energy-dependent method for providing a positive driving force to modulate drug release. These energy sources may be as diverse as osmotic pressure gradients or electromechanical drives.

Passive implants

Passive implants tend to be relatively simple, homogenous and singular devices, typically comprising the simple packaging of drugs in a biocompatible material or matrix. A typical passive actuator relies on a drug infusion process in which the drug is slowly released through a porous membrane or a biodegradable membrane that degrades over time. Other passive methods include an array of small sealed drug wells that make up the reservoir such that dissolving the individual seals by applying an electrical stimulus releases a precise drug dose. In either case, the released drug diffuses into the target delivery site. By definition, they do not contain any moving parts, and depend on a passive, diffusion-mediated phenomenon to modulate drug release. Delivery kinetics are partially tunable by the choice of drug, its concentration, overall implant morphology, matrix material and surface properties.

Dynamic implants

As defined earlier, dynamic implant systems harness a positive driving force to enable and control drug release. As a result, these are typically able to modulate drug doses and delivery rates much more precisely than passive systems. However, this comes at a higher cost, both in terms of complexity and actual device price. Because of the diverse range of active micropumps, a number of classifications have grouped micropumps into mechanical (reciprocating) and nonmechanical (no moving parts) pumps. However, micropumps can be grouped into displacement and dynamic pumps [121–123]. Displacement pumps exert pressure forces on the working fluid through one or more moving boundaries and dynamic pumps continuously add energy to the working fluid in a manner that increases either its momentum or its pressure directly [122]. Essentially, active micropumps respond to an electrical stimulus to cause an electrochemical or electromechanical response to affect a controlled drug release that can be continued or stopped at any time. Many forms of micropumps have been designed and implemented using actuators based on processes such as electrolysis, osmosis, hydrodynamics, electrophoresis, piezoelectrics, magnetics, pneumatics, hydrolysis, and material deformations [121–123].

External control of dosing is a requirement for many drugs, a feature that is difficult to obtain when using biodegradable or nondegradable delivery systems. Pump systems have been used to provide the higher precision and remote control needed in these situations. Additionally, they offer a number of advantages, such as evasion of the GI tract, avoidance of repeated injections, and improved release rates (faster than diffusion-limited systems). With advances in microelectronics since the 1970s, remote control over delivery rates or integration of implantable sensors to create feedback-controlled drug delivery is now feasible. Implantable pumps primarily utilize osmosis, propellant-driven fluids, or electromechanical drives to generate pressure gradients and enable controlled drug release.

While osmotic and propellant-driven constant pressure pumps work well for small volumes of medication, this may be a severe limitation for certain chronic diseases requiring daily infusion of medication, precluding their use over long timespans. In

such cases, it may be necessary to consider larger implants, wherein the storage capacity of the pump may be replenished from time to time, while the pumping mechanisms stay implanted. By necessity, this implies the use of electrically powered mechanical pumps, typically with moving parts and advanced control systems.

Electromechanical infusion technology has been rapidly growing and offers some unique solutions for biomedical applications, particularly to address unmet medical needs related to precision dosing. An IDDS in the micro/nano meter range can be fabricated to accurately and conveniently administer very small amounts of medication. Micro electromechanical systems (MEMS) technology enables the manufacture of small devices using microfabrication techniques, similar to that used to fabricate silicon-based computer chips. MEMS technology has been used to construct micro-reservoirs, micro-pumps, nano-porous membranes, nanoparticles, valves, sensors, micro-catheters, and other structures using biocompatible materials appropriate for drug administration [124,125].

Some of the latest IMDs have begun to incorporate numerous communication and networking functions, usually known as telemetry, as well as increasingly sophisticated computing capabilities [126,127]. This has resulted in implants with more intelligence and provided patients with more autonomy, as medical personnel can access data and re-configure the implant remotely, i.e., without the patient being physically present in a medical facility.

Apart from a significant cost reduction, telemetry and computing capabilities also allow healthcare providers to constantly monitor the patient's condition and to develop new diagnostic techniques based on the IntraBody Network (IBN) of medical devices.

2.2.2 Current therapeutic applications

IDDSs are finding increasing applications in the areas of chronic diseases (including lifestyle diseases), oncology, pain management, and neurology. In the following section, we review some of the major clinical areas in which implants have made a significant contribution to therapy and disease management.

Chronic diseases

Of all clinical use scenarios, IDDS perhaps find their best applicability in the treatment of chronic diseases. As such, devices for a wide variety of clinical applications against chronic illnesses have been developed.

- MicroCHIPS has a number of DDS in development for the treatment of osteoporosis, diabetes, and multiple sclerosis, and a remote control contraception implant [128]. The MicroCHIPS DDS contraceptive implant is an active system in that it contains microreservoirs of 30 μg of the hormone levonorgestrel released daily over a 16 year period and the process can be deactivated and reactivated at any time using a short-range wireless remote control unit. The DDS also incorporates a real-time clock and wireless telemetry circuits for active control of drug dose scheduling from an external remote control unit placed in contact with the skin over the site of implantation. The bidirectional communications link also provides information regarding dose delivery confirmation and implant status such as battery voltage. The MicroCHIPS structure consists of a silicon substrate into which are etched pyramidal microreservoirs that are filled with the prescribed drug dose and then hermetically sealed with an ultra-thin gold membrane covering that also serves as an anode electrode. Applying an anodal DC voltage of 1.04 V with reference to the cathode for a period of several seconds, results in the gold membrane to effectively dissolve such that the drug in the reservoir can diffuse into the surrounding tissue and subsequently enter the blood stream. The MicroCHIPS measures 20x20x7 mm and is designed to be implanted subcutaneously in the buttocks, upper arm, or abdomen under local anesthetic.
- The CODMANs 3000 Implantable infusion drug pump is an example of a passive DDS used to deliver medications at a constant rate for the treatment of chronic pain, severe spasticity and cancers of the liver. The CODMANs 3000 does not require batteries and is available in three sizes (16, 30, and 50 mL) to increase the delivery time between refills. The FLEXTIP Plus SureStream intraspinal catheter is used when medication is delivered to the

intraspinal space as required in the treatment for chronic pain and severe spasticity. The drug reservoir is refilled by inserting a needle through the skin into the central septum through a self-sealing silicone membrane. CODMANs 3000 pump contains two chambers, the inner drug reservoir and the permanently sealed outer propellant bellows chamber that contains a compressible fluorocarbon gas. When the drug reservoir is empty, the bellows contract under pressure from the gas in the propellant chamber which is dependent on the body temperature. Filling or refilling the drug reservoir chamber causes the bellows to expand, which forces the drug to flow out of the drug reservoir through a filter and a capillary restrictor tube which maintains an optimal flow rate of the drug through a catheter to the drug delivery site. The CODMANs 3000 Pump delivers the required medication, with typical flow rates between 0.5 and 2 mL/day. In cases in which a direct injection into the body is required or when the catheter needs flushing with saline, the CODMANs 3000 Bolus Needle is used which makes a direct connection to the tip of the catheter. The CODMANs Pump 3000 is housed in a titanium casing and is implanted subcutaneously in the lower abdomen.

- The SynchroMeds II Infusion System delivers pain medication directly to the intrathecal space surrounding the spinal cord [129]. The treatments include pain management for severe chronic nonmalignant, severe spasticity of spinal or cerebral origin, and treatment of primary or metastatic cancer [130]. The myPTM is a handheld personal therapy manager that gives patients the control to receive extra prescribed bolus doses of medication when the need arises. The N'Vision Clinician Programmer is used to create and store up to 50 clinician-created programs for the management of patient treatment, as well as to store all critical therapy and patient information. The SynchroMeds II Programmable Infusion Pump is implanted in the abdominal area and is connected to a small thin catheter that is implanted in the intrathecal space. Two sizes of drug reservoirs are available, 18 and 20 mL. An alarm is activated if the drug level decreases to less than 2 mL. The pump can be programmed to deliver medication at

therapeutic flow rates from 0.002 to 1.0 mL/h (0.048-24 mL/day). The battery life, depending on usage, is between 4 and 7 years. After 7 years, the pump automatically shuts off. The drug is delivered using a 22-gauge corning needle into the reservoir fill port, where it passes through the reservoir valve and into the pump reservoir. The micropump contains a sealant gas that begins to heat up from the body's temperature, exerting pressure on the pump reservoir forcing the drug into the pump tubing, where an electronically controlled motor pushes the required dose out through the catheter port and into the catheter to the infusion site. The catheter access port allows for direct access to the catheter tip using a 24-gauge noncoring needle. This allows for direct access to the infusion site and also for flushing of the catheter.

- The MIP Implantable pump from Debiotech is a piezo-actuated silicon micropump fabricated using MEMS technology working as a volumetric pump by the reciprocating action of a silicon micromachined membrane to periodically compress the fluidic chamber to pump the pharmaceutical drug out through one-way directional fabricated valves. The silicon layers are micromachined to form the circular fluidic chamber and valve structures, whereas the glass layers contain through holes for the fluid. On top of the stack is a piezoelectric ceramic disc that is bonded to the top silicon layer, which collectively acts as the micropump actuator. At the bottom of the stack are two titanium fluid connectors hermetically joined to the micropump. The piezoelectric actuator vibrates when a voltage is applied across the material, initiating a displacement of the silicon membrane, initiating a reciprocating pump action. The structure of the device is such that on the compression stroke, the membrane compresses the fluid chamber and directs the fluid flow through the inlet and outlet valves. The flow rate is linear with the actuation frequency up to 0.2 Hz and achieves a typical flow rate of 0.1 mL/h with a stroke volume of 150 nL. The whole chip measures 16x12x1.86 mm.

- The DebioStart is an implantable DDS that can be used for local and sustained delivery of pharmaceutical drugs subcutaneously,

intraperitoneally or intramuscularly for single or refillable use. DebioStart that contains a refillable drug reservoir and a controlled silicon nanoporous membrane, whereby the pore diameter and membrane thickness can be controlled to alter the drug delivery rate such that the drug can be delivered over several weeks or several months. The pore diameters can be altered with a range between 1 and 250 nm and the total membrane range thickness is from 50 nm to several hundred micrometres. A pore density of 1 billion pores/cm2 is possible. Also, by chemically altering the membrane surface properties, the drug delivery can be delayed over longer periods.

Figure 2-4 Implantable drug delivery systems for chronic disease

Cancer

The major challenge in anticancer therapy is to develop DDSs to deliver chemotherapeutic drugs safely and effectively without side effects. Therefore, IDDSs have a great potential to deliver chemotherapeutic drugs in a more effective and safe manner. Brain, prostate, and bladder cancer are a few examples, for which attempts have been made to enable treatment with a drug delivery implant [131,132]. The Gliadel Wafer described earlier has been approved as one of the first implantable brain cancer treatment to deliver chemotherapy directly to the tumor site. Another example is the Zoladex biodegradable implantable rod, delivering goserelin acetate for treating prostate cancer [133]. Similarly, Endo Pharmaceutical has developed a hydrogel subcutaneous implant, called Vantas, also targeting prostate cancer. This product is capable of delivering 50 mg of histrelin acetate over a 12-month period [134]. Also notable is a nonbiodegradable drug-eluting product from TARIS Biomedical, designed to provide relief for nonmuscle invasive bladder cancer [135].

2.3 Limitations and open challenges

2.3.1 Manipulators for robotic surgery

Flexible robotics research in the medical domain has generated increasing numbers of new concepts and feasibility studies over the last decade. Fundamental topics such as structural design, actuation, and kinematic modelling have achieved a sufficient level of sophistication for many applications and have thus led to commercialized and clinically relevant research systems. However, three grand challenges remain in order to bring those robots that have not yet been commercialized to clinical practice: A) Instrumentation, Visualization; B) Human–Machine Interaction; and C) Shape and Force Sensing.

A. *Instrumentation, Visualization*

Beyond reaching around corners and following curved paths, successful use of continuum robots in surgery also requires visualization of the anatomy and the ability to perform surgical tasks once the desired pathology is reached. In addition to instrumentation, minimally invasive surgery is highly dependent on

visualization of the surgical site and surrounding anatomy. There is a tradeoff between straight, rigid endoscopes delivering high-resolution visualization and flexible endoscopes (flexible fiber optic scopes) with a bendable tip but inferior visualization. High-definition 3-D visualization, such as in the daVinci surgical system, is highly preferred by surgeons as spatial depth perception is considered very helpful. Three concepts for addressing this challenge have been proposed: 1) follow the flexible manipulator with a conventional rigid endoscope (e.g., Burgner et al. [88]) ; 2) equip the flexible manipulator with (flexible) endoscope (e.g., Hendrick et al. [136]); or 3) integrate optical instrumentation within flexible manipulator to provide visualization (e.g., Can et al. [137]). The third concept is the most challenging due to space constraints. Optical fibers or chip-on-the-tip cameras may provide a solution, but attaining sufficient illumination, resolution, and depth perception remain unsolved challenges today. The operating room and surgical application itself also pose special requirements on medical devices. The federal regulatory frameworks ensure that medical devices meet essential requirements in terms of performance and safety. However, keeping the requirements of surgical applications in mind is essential during the development phase, such as characteristics of the surgical site (e.g., present body liquids, motion of organs), limited space in the operating room and at the patient, sterilizability of the device (e.g., Burgner et al. [138]), ease of use for surgical staff, and compatible design for medical imaging (MRI, X-ray [25]).

B. *Human-Machine Interactions*

Having a continuously curved manipulator, which is tele-operated rather than controlled manually, poses significant requirements on an efficient human-machine interface. The challenge is to provide the information necessary to the physician about the shape of the manipulator by means of an image-guidance system. In other words, to represent the morphology of a curved structure, its contact points with the anatomy, or the force profile acting on the structure to the operator. It is a challenge to adjust tissue contact forces, allow robot deflection through tissue contact, and use natural anatomical constraints in motion planning, while also compensating for undesired deflections. Not only is this a problem of

motion planning and control, but also of how to provide an interface for the operator (e.g., to inform about interaction forces between the manipulator and tissue).

Another important aspect of the human–machine interface is the design of input devices in those medical applications where the robot is teleoperated. The Geomagic Touch device (formerly Phantom Omni, now marketed by Geomagic Inc., USA) has been used in [32,88,89,90]. It features a pen-like stylus for commanding motion in 6 DOF and can apply force feedback in 3 DOF. Auris Monarch platform for bronchial tree has been using a XBOX type controller that allows physicians to navigate the continuum endoscope. Motion planning is essential to consider as a part of the human–machine interface. In order to be applicable in a medical scenario, effective motion planning for flexible robots will not only depend on scalable real-time algorithms, but also on the availability of real-time sensor information on the anatomy and robot shape.

C. Shape and Force Sensing

Sensing the 3-D shape of flexible robots in real time is a major research challenge as knowledge about the shape is key to advanced control methodologies, human-machine interaction, and interfaces. While the integration of existing external sensors such as camera systems or EM tracking coils are feasible in principal, the small size of flexible robots and the clinical setting usually impede straightforward implementation. External cameras require line of sight with the robot, which is not possible in minimally invasive surgeries, and EM tracking requires an environment without any magnetic objects that could interfere with the magnetic field and decrease accuracy. One promising strategy is fiber Bragg grating (FBG) [139–141], strain-based, shape sensing. Similar approaches to the continuous shape sensing challenge include bending sensors and cable displacement measurements. Chen *et al.,* proposed a two-axis flexible bending sensor surrounding a flexible spring coated in parylene and integrated into a layer of polyurethane [142]. Rone and Bentzvi estimate the shape of single- and multibackbone tendon-driven flexible robots from passive cable displacement in numerical case studies [143].

42

Application of flexible robots in the medical domain also suggests the possibility of using medical imaging for sensing purposes. Ultrasound is a cost-effective choice for real-time imaging in applications where the robot is surrounded by liquid or soft tissue (e.g., cardiac, vascular, or abdominal surgery). However, ultrasound images usually have poor resolution, and anatomical features are difficult to identify. Thus far, ultrasound has been used for guidance in flexible robotics research, i.e., a target position is either defined in ultrasound [144] or continuous ultrasound images are used for navigation [69]. Ren and Dupont used 3-D ultrasound to detect the curvature of a component tube of concentric-tube robots in intracardiac interventions [145]. Initial results using flouroscopic imaging have been reported by Burgner *et al.* [146] and further theoretical contributions were made by Lobaton *et al.* [147]. However, the risks of using radiation for imaging must be justified in terms of the surgical outcome.

Besides sensing the 3-D shape of flexible robots, sensing contact forces throughout the structure of the robot is a major challenge. Flexible robots have some natural passive force/displacement mapping at their end-effectors due to their elastic structure, yet the operator may desire different stiffness characteristics in different scenarios that may not match the passive stiffness of the robot. If end-effector displacements and/or applied forces can be sensed and compared with model computations [148], active stiffness control techniques similar to those employed for conventional robots can compensate for undesired deflection and implement a desired stiffness behaviour [149]. This also brings the possibility of compliant motion control with intrinsic contact and load sensing during insertion. These topics have been investigated by sensing both robot displacement and actuation forces in multibackbone flexible robots [32] [150–155].

Several technical and scientific issues are still open and research works are underway in many places to extend this endoluminal approach to more demanding therapeutic procedures. To list a few, progress is required in the design to transmit enough forces for performing the desired task, to improve triangulation for better visualization, etc., while continuing miniaturization. Progress is also required in control to better stabilize the surgical tools once on the operating site, to

compensate for flexibilities, backlashes, dead-bands, etc., in order to improve precision and dynamics. Concerning SPA, the challenge is in the design of the trocar and instruments going through it, such that they are deployed inside the abdominal cavity in an optimal working configuration. In other words, they should not collide with each other while offering sufficient triangulation to provide enough dexterity and field of view. A few products for manual procedures are now on the shelves such as, for instance, the ASC Triport and Quad-port8 or the X-Cone from Karl.

In a more dramatic approach to in vivo robotics, micro/nanotechnology is a multibillion dollar area of research, including investigation for various medical robotic uses such as inexpensive directable drug delivery devices, and other therapeutic approaches that may benefit from robots working at the cellular level. Construction of functional systems is an ongoing area of research, particularly with respect to generating and powering motion. Many current prototypes are propelled and guided via magnetic fields, though some utilize external electrical energy sources.

2.3.2 Implantable drug release system

- *Biocompatibility-related issues*

Biocompatibility is a critical design parameter for successful IDDS performance, given the need for a substantial time period of implantation. Since most IDDS are in close proximity to critical internal organs and in intimate contact with tissue, biocompatibility with the human environment is essential. Unfortunately, it is very unlikely that any synthetic material will be completely inert or harmonious with the living environment. For a substance to be considered as biocompatible, it must fulfill certain requirements. All implant materials, not including the drug cargo, must be chemically inert, hypoallergenic, and mechanically stable at the implant site [156]. The material should also not be physically or chemically modified by local tissue, and the implant should not cause any inflammatory response at the site of implantation. Specific issues associated with post-implantation stability and reactivity need to be investigated, such as the formation of fibrous capsules around

the implant. If acceptable biocompatibility is not achieved, many adverse effects may occur. These may range in severity, such as capsular contracture, to relatively serious complications, such as unexpected release of the drug, platelet adhesion, inflammation, fibrosis, thrombosis, tissue damage, or infection of the area surrounding the implant [157,158]. Biomaterial implantation is always accompanied by some unavoidable injury as a result of the implantation procedure. This initiates various responses at the tissue and molecular levels.

There are many factors to consider during the development of an IDDS which influence implant biocompatibility, such as implant size, shape, material composition, and surface wettability, roughness, and charge. Both the physical and chemical properties of the bulk material may be involved in provoking a particular tissue reaction, and soluble breakdown products may induce their own local tissue response. Implant size also has marked effect on tissue response [156].

- ***Patient compliance***

Some IDDSs require minor surgery for implantation and extraction, which lowers patient acceptance and demands a less invasive alternative. Implanting (and potential explanting) may require specialized training, in most cases where implants are designed for administration by lower level healthcare workers instead of surgeons. Patient acceptance is typically lowered if the IDDS exert pain and discomfort while implanted in the body [159,160]. However, in most cases where implants are indicated, the potential cumulative benefits of the prolonged therapy, minimal ongoing compliance burden, and optimized or localized delivery far outweigh the potential risks. As such, most patients in need of such therapy may be suitably counseled to comply with the temporary morbidity associated with implantation and extraction, if needed.

- ***Regulatory aspects***

With respect to IMDs, the evolution of technologies from mere electromechanical devices to ones with more advanced computing and communication capabilities have many benefits, but also entail numerous security and privacy risks for the patient. The majority of such risks are relatively well known in classic computing

scenarios, although, in many respects, their repercussions are far more critical in the case of implants. Furthermore, these devices store and transmit very sensitive medical information that requires protection, as dictated by European and US Directives.

- ***Cost-effectiveness***

The inherent complexity of implantable systems, particularly in comparison with simpler oral dosage forms, potentially makes the vital and necessary regulatory path for approval longer and prohibitively expensive for some companies to pursue. The cost-benefit ratio is a vital parameter influencing patient acceptance and commercial success. It is possible that, after considering the costs for development, manufacturing, and regulatory approval, the IDDSs may not be cost effective enough for reimbursement, insurance coverage, or out-of-pocket purchase in uninsured markets. Major pharmaceutical companies will usually not undertake the cost involved, unless reimbursement is highly probable or is negotiated beforehand. This leaves smaller companies to accept the risk and expenses incurred during the development and approval process. Nonetheless, as reviewed earlier, there are multiple clinical situations where implantable systems are not only cost-effective, but may substantially lower the overall cost of treatment when subjective factors like patient compliance and satisfaction are accounted for. This is perhaps a significant reason why both large medtech multinational companies, as well as small startups operating in niche areas, find it profitable to compete for the same market.

- ***Future perspectives***

Overall, there is an ongoing a drive to make IDDSs more cost-effective and patient-friendly. This trend indicates that future devices will probably be smaller, less invasive, and more site-specific. All these features will need to be accomplished while maintaining the dose at precise therapeutic levels for the desired duration. Micro/nano-fabricated devices lend themselves precisely to this task, since manufacturability is well established by borrowing concepts from the semiconductor industry. Some IDDSs may even be hybrids that contain a targeting therapeutic molecule and include a diagnostic feature, creating a new class of so-

called next generation theranostics. Future versions of IDDSs may additionally have a remotely controllable feature, whereby a physician located at considerable distance may precisely control their operation. This may enable them to become even more patient-friendly and increase their long-term cost-effectiveness. However, it certainly appears that the key drivers in the future will be IDDS applications that are more cost-effective while improving patient compliance and acceptance. Most of the electromechanical IDDSs use batteries, which must be changed frequently by surgical procedures, or require the power source to remain externally placed outside the body. To overcome these problems, Dagdeviren recently developed a flexible micro-generator that can harvest energy from the natural movements (contraction and relaxation) of organs to power implantable devices [161]. Consequently, it is possible that, in the near future, we may see IDDSs with micro-bionic dynamos to power the next generation of dynamic drug delivery implants. However, further investigation into the safety profile of these types of systems is needed to evaluate whether they could be safely integrated into drug delivery implants. Environmentally sensitive polymeric delivery systems are currently designed to achieve targeted and controlled in vivo delivery in response to specific stimuli, such as pH, ionic strength, enzyme-substrate, magnetic, thermal, electrical, ultrasound, etc. [162]. It is expected that implantable system will leverage such materials to generate a feedback-controlled release mechanism to modulate zero-order or nonzero-order release profiles. It is hoped that, in the future, development of new implantable systems will help reduce the cost of drug therapy, increase the efficacy of drugs, and enhance patient compliance.

2.4 Conclusion

While the first flexible robots were created almost 50 years ago, medical applications have clearly been a primary driving factor for continuum robot research over the last decade. Substantial progress has been made in design, modelling, control, sensing, and application to specific medical problems. We have surveyed the core principles underlying flexible robotics research in medical applications and given an overview of surgical systems that are either commercialized or relatively far advanced in terms of clinical readiness. Apart

from the progress that has been made in medical continuum robotics research, several major challenges require future research. The small size and compliance of continuum robots is favorable from a medical point of view but place high demands on sensing, control, and human–machine interaction. We anticipate that the next decade will see flexible robots increasingly benefiting surgeons and patients by providing less invasive access pathways and manipulation possibilities.

In the field of artificial organs, many research programs are being performed on all major organ systems. However, only a limited number of the approaches have reached the phase of application in clinical use. Established organ support devices exist as a bridge to transplant or long-term chronical support for the heart, the pancreas and the bladder. Clinical trials are going on with a total artificial heart device, liver and kidney support devices and with cell therapy for the heart and a tissue-engineered bioreactor combined with dialysis functions to replace failing kidneys.

For over 40 years now, studies have been performed on the development of a closed-loop glucose measurement and insulin delivery system. In the last decennia progress has been made in the development of essential components: glucose monitors and insulin pumps. Both are commercially available, including those advising algorithms and data management options, and the application possibilities become more sophisticated year after year. However, fully closed loops systems are still not reliable and sufficiently accurate to be marketed. This is mainly due to problems with long term glucose measurement and to the complexity of dose controlling algorithms that have to respond to many different physiological circumstances.

IDDSs have seen reasonable clinical and commercial success as a mode of enhanced drug therapy. However, optimization of performance characteristics, including long-term biocompatibility and drug release kinetics is critical. Furthermore, clinical validation of current systems under development is essential for regulatory approval and their commercial success. However, as reviewed here, numerous commercial systems are able to attain nearly ideal zero-order release kinetics profiles in vivo, over extended time periods. IDDSs therefore present a

viable, cost-effective and clinically acceptable alternative route of sustained drug delivery for chronically ill patients.

References:

1. Harrell AG, Heniford BT. Minimally invasive abdominal surgery: lux et veritas past, present, and future. *Am J Surg*. 2005;190(2):239-243. doi:10.1016/j.amjsurg.2005.05.019

2. Gomes P. Surgical robotics: Reviewing the past, analysing the present, imagining the future. *Robot Comput Integr Manuf*. 2011;27(2):261-266. doi:10.1016/j.rcim.2010.06.009

3. Dogangil G, Davies BL, Rodriguez y Baena F. A review of medical robotics for minimally invasive soft tissue surgery. *Proc Inst Mech Eng Part H J Eng Med*. 2010;224(5):653-679. doi:10.1243/09544119JEIM591

4. Davies B. A review of robotics in surgery. *Proc Inst Mech Eng Part H J Eng Med*. 2000;214(1):129-140. doi:10.1243/0954411001535309

5. Ayvali E, Liang CP, Ho M, Chen Y, Desai JP. Towards a discretely actuated steerable cannula for diagnostic and therapeutic procedures. *Int J Rob Res*. 2012;31(5):588-603. doi:10.1177/0278364912442429

6. Camarillo DB, Milne CF, Carlson CR, Zinn MR, Salisbury JK. Mechanics modeling of tendon-driven continuum manipulators. *IEEE Trans Robot*. 2008;24(6):1262-1273. doi:10.1109/TRO.2008.2002311

7. Burgner-Kahrs J, Rucker DC, Choset H. Continuum Robots for Medical Applications: A Survey. *IEEE Trans Robot*. 2015;31(6):1261-1280. doi:10.1109/TRO.2015.2489500

8. Simaan N, Kai Xu, Wei Wei, et al. Design and Integration of a Telerobotic System for Minimally Invasive Surgery of the Throat. *Int J Rob Res*. 2009;28(9):1134-1153. doi:10.1177/0278364908104278

9. Xu K, Zhao J, Fu M. Development of the SJTU Unfoldable Robotic System (SURS) for Single Port Laparoscopy. *IEEE/ASME Trans Mechatronics*. 2015;20(5):2133-2145. doi:10.1109/TMECH.2014.2364625

10. Till J, Bryson CE, Chung S, Orekhov A, Rucker DC. Efficient computation of

multiple coupled Cosserat rod models for real-time simulation and control of parallel continuum manipulators. In: *2015 IEEE International Conference on Robotics and Automation (ICRA).* IEEE; 2015:5067-5074. doi:10.1109/ICRA.2015.7139904

11.   Moses MS, Kutzer MDM, Hans Ma, Armand M. A continuum manipulator made of interlocking fibers. In: *2013 IEEE International Conference on Robotics and Automation.* IEEE; 2013:4008-4015. doi:10.1109/ICRA.2013.6631142

12.   Ikuta K, Ichikawa H, Suzuki K, Yajima D. Multi-degree of freedom hydraulic pressure driven safety active catheter. In: *Proceedings 2006 IEEE International Conference on Robotics and Automation, 2006. ICRA 2006.* IEEE; :4161-4166. doi:10.1109/ROBOT.2006.1642342

13.   Bailly Y, Amirat Y, Fried G. Modeling and Control of a Continuum Style Microrobot for Endovascular Surgery. *IEEE Trans Robot.* 2011;27(5):1024-1030. doi:10.1109/TRO.2011.2151350

14.   Ikuta K, Matsuda Y, Yajima D, Ota Y. Pressure Pulse Drive: A Control Method for the Precise Bending of Hydraulic Active Catheters. *IEEE/ASME Trans Mechatronics.* 2012;17(5):876-883. doi:10.1109/TMECH.2011.2138711

15.   Chen G, Pham MT, Redarce T. A Guidance Control Strategy for Semi-autonomous Colonoscopy Using a Continuum Robot. In: *Recent Progress in Robotics: Viable Robotic Service to Human.* Berlin, Heidelberg: Springer Berlin Heidelberg; :63-78. doi:10.1007/978-3-540-76729-9_6

16.   Chen G, Pham MT, Redarce T. Sensor-based guidance control of a continuum robot for a semi-autonomous colonoscopy. *Rob Auton Syst.* 2009;57(6-7):712-722. doi:10.1016/j.robot.2008.11.001

17.   Jayender J, Azizian M, Patel RV. Autonomous Image-Guided Robot-Assisted Active Catheter Insertion. *IEEE Trans Robot.* 2008;24(4):858-871. doi:10.1109/TRO.2008.2001353

18.   Jayender J, Patel RV, Nikumb S. Robot-assisted Active Catheter Insertion: Algorithms and Experiments. *Int J Rob Res.* 2009;28(9):1101-1117. doi:10.1177/0278364909103785

19.   Ayvali E, Liang C-P, Ho M, Chen Y, Desai JP. Towards a discretely actuated steerable cannula for diagnostic and therapeutic procedures. *Int J Rob Res.*

2012;31(5):588-603. doi:10.1177/0278364912442429

20. Crews JH, Buckner GD. Design optimization of a shape memory alloy–actuated robotic catheter. *J Intell Mater Syst Struct*. 2012;23(5):545-562. doi:10.1177/1045389X12436738

21. Noonan DP, Vitiello V, Shang J, Payne CJ, Yang G-Z. A modular, mechatronic joint design for a flexible access platform for MIS. In: *2011 IEEE/RSJ International Conference on Intelligent Robots and Systems*. IEEE; 2011:949-954. doi:10.1109/IROS.2011.6094907

22. Bishop-Moser J, Kota S. Towards snake-like soft robots: Design of fluidic fiber-reinforced elastomeric helical manipulators. In: *2013 IEEE/RSJ International Conference on Intelligent Robots and Systems*. IEEE; 2013:5021-5026. doi:10.1109/IROS.2013.6697082

23. Berg DR, Li PY, Erdman AG. Achieving Dexterous Manipulation for Minimally Invasive Surgical Robots Through the Use of Hydraulics. In: *Volume 3: Renewable Energy Systems; Robotics; Robust Control; Single Track Vehicle Dynamics and Control; Stochastic Models, Control and Algorithms in Robotics; Structure Dynamics and Smart Structures;*. ASME; 2012:429-438. doi:10.1115/DSCC2012-MOVIC2012-8685

24. McMahan W, Chitrakaran V, Csencsits M, et al. Field trials and testing of the OctArm continuum manipulator. In: *Proceedings 2006 IEEE International Conference on Robotics and Automation, 2006. ICRA 2006.* IEEE; :2336-2341. doi:10.1109/ROBOT.2006.1642051

25. Greigarn T, Cavusoglu MC. Task-space motion planning of MRI-actuated catheters for catheter ablation of atrial fibrillation. In: *2014 IEEE/RSJ International Conference on Intelligent Robots and Systems*. IEEE; 2014:3476-3482. doi:10.1109/IROS.2014.6943047

26. Liu T, Cavusoglu MC. Three dimensional modeling of an MRI actuated steerable catheter system. In: *2014 IEEE International Conference on Robotics and Automation (ICRA)*. IEEE; 2014:4393-4398. doi:10.1109/ICRA.2014.6907499

27. Dario P, Carrozza MC, Marcacci M, et al. A novel mechatronic tool for computer-assisted arthroscopy. *IEEE Trans Inf Technol Biomed*. 2000;4(1):15-29. doi:10.1109/4233.826855

28. Kato T, Okumura I, Kose H, Takagi K, Hata N. Extended kinematic mapping of tendon-driven continuum robot for neuroendoscopy. In: *2014 IEEE/RSJ International Conference on Intelligent Robots and Systems*. IEEE; 2014:1997-2002. doi:10.1109/IROS.2014.6942828

29. Hyun-Soo Yoon, Byung-Ju Yi. A 4-DOF flexible continuum robot using a spring backbone. In: *2009 International Conference on Mechatronics and Automation*. IEEE; 2009:1249-1254. doi:10.1109/ICMA.2009.5246612

30. Camarillo DB, Milne CF, Carlson CR, Zinn MR, Salisbury JK. Mechanics Modeling of Tendon-Driven Continuum Manipulators. *IEEE Trans Robot*. 2008;24(6):1262-1273. doi:10.1109/TRO.2008.2002311

31. Kutzer MDM, Segreti SM, Brown CY, Armand M, Taylor RH, Mears SC. Design of a new cable-driven manipulator with a large open lumen: Preliminary applications in the minimally-invasive removal of osteolysis. In: *2011 IEEE International Conference on Robotics and Automation*. IEEE; 2011:2913-2920. doi:10.1109/ICRA.2011.5980285

32. Bajo A, Pickens RB, Herrell SD, Simaan N. Constrained motion control of multisegment continuum robots for transurethral bladder resection and surveillance. In: *2013 IEEE International Conference on Robotics and Automation*. IEEE; 2013:5837-5842. doi:10.1109/ICRA.2013.6631417

33. Jiangran Zhao, Xidian Zheng, Minhua Zheng, Shih AJ, Kai Xu. An endoscopic continuum testbed for finalizing system characteristics of a surgical robot for NOTES procedures. In: *2013 IEEE/ASME International Conference on Advanced Intelligent Mechatronics*. IEEE; 2013:63-70. doi:10.1109/AIM.2013.6584069

34. Ding J, Goldman RE, Xu K, Allen PK, Fowler DL, Simaan N. Design and Coordination Kinematics of an Insertable Robotic Effectors Platform for Single-Port Access Surgery. *IEEE/ASME Trans Mechatronics*. 2013;18(5):1612-1624. doi:10.1109/TMECH.2012.2209671

35. Kwok K-W, Hung Tsoi K, Vitiello V, et al. Dimensionality Reduction in Controlling Articulated Snake Robot for Endoscopy Under Dynamic Active Constraints. *IEEE Trans Robot*. 2013;29(1):15-31. doi:10.1109/TRO.2012.2226382

36. Kwok K-W, Vitiello V, Yang G-Z. Control of Articulated Snake Robot under Dynamic Active Constraints. In: ; 2010:229-236. doi:10.1007/978-3-642-15711-0_29

37. Lee SL, Lerotic M, Vitiello V, et al. From medical images to minimally invasive intervention: Computer assistance for robotic surgery. *Comput Med Imaging Graph*. 2010;34(1):33-45. doi:10.1016/j.compmedimag.2009.07.007

38. Shang J, Noonan DP, Payne C, et al. An articulated universal joint based flexible access robot for minimally invasive surgery. In: *2011 IEEE International Conference on Robotics and Automation*. IEEE; 2011:1147-1152. doi:10.1109/ICRA.2011.5980261

39. Newton RC, Noonan DP, Vitiello V, et al. Robot-assisted transvaginal peritoneoscopy using confocal endomicroscopy: a feasibility study in a porcine model. *Surg Endosc*. 2012;26(9):2532-2540. doi:10.1007/s00464-012-2228-1

40. Shang J, Payne CJ, Clark J, et al. Design of a multitasking robotic platform with flexible arms and articulated head for Minimally Invasive Surgery. In: *2012 IEEE/RSJ International Conference on Intelligent Robots and Systems*. IEEE; 2012:1988-1993. doi:10.1109/IROS.2012.6385567

41. Kim Y-J, Cheng S, Kim S, Iagnemma K. A Stiffness-Adjustable Hyperredundant Manipulator Using a Variable Neutral-Line Mechanism for Minimally Invasive Surgery. *IEEE Trans Robot*. 2014;30(2):382-395. doi:10.1109/TRO.2013.2287975

42. Hyun-Soo Yoon, Hyo-Jeong Cha, Jaeheon Chung, Byung-Ju Yi. Compact design of a dual master-slave system for maxillary sinus surgery. In: *2013 IEEE/RSJ International Conference on Intelligent Robots and Systems*. IEEE; 2013:5027-5032. doi:10.1109/IROS.2013.6697083

43. Conrad BL, Jung J, Penning RS, Zinn MR. Interleaved continuum-rigid manipulation: An augmented approach for robotic minimally-invasive flexible catheter-based procedures. In: *2013 IEEE International Conference on Robotics and Automation*. IEEE; 2013:718-724. doi:10.1109/ICRA.2013.6630652

44. Conrad BL, Zinn MR. Interleaved continuum-rigid manipulation approach: Development and functional evaluation of a clinical scale manipulator. In: *2014 IEEE/RSJ International Conference on Intelligent Robots and Systems*. IEEE;

2014:4290-4296. doi:10.1109/IROS.2014.6943168

45. Xu K, Fu M, Zhao J. An experimental kinestatic comparison between continuum manipulators with structural variations. In: *2014 IEEE International Conference on Robotics and Automation (ICRA)*. IEEE; 2014:3258-3264. doi:10.1109/ICRA.2014.6907327

46. Chirikjian GS, Burdick JW. A hyper-redundant manipulator. *IEEE Robot Autom Mag*. 1994;1(4):22-29. doi:10.1109/100.388263

47. Robinson G, Davies JBC. Continuum robots - a state of the art. In: *Proceedings 1999 IEEE International Conference on Robotics and Automation (Cat. No.99CH36288C)*. Vol 4. IEEE; :2849-2854. doi:10.1109/ROBOT.1999.774029

48. Webster RJ, Jones BA. Design and Kinematic Modeling of Constant Curvature Continuum Robots: A Review. *Int J Rob Res*. 2010;29(13):1661-1683. doi:10.1177/0278364910368147

49. Hirose S. Hirose, Shigeo. Biologically inspired robots: snake-like locomotors and manipulators. *Oxford Oxford Univ Press*. 1993;1093.

50. Chirikjian GS, Burdick JW. A modal approach to hyper-redundant manipulator kinematics. *IEEE Trans Robot Autom*. 1994;10(3):343-354. doi:10.1109/70.294209

51. Chirikjian GS, Burdick JW. The kinematics of hyper-redundant robot locomotion. *IEEE Trans Robot Autom*. 1995;11(6):781-793. doi:10.1109/70.478426

52. Chirikjian GS, Burdick JW. Kinematically optimal hyper-redundant manipulator configurations. *IEEE Trans Robot Autom*. 1995;11(6):794-806. doi:10.1109/70.478427

53. Walker ID. Robot strings: Long, thin continuum robots. In: *2013 IEEE Aerospace Conference*. IEEE; 2013:1-12. doi:10.1109/AERO.2013.6496902

54. Hirose S, Yamada H. Snake-like robots [Tutorial]. *IEEE Robot Autom Mag*. 2009;16(1):88-98. doi:10.1109/MRA.2009.932130

55. Trivedi D, Rahn CD, Kier WM, Walker ID. Soft robotics: Biological inspiration, state of the art, and future research. *Appl Bionics Biomech*. 2008;5(3):99-117. doi:10.1080/11762320802557865

56. Kim S, Laschi C, Trimmer B. Soft robotics: a bioinspired evolution in robotics.

Trends Biotechnol. 2013;31(5):287-294. doi:10.1016/j.tibtech.2013.03.002

57.   Gilbert HB, Rucker DC, Webster III RJ. Concentric Tube Robots: The State of the Art and Future Directions. In: ; 2016:253-269. doi:10.1007/978-3-319-28872-7_15

58.   Chirikjian GS. Conformational Modeling of Continuum Structures in Robotics and Structural Biology: A Review. *Adv Robot*. 2015;29(13):817-829. doi:10.1080/01691864.2015.1052848

59.   Fu Y, Liu H, Huang W, Wang S, Liang Z. Steerable catheters in minimally invasive vascular surgery. *Int J Med Robot Comput Assist Surg*. 2009;5(4):381-391. doi:10.1002/rcs.282

60.   Bonatti J, Vetrovec G, Riga C, Wazni O, Stadler P. Robotic technology in cardiovascular medicine. *Nat Rev Cardiol*. 2014;11(5):266-275. doi:10.1038/nrcardio.2014.23

61.   Rafii-Tari H, Payne CJ, Yang G-Z. Current and Emerging Robot-Assisted Endovascular Catheterization Technologies: A Review. *Ann Biomed Eng*. 2014;42(4):697-715. doi:10.1007/s10439-013-0946-8

62.   Reddy VY, Neuzil P, Malchano ZJ, et al. View-Synchronized Robotic Image-Guided Therapy for Atrial Fibrillation Ablation. *Circulation*. 2007;115(21):2705-2714. doi:10.1161/CIRCULATIONAHA.106.677369

63.   Chun KRJ, Schmidt B, Köktürk B, et al. Catheter Ablation – New Developments in Robotics. *Herz Kardiovaskuläre Erkrankungen*. 2008;33(8):586-589. doi:10.1007/s00059-008-3180-7

64.   Riga C V., Bicknell CD, Wallace D, Hamady M, Cheshire N. Robot-Assisted Antegrade In-Situ Fenestrated Stent Grafting. *Cardiovasc Intervent Radiol*. 2009;32(3):522-524. doi:10.1007/s00270-008-9459-5

65.   RILLIG A, SCHMIDT B, STEVEN D, et al. Study Design of the Man and Machine Trial: A Prospective International Controlled Noninferiority Trial Comparing Manual with Robotic Catheter Ablation for Treatment of Atrial Fibrillation. *J Cardiovasc Electrophysiol*. 2013;24(1):40-46. doi:10.1111/j.1540-8167.2012.02418.x

66.   Ernst S, Ouyang F, Linder C, et al. Initial Experience With Remote Catheter Ablation Using a Novel Magnetic Navigation System. *Circulation*.

2004;109(12):1472-1475. doi:10.1161/01.CIR.0000125126.83579.1B

67. Chun JK-R, Ernst S, Matthews S, et al. Remote-controlled catheter ablation of accessory pathways: results from the magnetic laboratory. *Eur Heart J*. 2006;28(2):190-195. doi:10.1093/eurheartj/ehl447

68. Kesner SB, Howe RD. Position Control of Motion Compensation Cardiac Catheters. *IEEE Trans Robot*. 2011;27(6):1045-1055. doi:10.1109/TRO.2011.2160467

69. Kesner SB, Howe RD. Robotic catheter cardiac ablation combining ultrasound guidance and force control. *Int J Rob Res*. 2014;33(4):631-644. doi:10.1177/0278364913511350

70. Lang JE, Mannava S, Floyd AJ, et al. Robotic systems in orthopaedic surgery. *J Bone Joint Surg Br*. 2011;93-B(10):1296-1299. doi:10.1302/0301-620X.93B10.27418

71. Pearle AD, O'Loughlin PF, Kendoff DO. Robot-Assisted Unicompartmental Knee Arthroplasty. *J Arthroplasty*. 2010;25(2):230-237. doi:10.1016/j.arth.2008.09.024

72. Schulz AP, Seide K, Queitsch C, et al. Results of total hip replacement using the Robodoc surgical assistant system: clinical outcome and evaluation of complications for 97 procedures. *Int J Med Robot Comput Assist Surg*. 2007;3(4):301-306. doi:10.1002/rcs.161

73. Pearle AD, Kendoff D, Stueber V, Musahl V, Repicci JA. Perioperative management of unicompartmental knee arthroplasty using the MAKO robotic arm system (MAKOplasty). *Am J Orthop (Belle Mead NJ)*. 2009;38(2 Suppl):16-19. http://www.ncbi.nlm.nih.gov/pubmed/19340378.

74. Plaskos C, Cinquin P, Lavallée S, Hodgson AJ. Praxiteles: a miniature bone-mounted robot for minimal access total knee arthroplasty. *Int J Med Robot Comput Assist Surg*. 2005;1(4):67-79. doi:10.1002/rcs.59

75. Koulalis D, O'Loughlin PF, Plaskos C, Kendoff D, Cross MB, Pearle AD. Sequential versus automated cutting guides in computer-assisted total knee arthroplasty. *Knee*. 2011;18(6):436-442. doi:10.1016/j.knee.2010.08.007

76. Yen P-L, Davies BL. Active constraint control for image-guided robotic surgery. *Proc Inst Mech Eng Part H J Eng Med*. 2010;224(5):623-631.

doi:10.1243/09544119JEIM606

77.   Nathoo N, Çavuşoğlu MC, Vogelbaum MA, Barnett GH. In Touch with Robotics: Neurosurgery for the Future. *Neurosurgery*. 2005;56(3):421-433. doi:10.1227/01.NEU.0000153929.68024.CF

78.   Kwoh YS, Hou J, Jonckheere EA, Hayati S. A robot with improved absolute positioning accuracy for CT guided stereotactic brain surgery. *IEEE Trans Biomed Eng*. 1988;35(2):153-160. doi:10.1109/10.1354

79.   Brodie J, Eljamel S. Evaluation of a neurosurgical robotic system to make accurate burr holes. *Int J Med Robot Comput Assist Surg*. 2011;7(1):101-106. doi:10.1002/rcs.376

80.   Cleary K, Peters TM. Image-Guided Interventions: Technology Review and Clinical Applications. *Annu Rev Biomed Eng*. 2010;12(1):119-142. doi:10.1146/annurev-bioeng-070909-105249

81.   Varma TRK, Eldridge P. Use of the NeuroMate stereotactic robot in a frameless mode for functional neurosurgery. *Int J Med Robot Comput Assist Surg*. 2006;2(2):107-113. doi:10.1002/rcs.88

82.   Li QH, Zamorano L, Pandya A, Perez R, Gong J, Diaz F. The application accuracy of the NeuroMate robot?A quantitative comparison with frameless and frame-based surgical localization systems. *Comput Aided Surg*. 2002;7(2):90-98. doi:10.1002/igs.10035

83.   Morgan PS, Carter T, Davis S, et al. The application accuracy of the Pathfinder neurosurgical robot. *Int Congr Ser*. 2003;1256:561-567. doi:10.1016/S0531-5131(03)00421-7

84.   Deacon G, Harwood A, Holdback J, et al. The Pathfinder image-guided surgical robot. *Proc Inst Mech Eng Part H J Eng Med*. 2010;224(5):691-713. doi:10.1243/09544119JEIM617

85.   Devito DP, Kaplan L, Dietl R, et al. Clinical Acceptance and Accuracy Assessment of Spinal Implants Guided With SpineAssist Surgical Robot. *Spine (Phila Pa 1976)*. 2010;35(24):2109-2115. doi:10.1097/BRS.0b013e3181d323ab

86.   Stammberger H, Posawetz W. Functional endoscopic sinus surgery. *Eur Arch Oto-Rhino-Laryngology*. 1990;247(2). doi:10.1007/BF00183169

87.   Hyun-Soo Yoon, Se Min Oh, Jin Hyeok Jeong, et al. Active bending endoscope

robot system for navigation through sinus area. In: *2011 IEEE/RSJ International Conference on Intelligent Robots and Systems*. IEEE; 2011:967-972. doi:10.1109/IROS.2011.6094774

88. Burgner J, Rucker DC, Gilbert HB, et al. A Telerobotic System for Transnasal Surgery. *IEEE/ASME Trans Mechatronics*. 2014;19(3):996-1006. doi:10.1109/TMECH.2013.2265804

89. Bajo A, Dharamsi LM, Netterville JL, Garrett CG, Simaan N. Robotic-assisted micro-surgery of the throat: The trans-nasal approach. In: *2013 IEEE International Conference on Robotics and Automation*. IEEE; 2013:232-238. doi:10.1109/ICRA.2013.6630581

90. Gosline AH, Vasilyev N V, Butler EJ, et al. Percutaneous intracardiac beating-heart surgery using metal MEMS tissue approximation tools. *Int J Rob Res*. 2012;31(9):1081-1093. doi:10.1177/0278364912443718

91. Vasilyev N V., Gosline AH, Butler E, et al. Percutaneous Steerable Robotic Tool Delivery Platform and Metal Microelectromechanical Systems Device for Tissue Manipulation and Approximation. *Circ Cardiovasc Interv*. 2013;6(4):468-475. doi:10.1161/CIRCINTERVENTIONS.112.000324

92. Yuen SG, Novotny PM, Howe RD. Quasiperiodic predictive filtering for robot-assisted beating heart surgery. In: *2008 IEEE International Conference on Robotics and Automation*. IEEE; 2008:3875-3880. doi:10.1109/ROBOT.2008.4543806

93. Patronik NA, Riviere CN, El Qarra S, Zenati MA. The HeartLander: A novel epicardial crawling robot for myocardial injections. *Int Congr Ser*. 2005;1281:735-739. doi:10.1016/j.ics.2005.03.325

94. Moral del Agua D, Wood NA, Riviere CN. Improved synchronization of HeartLander locomotion with physiological cycles. In: *2011 IEEE 37th Annual Northeast Bioengineering Conference (NEBEC)*. IEEE; 2011:1-2. doi:10.1109/NEBC.2011.5778630

95. Moore JT, Chu MWA, Kiaii B, et al. A Navigation Platform for Guidance of Beating Heart Transapical Mitral Valve Repair. *IEEE Trans Biomed Eng*. 2013;60(4):1034-1040. doi:10.1109/TBME.2012.2222405

96. Zhe Luo, Junfeng Cai, Su Wang, Qiang Zhao, Peters TM, Lixu Gu. Magnetic

Navigation for Thoracic Aortic Stent-graft Deployment Using Ultrasound Image Guidance. *IEEE Trans Biomed Eng*. 2013;60(3):862-871. doi:10.1109/TBME.2012.2206388

97. Ota T, Degani A, Schwartzman D, et al. A Highly Articulated Robotic Surgical System for Minimally Invasive Surgery. *Ann Thorac Surg*. 2009;87(4):1253-1256. doi:10.1016/j.athoracsur.2008.10.026

98. Degani A, Choset H, Wolf A, Zenati MA. Highly articulated robotic probe for minimally invasive surgery. *Proc - IEEE Int Conf Robot Autom*. 2006;2006:4167-4172. doi:10.1109/ROBOT.2006.1642343

99. Liu Y, Lv C, Xu Q, Li S, Huang H, Ouyang P. Enhanced acid tolerance of Rhizopus oryzae during fumaric acid production. *Bioprocess Biosyst Eng*. 2015;38(2):323-328. doi:10.1007/s00449-014-1272-8

100. Martín del Valle EM, Galán MA, Carbonell RG. Drug Delivery Technologies: The Way Forward in the New Decade. *Ind Eng Chem Res*. 2009;48(5):2475-2486. doi:10.1021/ie800886m

101. Kleiner LW, Wright JC, Wang Y. Evolution of implantable and insertable drug delivery systems. *J Control Release*. 2014;181:1-10. doi:10.1016/j.jconrel.2014.02.006

102. Folkman J, Long DM. The use of silicone rubber as a carrier for prolonged drug therapy. *J Surg Res*. 1964;4(3):139-142. doi:10.1016/S0022-4804(64)80040-8

103. Amory JK, Page ST, Bremner WJ. Drug Insight: recent advances in male hormonal contraception. *Nat Clin Pract Endocrinol Metab*. 2006;2(1):32-41. doi:10.1038/ncpendmet0069

104. Forwith KD, Chandra RK, Yun PT, Miller SK, Jampel HD. ADVANCE: A multisite trial of bioabsorbable steroid-eluting sinus implants. *Laryngoscope*. 2011;121(11):2473-2480. doi:10.1002/lary.22228

105. Matheny KE, Carter KB, Tseng EY, Fong KJ. Safety, feasibility, and efficacy of placement of steroid-eluting bioabsorbable sinus implants in the office setting: a prospective case series. *Int Forum Allergy Rhinol*. 2014;4(10):808-815. doi:10.1002/alr.21416

106. Mohamed M, Borchard G, Jordan O. In situ forming implants for local chemotherapy and hyperthermia of bone tumors. *J Drug Deliv Sci Technol*.

2012;22(5):393-408. doi:10.1016/S1773-2247(12)50066-3

107. Schmidmaier G, Lucke M, Wildemann B, Haas NP, Raschke M. Prophylaxis and treatment of implant-related infections by antibiotic-coated implants: a review. *Injury*. 2006;37(2):S105-S112. doi:10.1016/j.injury.2006.04.016

108. Schaepelynck P, Renard E, Jeandidier N, et al. A Recent Survey Confirms the Efficacy and the Safety of Implanted Insulin Pumps During Long-Term Use in Poorly Controlled Type 1 Diabetes Patients. *Diabetes Technol Ther*. 2011;13(6):657-660. doi:10.1089/dia.2010.0209

109. Yang HS, La W-G, Bhang SH, Jeon J-Y, Lee JH, Kim B-S. Heparin-Conjugated Fibrin as an Injectable System for Sustained Delivery of Bone Morphogenetic Protein-2. *Tissue Eng Part A*. 2010;16(4):1225-1233. doi:10.1089/ten.tea.2009.0390

110. Fumimoto Y, Matsuyama A, Komoda H, et al. Creation of a Rich Subcutaneous Vascular Network with Implanted Adipose Tissue–Derived Stromal Cells and Adipose Tissue Enhances Subcutaneous Grafting of Islets in Diabetic Mice. *Tissue Eng Part C Methods*. 2009;15(3):437-444. doi:10.1089/ten.tec.2008.0555

111. Birch DG, Weleber RG, Duncan JL, Jaffe GJ, Tao W. Randomized Trial of Ciliary Neurotrophic Factor Delivered by Encapsulated Cell Intraocular Implants for Retinitis Pigmentosa. *Am J Ophthalmol*. 2013;156(2):283-292.e1. doi:10.1016/j.ajo.2013.03.021

112. Knight KH, Brand FM, Mchaourab AS, Veneziano G. Implantable intrathecal pumps for chronic pain: highlights and updates. *Croat Med J*. 2007;48(1):22-34. http://www.ncbi.nlm.nih.gov/pubmed/17309136.

113. Grabowska-Derlatka L, Derlatka P, Szeszkowski W, Cieszanowski A. Diffusion-Weighted Imaging of Small Peritoneal Implants in "Potentially" Early-Stage Ovarian Cancer. *Biomed Res Int*. 2016;2016:1-5. doi:10.1155/2016/9254742

114. De Oliveira LG, Figueiredo LA, Fernandes-Cunha GM, et al. Methotrexate Locally Released from Poly(e-Caprolactone) Implants: Inhibition of the Inflammatory Angiogenesis Response in a Murine Sponge Model and the Absence of Systemic Toxicity. *J Pharm Sci*. 2015;104(11):3731-3742. doi:10.1002/jps.24569

115. Lueshen E, Venugopal I, Soni T, Alaraj A, Linninger A. Implant-Assisted

Intrathecal Magnetic Drug Targeting to Aid in Therapeutic Nanoparticle Localization for Potential Treatment of Central Nervous System Disorders. *J Biomed Nanotechnol*. 2015;11(2):253-261. doi:10.1166/jbn.2015.1907

116. Rajgor N, Bhaskar V, Patel M. Implantable drug delivery systems: An overview. *Syst Rev Pharm*. 2011;2(2):91. doi:10.4103/0975-8453.86297

117. Westphal M, Hilt DC, Bortey E, et al. A phase 3 trial of local chemotherapy with biodegradable carmustine (BCNU) wafers (Gliadel wafers) in patients with primary malignant glioma. *Neuro Oncol*. 2003;5(2):79-88. doi:10.1093/neuonc/5.2.79

118. Loudon JA. Downsides of implants. *Br Dent J*. 2007;203(5):228-229. doi:10.1038/bdj.2007.801

119. McGregor D., Baan R., Partensky C, Rice J., Wilbourn J. Evaluation of the carcinogenic risks to humans associated with surgical implants and other foreign bodies — a report of an IARC Monographs Programme Meeting. *Eur J Cancer*. 2000;36(3):307-313. doi:10.1016/S0959-8049(99)00312-3

120. Takamura K, Hayashi K, Ishinishi N, Yamada T, Sugioka Y. Evaluation of carcinogenicity and chronic toxicity associated with orthopedic implants in mice. *J Biomed Mater Res*. 1994;28(5):583-589. doi:10.1002/jbm.820280508

121. Abhari F, Jaafar H, Md Yunus NA. A comprehensive study of micropumps technologies. *Int J Electrochem Sci*. 2012;7(10):9765-9780. doi:10.3390/mi2020179

122. Laser DJ, Santiago JG. A review of micropumps. *J Micromechanics Microengineering*. 2004;14(6):R35-R64. doi:10.1088/0960-1317/14/6/R01

123. Nguyen N-T, Huang X, Chuan TK. MEMS-Micropumps: A Review. *J Fluids Eng*. 2002;124(2):384. doi:10.1115/1.1459075

124. Brady ML, Raghavan R, Singh D, et al. In vivo performance of a microfabricated catheter for intraparenchymal delivery. *J Neurosci Methods*. 2014;229:76-83. doi:10.1016/j.jneumeth.2014.03.016

125. Elman NM, Masi BC, Cima MJ, Langer R. Electro-thermally induced structural failure actuator (ETISFA) for implantable controlled drug delivery devices based on Micro-Electro-Mechanical-Systems. *Lab Chip*. 2010;10(20):2796. doi:10.1039/c005135g

126. Cordes JS, Heyen JR, Volberg ML, et al. Validation and utility of the PhysioTel^{TM} Digital M11 telemetry implant for cardiovascular data evaluation in cynomolgus monkeys and Beagle dogs. *J Pharmacol Toxicol Methods*. 2016;79:72-79. doi:10.1016/j.vascn.2016.01.006

127. Jiang D, Cirmirakis D, Schormans M, Perkins TA, Donaldson N, Demosthenous A. An Integrated Passive Phase-Shift Keying Modulator for Biomedical Implants With Power Telemetry Over a Single Inductive Link. *IEEE Trans Biomed Circuits Syst*. 2017;11(1):64-77. doi:10.1109/TBCAS.2016.2580513

128. Farra R, Sheppard NF, McCabe L, et al. First-in-Human Testing of a Wirelessly Controlled Drug Delivery Microchip. *Sci Transl Med*. 2012;4(122):122ra21-122ra21. doi:10.1126/scitranslmed.3003276

129. Michael A, Buffen E, Rauck R, Anderson W, McGirt M, Mendenhall HV. An In Vivo Canine Study to Assess Granulomatous Responses in the MedStream Programmable Infusion System^{TM} and the SynchroMed II Infusion System®. *Pain Med*. 2012;13(2):175-184. doi:10.1111/j.1526-4637.2011.01308.x

130. Yue B, Brendel R, Lukitsch A, Prentice T, Doty B. Solubility and Stability of Baclofen 3 mg/mL Intrathecal Formulation and Its Compatibility With Implantable Programmable Intrathecal Infusion Systems. *Neuromodulation Technol Neural Interface*. 2017;20(4):397-404. doi:10.1111/ner.12535

131. Exner AA, Saidel GM. Drug-eluting polymer implants in cancer therapy. *Expert Opin Drug Deliv*. 2008;5(7):775-788. doi:10.1517/17425247.5.7.775

132. Barros AA, Browne S, Oliveira C, et al. Drug-eluting biodegradable ureteral stent: New approach for urothelial tumors of upper urinary tract cancer. *Int J Pharm*. 2016;513(1-2):227-237. doi:10.1016/j.ijpharm.2016.08.061

133. Goldspiel BR, Kohler DR. Goserelin Acetate Implant: A Depot Luteinizing Hormone-Releasing Hormone Analog for Advanced Prostate Cancer. *DICP*. 1991;25(7-8):796-804. doi:10.1177/106002809102500716

134. Schlegel P. A review of the pharmacokinetic and pharmacological properties of a once-yearly administered histrelin acetate implant in the treatment of prostate cancer. *BJU Int*. 2009;103:7-13. doi:10.1111/j.1464-410X.2009.08383.x

135. Burt HM, Hunter WL. Drug-eluting stents: A multidisciplinary success story. *Adv Drug Deliv Rev*. 2006;58(3):350-357. doi:10.1016/j.addr.2006.01.014

136. Hendrick RJ, Mitchell CR, Herrell SD, Webster RJ. Hand-held transendoscopic robotic manipulators: A transurethral laser prostate surgery case study. *Int J Rob Res*. 2015;34(13):1559-1572. doi:10.1177/0278364915585397

137. Can S, Staub C, Knoll A, Fiolka A, Schneider A, Feussner H. Design, development and evaluation of a highly versatile robot platform for minimally invasive single-port surgery. In: *2012 4th IEEE RAS & EMBS International Conference on Biomedical Robotics and Biomechatronics (BioRob)*. IEEE; 2012:817-822. doi:10.1109/BioRob.2012.6290766

138. Burgner J, Swaney PJ, Bruns TL, et al. An Autoclavable Steerable Cannula Manual Deployment Device: Design and Accuracy Analysis. *J Med Device*. 2012;6(4):041007. doi:10.1115/1.4007944

139. Roesthuis RJ, Janssen S, Misra S. On using an array of fiber Bragg grating sensors for closed-loop control of flexible minimally invasive surgical instruments. In: *2013 IEEE/RSJ International Conference on Intelligent Robots and Systems*. IEEE; 2013:2545-2551. doi:10.1109/IROS.2013.6696715

140. Ryu SC, Dupont PE. FBG-based shape sensing tubes for continuum robots. In: *2014 IEEE International Conference on Robotics and Automation (ICRA)*. IEEE; 2014:3531-3537. doi:10.1109/ICRA.2014.6907368

141. Kim B, Ha J, Park FC, Dupont PE. Optimizing curvature sensor placement for fast, accurate shape sensing of continuum robots. In: *2014 IEEE International Conference on Robotics and Automation (ICRA)*. IEEE; 2014:5374-5379. doi:10.1109/ICRA.2014.6907649

142. Chen Y, Oliveira JM, Hunter IW. Two-axis bend sensor design, kinematics and control for a continuum robotic endoscope. In: *2013 IEEE International Conference on Robotics and Automation*. IEEE; 2013:704-710. doi:10.1109/ICRA.2013.6630650

143. Rone WS, Ben-Tzvi P. Multi-segment continuum robot shape estimation using passive cable displacement. In: *2013 IEEE International Symposium on Robotic and Sensors Environments (ROSE)*. IEEE; 2013:37-42. doi:10.1109/ROSE.2013.6698415

144. Swaney PJ, Burgner J, Pheiffer TS, et al. Tracked 3D ultrasound targeting with an active cannula. In: Holmes III DR, Wong KH, eds. ; 2012:83160R.

doi:10.1117/12.912021

145. Ren H, Dupont PE. Tubular Enhanced Geodesic Active Contours for continuum robot detection using 3D ultrasound. In: *2012 IEEE International Conference on Robotics and Automation*. IEEE; 2012:2907-2912. doi:10.1109/ICRA.2012.6225033

146. Burgner J, Herrell SD, Webster RJ. Toward Fluoroscopic Shape Reconstruction for Control of Steerable Medical Devices. In: *ASME 2011 Dynamic Systems and Control Conference and Bath/ASME Symposium on Fluid Power and Motion Control, Volume 2*. ASME; 2011:791-794. doi:10.1115/DSCC2011-6029

147. Lobaton EJ, Fu J, Torres LG, Alterovitz R. Continuous shape estimation of continuum robots using X-ray images. In: *2013 IEEE International Conference on Robotics and Automation*. IEEE; 2013:725-732. doi:10.1109/ICRA.2013.6630653

148. Rucker DC, Webster RJ. Deflection-based force sensing for continuum robots: A probabilistic approach. In: *2011 IEEE/RSJ International Conference on Intelligent Robots and Systems*. IEEE; 2011:3764-3769. doi:10.1109/IROS.2011.6094526

149. Mahvash M, Dupont PE. Stiffness Control of Surgical Continuum Manipulators. *IEEE Trans Robot*. 2011;27(2):334-345. doi:10.1109/TRO.2011.2105410

150. Bajo A, Goldman RE, Wang L, Fowler D, Simaan N. Integration and preliminary evaluation of an Insertable Robotic Effectors Platform for Single Port Access Surgery. In: *2012 IEEE International Conference on Robotics and Automation*. IEEE; 2012:3381-3387. doi:10.1109/ICRA.2012.6224986

151. Kai Xu, Simaan N. Intrinsic Wrench Estimation and Its Performance Index for Multisegment Continuum Robots. *IEEE Trans Robot*. 2010;26(3):555-561. doi:10.1109/TRO.2010.2046924

152. Xu K, Simaan N. An Investigation of the Intrinsic Force Sensing Capabilities of Continuum Robots. *IEEE Trans Robot*. 2008;24(3):576-587. doi:10.1109/TRO.2008.924266

153. Goldman RE, Bajo A, Simaan N. Compliant Motion Control for Multisegment Continuum Robots With Actuation Force Sensing. *IEEE Trans Robot*. 2014;30(4):890-902. doi:10.1109/TRO.2014.2309835

154. Goldman RE, Bajo A, Simaan N. Compliant motion control for continuum robots with intrinsic actuation sensing. In: *2011 IEEE International Conference on Robotics and Automation*. IEEE; 2011:1126-1132. doi:10.1109/ICRA.2011.5980000

155. Bajo A, Simaan N. Finding lost wrenches: Using continuum robots for contact detection and estimation of contact location. In: *2010 IEEE International Conference on Robotics and Automation*. IEEE; 2010:3666-3673. doi:10.1109/ROBOT.2010.5509569

156. Williams DF. Regulatory biocompatibility requirements for biomaterials used in regenerative medicine. *J Mater Sci Mater Med*. 2015;26(2):89. doi:10.1007/s10856-015-5421-7

157. Flamant Q, Caravaca C, Meille S, et al. Selective etching of injection molded zirconia-toughened alumina: Towards osseointegrated and antibacterial ceramic implants. *Acta Biomater*. 2016;46:308-322. doi:10.1016/j.actbio.2016.09.017

158. Nuss KMR, Rechenberg B von. Biocompatibility Issues with Modern Implants in Bone - A Review for Clinical Orthopedics. *Open Orthop J*. 2008;2(1):66-78. doi:10.2174/1874325000802010066

159. Patel K, Brandstetter K. Solid Implants in Facial Plastic Surgery: Potential Complications and How to Prevent Them. *Facial Plast Surg*. 2016;32(05):520-531. doi:10.1055/s-0036-1586497

160. Zernotti ME, Suárez A, Slavutsky V, Nicenboim L, Di Gregorio MF, Soto JA. Comparación de complicaciones según la técnica utilizada en los implantes cocleares. *Acta Otorrinolaringológica Española*. 2012;63(5):327-331. doi:10.1016/j.otorri.2012.01.012

161. Dagdeviren C. The future of bionic dynamos. *Science (80-)*. 2016;354(6316):1109-1109. doi:10.1126/science.aal2190

162. Fu Y, Kao WJ. Drug release kinetics and transport mechanisms of non-degradable and degradable polymeric delivery systems. *Expert Opin Drug Deliv*. 2010;7(4):429-444. doi:10.1517/17425241003602259

3 Robotic Approach for Minimally Invasive Aortic Heart Valve Surgery

Part of the material reported in this chapter has been published in:

- V. Mamone, S. Condino, F. Cutolo, **I. Tamadon**, M. Murzi, A. Menciassi and V. Ferrari "Low Computational Cost Stitching Method in a Three-Eyed Endoscope" Journal of Healthcare Engineering, Augmented Reality in Healthcare, (Accepted)

- **Tamadon**, Y. Huan, A. G. de Groot, A. Menciassi and E. Sinibaldi "Smooth positioning and pose-preserving stiffening for an articulated/continuum manipulator for minimally invasive surgery" IEEE/ASME Transactions on Mechatronics, (Under review)

- **Tamadon,** G. Soldani, P. Dario, A. Menciassi "Novel Robotic Approach for Minimally Invasive Aortic Heart Valve Surgery" 40th International conference of the IEEE Engineering in Medicine and Biology Society, 17-21 Jul., 2018, Honolulu, USA. **DOI:** 10.1109/EMBC.2018.8513309

- **I. Tamadon**, A. Menciassi, G. Soldani, et al. "Flexible robotic platform for minimally invasive delivery of novel artificial heart valve under endoscopic guidance" Patent, Submitted in May, 2018.

- **I. Tamadon**, S. Tognarelli, C. Quaglia, et al. "Development of a robotic platform for minimally invasive aortic heart valve surgery" 29th Conference of the international Society for Medical Innovation and Technology, 9-10 Nov. 2017, Torino, Italy

- G. Turini, S. Condino, S. Sinceri, **I. Tamadon** et al. "Patient Specific Virtual and Physical Simulation Platform for Surgical Robot Movability Evaluation in Single-Access Robot-Assisted Minimally-Invasive Cardiothoracic Surgery" AVR 2017: 4th International conference on Augmented Reality, Virtual Reality, and Computer Graphics, June 12-15, 2017, Lecce, Italy. **DOI:** 10.1007/978-3-319-60928-7_18

In this chapter the design, fabrication and performance evaluation (in-vitro) of a robotic system for heart valve delivery is reported. The robotic manipulator is compatible with MIS approach and equipped with endoscopic visualization, for aortic heart valve replacement. The robotic manipulator is able to reach the

intervention site and place the valve in a safe, effective and fast way. The results show successful implantation of a commercial valve with the aid of endoscopic vision of the aortic root. This paves the way to future applications of these systems in the field of robotic-assisted heart surgery.

3.1 Ideas behind the project

Valvular heart disease is characterized by damage or defect of one of the four heart valves. One common valvular disease is Aortic Stenosis (AS – narrowing of the aortic valve opening): the AS prevalence in the elderly is around 12% and the prevalence of severe AS is 3.4% [1]. Valvular heart diseases have different causes (e.g. infections, diabetes, metabolic or hormonal conditions, genetic and aging) and lead to stenosis, failure (valve incontinence) or mixed disorders (Steno-insufficiency) [2]. These diseases, which lead progressively to the patient's death, are becoming more frequent, with an estimated number of 300,000 surgical replacement procedures annually worldwide; that number is expected to grow to 850,000 in 2050 with the increase in the average age of the population [1]. The aortic valve replacement is the second most common surgery after coronary artery bypass [3]. Current treatment for stenosis includes Balloon Aortic Valvuloplasty (BAV) [4], Surgical Aortic Valve Replacement (SAVR) [5,6], Transcatheter Aortic Valve Replacement (TAVR) [7] and Minimally Invasive Aortic Valve Surgery (MIAVS) [8]. However, all therapies utilize straight and rigid introducers for the delivery of the valve. So, with conventional introducers, the access point for valve deployment is constrained and it is more challenging to tune deployment position/orientation [9]. Moreover, it has risk to damage surrounding tissues since the deployment is not totally under control (e.g. lack of sensing, limited vision, collapsing of aorta vessels) [10].

With evolving robotics in MIS [11], there are further benefits in term of 3-dimensional visualization, tele-manipulation, motion scaling, even smaller incisions and precise adjustment [12,13]. However, there are certain challenges before the widespread usage of this technique in heart surgery [14]. The da Vinci robotic surgical system was successfully demonstrated in 2005 [15] and in 2010 with

complete excision of diseased native aortic valve cups and accurate Sorin Perceval valve placement [16]. But, there has been slow adoption of this technology in cardiac surgery for reasons related to procedural cost and lack of proper training [17]. Moreover, in robotic delivery with small incision, visualization is also a major bottleneck. So, intraoperative MRI technology [18,19] and 2D fluoroscopic image [20] have been used to track aortic heart valve more precisely, however these solutions required bulky equipment and were limited by the beating heart and the respiratory motions, causing misalignment [21].

On the other hand, the progress of modern surgery is closely related to the development of radiological technologies to provide the surgeon with more information about precise anatomy of the patient. The simulation, as part of the preoperative planning, is now common in various surgical areas [22,23] and also in vascular/cardiac [24] fields. In the context of cardiac valve disease, numerous literature studies have recently been addressed to the segmentation of the aortic root and annulus from CT angiography or 3D transesophageal echocardiography [25–33]. The objective of these studies is to ensure the accuracy of results and the improvement and/or automation of methods of segmentation and 3D measurement [32,34,35]. An accurate 3D evaluation of the anatomical structures and dimensions such as annulus aortic arch, length of the ascending aorta, distance between the planned surgical site and the aortic valve, are fundamental for the most surgical approaches. For example, in the system of interventions of TAVR, undersizing of the prosthesis can lead to migration or severe deficiency, while oversizing can result in rupture of the annulus [31,33].

The use of simulators depicting human anatomy also provides a viable alternative to experimentation of animal, overcoming the ethical problems. Although extremely interesting, the solutions on the market are often limited to the simulation of standard anatomical models and are thus lacking of anatomical realism. It can only be achieved through patient-specific simulators. For this reason, recent literature studies have proposed manufacturing techniques based on the development of real radiological images to extract the 3D model of the

anatomical structures of interests, then for playing in a synthetic material through rapid prototyping techniques/molding [24,36].

3.2 State of the art in the field of heart valve surgery

This section is organized into five parts, which illustrate the sectors of the state of the art for each treatment and finally the development of the video/robotic delivery solutions for heart valve surgery.

3.2.1 Balloon Aortic Valvuloplasty (BAV)

Balloon aortic valvuloplasty (BAV) was introduced in 1986 as the first less invasive, percutaneous treatment option for treatment of AS. The procedure was performed in local anesthesia via percutaneous transfemoral approach. A balloon catheter (2-5 mm x 4.0 cm) is introduced and positioned across the stenotic aortic valve. Aortic valvuloplasty was performed with balloon inflation (25–30 ml, 2-3 atm) with the aim to increase area and reduce transaortic pressure gradient. The goal of the procedure was a reduction of the pressure gradient by at least 50% and if necessary, the balloon inflation could be repeated. Unfortunately, early restenosis of the enlarged valve and poor long term survival limits the use of this procedure with symptom reappearance. Today BAV is considered as a relaxing technique in patients with high perioperative risk; or a bridge to open heart surgery in unstable patients; or in patients who require urgent surgery. In the last few years new therapeutic options are being developed such as TAVI, where BAV plays an important role in preparing the stenotic aortic valve for the prosthesis implantation. Before and during valvuloplasty procedure a coronary angiography was performed [4].

3.2.2 Surgical Aortic Valve Replacement (SAVR)

Surgical aortic valve replacement is most frequently performed through an incision in the sternum. Once the pericardium has been opened, the patient is attached to a heart-lung machine that takes over the task of breathing and pumping their blood around while the surgeon replaces the heart valve. Once the patient is on bypass and heart is stopped, a cut is made in the aorta and a cross

clamp applied. The surgeon then removes the patient's calcified aortic valve and a mechanical or tissue valve is replaced in its place. Once the valve is in place and the aorta has been closed, the patient is taken off the heart-lung machine [5]. Echocardiogram can be used to verify that the new valve is functioning properly. Drainage tubes are usually removed within 36 hours while the pacing wires are generally left in place until the patient is discharged from the hospital (about four days). After aortic valve replacement, the patient will frequently stay in an intensive care unit for 12–36 hours unless complications arise [37]. Common complications include heart block, which typically requires the permanent insertion of a cardiac pacemaker. Recovery from aortic valve replacement will take about three months, if the patient is in good health. Patients are advised not to lift heavy items for several weeks to avoid damage to the sternum. Often patients will be referred to participate in cardiopulmonary rehabilitation, which deals with optimizing recovery and physical function in patients with recent cardiac surgeries. The risk of death or serious complications from aortic valve replacement is typically quoted as being between 1-3%, depending on the health and age of the patient. Older patients, as well as those who are frail and/or have multiple health problems, may face significantly higher surgical risk [6].

3.2.3 Transcatheter Aortic Valve Replacement (TAVR)

The first transcatheter aortic stent valve in animals was described in 1992, by presenting the results of the implantation in pigs [38] and then was implanted in humans [39], in 2002, using the transeptal approach and femoral vein access due to the bulky measures of the first device. In 2005, novel techniques and tools led to change the way of approaching to the transfemoral artery position, making the technique easier for the doctor and the patient [40]. TAVR, in general, is indicated for high risk patients, using the appropriate risk scores, who suffered from severe symptomatic AS. Currently, FDA expanded the approval for the TAVR technique, for special device, in case of people with symptomatic AS in intermediate and high risk scores [41]. The choice of proceeding between SAVR and TAVR is based on multiple factors, including surgical risk, patient frailty, diseases and patient preferences. Also, surgeons' experience in performing transcatheter procedures in

different centers, as well as the financial aspect, referring to the ability to cover the expenses. In the last decade, TAVR has been performed in about 400,000 patients worldwide and indications keep growing at a rate of 40% annually [40]. Real-world data published confirm the rapid adoption of TAVR, especially in the developed countries, shifting the treatment of AS from conventional surgery to a percutaneous transcatheter approach. The positive results of the randomized clinical trials (CHOICE, PARTNER 1A&1B, STACCATO, NOTION, SURTAVI study) recommend, TAVR can be performed in patients not suitable for conventional surgical treatment and as an alternative to surgery in high risk patients after approval by a multidisciplinary heart team, based on the individual risk profile and anatomy [7].

3.2.4 Minimally Invasive Aortic Valve Surgery (MIAVS)

Since Cosgrove and Sabik first described MIAVS in 1996 [42], there has been a significant expansion in popularity, experience and techniques associated with MIAVS [43]. Various techniques for obtaining appropriate exposure have been developed and put into practice including variations of a hemi- or mini-sternotomy and the right anterior thoracotomy [44]. With the greater use of MIAVS, there is a growing understanding of the outcomes following MIAVS compared with SAVR, including survival rate, perioperative times and complications [45]. Currently, the most common approaches used in the mini-sternotomy are J-shaped, inverted T or other similar incisions [46]. This approach provides several advantages over other incisions [47]. It provides adequate exposure while minimizing postoperative pain and minimally affecting thoracic cage stability. If necessary, it can be extended to provide additional exposure (femoral/aortic cannulation is also feasible [48]).
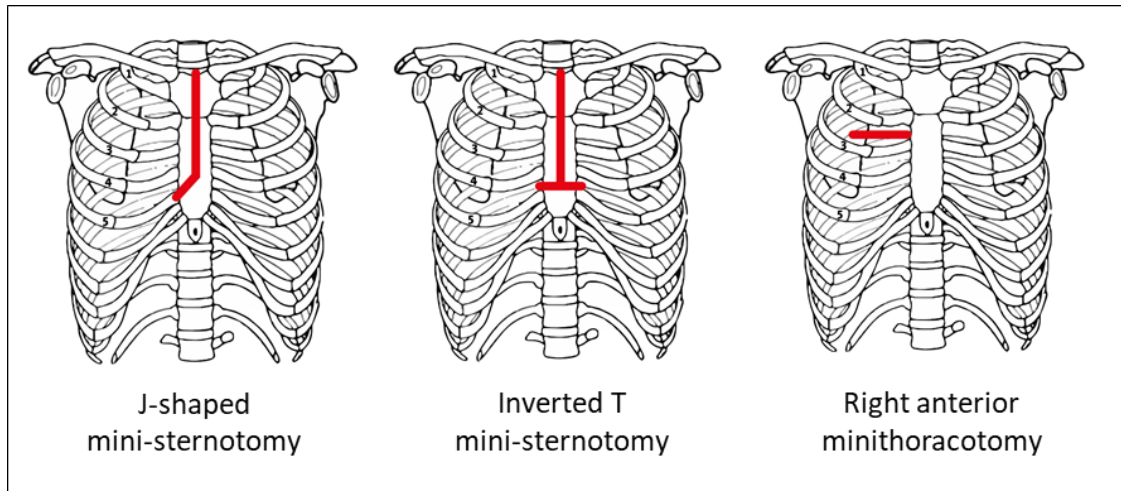
Figure 3-1 The most common approaches in MIAVS [45].

Most studies have demonstrated no difference in morbidity or mortality between MIAVS and SAVR [49]. In contrast with early studies associated MIAVS, operative times have improved and are comparable between groups in more recent studies. This suggests that there is a learning curve, but also that minimally invasive approaches do not require longer operative times in experienced hands. Most importantly, even in studies showing longer operative times for MIAVS, there remained no evidence of a difference in major outcomes, further supporting MIAVS as a safe and feasible alternative to SAVR [50]. In fact, MIAVS is more often associated with improvements in postoperative outcomes. Decreased length of stay in intensive care, days of ventilator support and hospital length of stay have been demonstrated. This coincides with an earlier return to work and return to normal activity in MIAVS patients as well. Of interest, in-hospital postoperative pain levels have been noted to be similar in MIAVS and SAVR patients, reflecting a relatively low overall pain level for traditional median sternotomy. However, using pain medication has been shown to be lower for MIAVS patients. Studies have demonstrated blood transfusion rates that are similar or lower for MIAVS patients.

Furthermore, sutureless aortic bioprostheses possess the potential for easy and fast implantation in MIAVS. Clinical reports of these valves showed a short cross-clamp time of 18–39 minutes reducing cross-clamp time up to 40% compared to the implantation of stented bioprosthesis [51,52]. The hemodynamic performance of sutureless valves is excellent, and after 4-year follow-up valvular gradients

remained stable [53]. The disadvantage of sutureless valves is the higher incidence of paravalvular leakage. With the Perceval S bioprosthesis (Sorin, Saluggia, Italy), perioperative leakage, requiring new aortic cross-clamping and valve explantation, occurred in 1.2–1.8% of the patients [52,53]. Postoperatively, there was no severe paravalvular leakage noted, moderate paravalvular leakage occurred in only one of the 396 patients (0.3%), and mild paravalvular leakage occurred in 0–15.6% [54]. Using the 3F Enable (Medtronic, Minneapolis, Minnesota, USA), Aymard reported one patient in a series of 28 patients that required reoperation because of significant paravalvular leakage and two patients with paravalvular leakage who did not require additional treatment [55]. Also with the 3F Enable, Martens showed three patients in a series of 140 patients with major paravalvular leakage that needed reoperation and another three patients with minor paravalvular leakage who did not require additional treatment [56]. Because of the shorter cross-clamp and therefore ischemic time, the sutureless valve may offer an advantage in high-risk patients, especially if this is combined with a MIAVS approach. The learning curve is fast, and after about 10 cases, a reduction in deployment time is expected [57].

3.2.5 Video/Robotic-Assisted systems for cardiovascular surgery

Currently, there are trials including over 1000 patients who have undergone video-assisted mitral valve surgery [58] and over 100 who have undergone robot-assisted aortic valve surgery [59]. However, the role of video/robotic- assisted aortic surgery is not on the same level as in mitral valve surgery, and only a few cases have been reported. The first example of use of robotics in the field of cardiovascular surgery and cardiothoracic dates back to 1997, when Falk et al. took the AESOPTM 3000 system in an endoscopic surgical procedure of mitral valve [60]. In 1999, the robotic system ZEUS was employed for the first time by Reichenspurner et al. in a coronary artery by-pass [61]. Also, Benetti et al. was the first to report AVR with video-assistance through a right anterior thoracotomy in seven patients [62]. The video- assistance resulted in a less traumatic and less painful approach because the removal of ribs and cartilage fragments was not necessary. The da Vinci system

was used for the first time in a complete repair procedure mitral valve in 2002 [63]. Currently the da Vinci robotic system is used in endoscopic surgery for repair/replacement of the mitral valve [63] and revascularization operations (i.e., surgical for coronary by-pass) [61] with documented advantages over traditional surgery. In 2005, Folliquet et al. reported a successful AVR using the Da Vinci robot system in five patients using one or two ports and a 5-cm incision in the right 3rd or 4th intercostal space with a mean procedure time of 231 minutes, CPB time of 122 minutes, and mean cross-clamp time of 98 minutes [64]. In 2006, Francesco et al. published a series of 12 patients who underwent video- assisted AVR. However, one patient had to be converted to sternotomy and one patient underwent re-exploration for bleeding. Francesco addressed the learning curve associated with video-assisted AVR. Their learning curve was short because they already had experience with video- assisted mitral valve surgery. In their opinion, at least 20–30 cases are needed to acquire confidence in the procedure [62]. In 2009, Poffo et al. published the results of video-assisted AVR in 14 patients, with no mortality or major postoperative complications, a mean CPB time of 124 minutes, and mean cross-clamp time of 102 minutes [65]. Also, CPB and aortic clamping time decreased after 40 cases [65]. However, the robotic system da Vinci cannot be employed or readily adapted to release operations into a valve site by means of thoracic aortic single port access [66] [67], which is the clinical objective of our research project.

The only specific robotic system dedicated to aortic heart valve surgery has been introduced by Horvath et al. [18] but it lacks the flexibility for accessing with safe site. Also actuated delivery sheath [68] demonstrates preliminary validation for better positioning of the transapical aortic valve implantation.

In conclusion, AVR with video- and robotic-assistance is possible in low-risk patients. However, video-assistance does not add much to the procedure of AVR and the disadvantages of long operating time, increased costs, and a steep learning curve outweigh the advantages of the smaller incisions. Therefore, video and robot-assisted AV surgery are still in their infancy, and for now, it only plays a very small role in the field. On the other hand, there has been a slow adoption of this technology in cardiac surgery for reasons related to procedural cost and lack of proper training [17].

3.3 Reference application and main scope

In this study, to perform a right anterior minitorocatomy MIAVS via transaortic approach (**Figure 3-1**), we present a hyperredundant manipulator with the possibility of view under endoscopic vision. It includes also an operating channel which acts to deliver the valve and guarantees its proper positioning. The robotic manipulator (called VALVETECH) will have a patient-specific simulation platform for preoperative planning and valve design. This simulation environment will be based on the patient volumetric radiological information (e.g. CT, MRI) of anatomical structures involved. Preoperative imaging will allow the definition of the surgical strategy and the optimal choice of the most suitable surgical access site. The robotic manipulator (with distal articulation for micro-placements that ensures the positioning and release of the valve in optimal conditions) can then be inserted according to the specifications of the pre-operative planning.

A 3D printing anatomical model of the human chest from CT images including the heart and other anatomical structures involved in the surgical delivery is provided. This model will be used for the following purposes: (I) Validation of the robot (including tests of maneuverability, ease of positioning of the valve and assessment of the reduction of the intervention times); (II) Simulation of MIAVS and (III) Training of heart surgeons.

In conclusion, the proposed technological advancement from the VALVETECH manipulator is to minimize the possible risks associated with valve replacement procedure using mini-invasive approach. Therefore, the cardiac surgeons will provide, a continuous feedback on the device under study and its application systems that will guide developers toward the final and optimized version of the system. The success of the manipulator, when finally developed at a clinical stage, could revolutionize the field of MIAVS with drastic reduction of the surgery time (less than 1 h) and the costs (about 1/10) compared to the devices currently on the market. Finally, the overall project would pave the way for the use in clinical practice of a highly reliable robotic system in the MIAVS interventions.

3.4 Design overview

For this study, among commercially available sutureless heart valves, Sorin Perceval is considered as ideal prosthesis for its promising long-term outcome [57]. The dedicated delivery tool is straight and rigid while manually actuated, through direct access to the aortic valve. Although being functional to effectively deliver the valve, it does not permit altering the access point and may damage surrounding tissue. In order to overcome the aforementioned drawbacks, we envisioned valve deployment through a bendable manipulator equipped with three endoscopic cameras, 120° angular shifted and embedded laterally on distal tip. The robot is following a two-phase procedure sketched in Figure 3-2. So, after charging the Sorin valve to the introducer, the manipulator is preliminarily fastened to a common holder such as a Martin's arm (MARINAMEDICAL, FL, US). The system is manually gross-positioned by a surgical operator so as to enter the keyhole (a safe point derived from patient specific simulation and CT). During phase-I (shown in Figure 3-2a) the manipulator, kept in a relatively compliant state, is teleoperated by the surgeon (based on endoscopic images recorded at the manipulator tip) to be fine-positioned 3-4 cm behind the target site. Additionally, three flaps in the distal end are used to keep the aorta open and stabilize the manipulator in the intervention site. When satisfied with positioning, the stiffening process starts and can improve the rigidity up to 2-3 times (depending on the position, see section 3.10). The surgeon can compensate the small deviation made by shortening cable and reach the previous position by the help of endoscopic vision. During phase-II (shown in Figure 3-2b), the introducer is moved to leaflet site satisfying the accurate translational movement and rotation based on anatomical hinge points. Finally, the expansion is commanded by the surgeons in two stages, first the skirt part for anchoring the prosthesis to the aortic wall and second the frame for fully attachment. The introducer can come out of the implanted valve and prepare the robot for retraction (i.e. closing of flaps and manipulator moving out of the body).
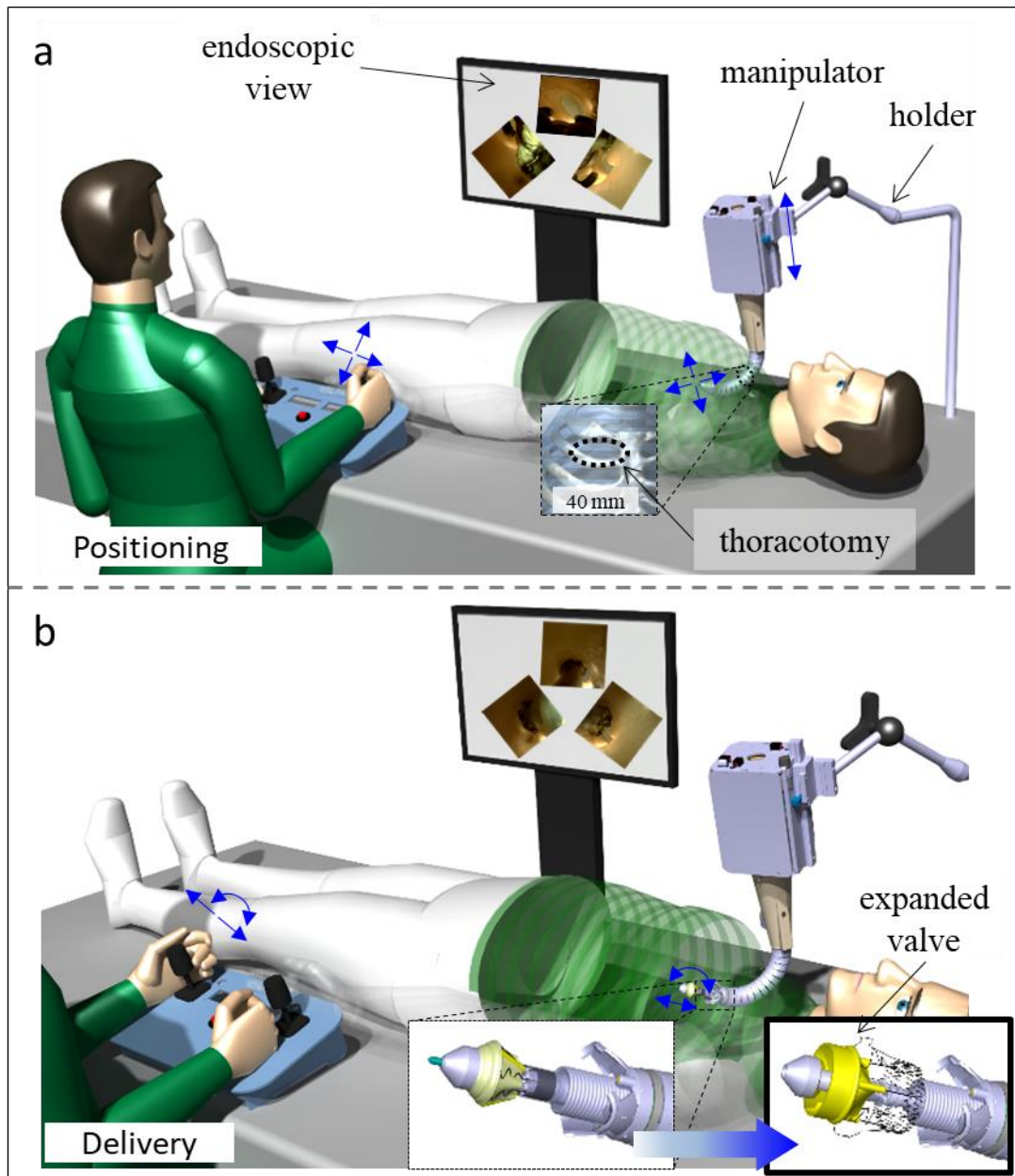
Figure 3-2 Schematic of the two-phase procedure, here illustrated through aortic valve replacement. a) The manipulator is tele-operated by the surgeon to the desired pose (potential contacts with tissues are mitigated by the relatively compliant status of the manipulator); b) The introducer is moved and the valve is rotated for fine adjustment with respect to nadir points; afterward, the valve can be expanded

The above procedure was envisioned in collaboration with cardiac surgeons. Besides highlighting the benefits of the hands-on gross-positioning in terms of reduced procedural times, they provided a reference length (130-150 mm) for the manipulator, and a reference diameter (20-25 mm) for its working channel to allow for Sorin valves delivery.

A number of flexible manipulators were proposed to suitably reach the target while circumventing the limitations posed, e.g., by deployment along a straight line. Commonly, a distinction is made between articulated systems (manipulators composed of discrete rigid links connected by joints [69,70]) and continuum systems (manipulators typically featuring an elastic structure, whose deformed shape can be swept with continuity by a tangent frame [71]). A few "hybrid" articulated/continuum designs, however, have been recently proposed. The manipulator in [72] introduced rigid wire-guides acting as links (connected by rolling friction joints) around a cylindrical elastic backbone, in order to avoid transmitting axial forces to such a backbone. An elastic tube surrounded by rigid vertebras also acting as wire-guides was similarly introduced in [73]: the vertebras formed rotational (friction-based sliding) joints, and the authors proposed to insert a rigid tube within the aforementioned elastic one in order to also control the length of the bendable section. A different embodiment was introduced in [74], with the continuum backbone provided by a couple of elastic tubes passing through the links (connected by ball-socket joints), perpendicular to the passages of the actuation wires, thus only allowing for planar bending. Finally, a further embodiment was proposed in [75], where the continuum backbone was provided by elastic push/pull tubes/rods external to an articulated chain of links (connected by revolute joints). Relative sliding respect to the continuum backbone was used to continuously change the stiffness of the compound system. Therefore, in some cases the articulated/continuum design was purposely introduced for locally tuning the manipulator stiffness, since continuum manipulators can allow for enhanced safety and adaptability when interacting with anatomical structures, yet at the cost of reduced effectiveness and stability.

We firstly introduced an articulated structure made of 26 hollow links ($\phi_{out} = 28$ mm, $\phi_{in} = 23$ mm), interleaved with 1 DoF pin joints alternately rotated by 90 deg, for the manipulator to achieve 2 DoFs bending (Figure 3-3a). The joint axes in the undeformed configuration implicitly introduced a 2D reference frame useful for identifying the bending direction. The joints were profiled (Figure 3-3a) for the manipulator to achieve 90 deg bending when

consistently compacting a set of parallel joints (axial bending), and 120 deg when consistently compacting all the joints (cross-axial bending). Each joints hosts four pair holes (ϕ = 1.1 mm) for the passing-through actuation cables, three slots for camera wires (the slots being shaped to easily insert the wires and hold them in place during operation), and a hole for passing a flexible shaft (functional to flaps actuation). We devised the actuation cables to have both ends connected at the manipulator base: we adopted ϕ = 0.42 mm braided fishing lines in order to allow for the small bending radius (2.8 mm) needed to route the cables back at the distal link (Figure 3-3a). Actuation and sensing devices were integrated at the manipulator base (Figure 3-3b). One end of each actuation cable was pulled by a brushless DC servomotor (Faulhaber 2250BX4, Germany), able to provide up to 25mN/m torque and high-resolution positioning (3000 increment/turn). The other end was connected to a force sensor (LSB200 by Futek, CA, US) able to read up to 44.5 N and fixed to the base frame. More in detail, the motor torque was transmitted to a ϕ = 13 mm pulley through a 1:10 ratio worm gear (RS Components S.r.l., Italy), which also supported the possibility to effectively transfer external actions toward the force sensors by virtue of its reduced back-drivability. The four actuation subsystems (each consisting of servomotor, worm-gear and pulley) were assembled so as to obtain a compact (10x10x15 cm) actuation unit; the sensors were correspondingly integrated in a sensing unit close to the manipulator proximal section (Figure 3-3b). Additionally, on the connection of the actuation unit to Martin arm a linear rail and ball screw (Faulhaber, BS22-1.5) actuator is positioned to provide linear insertion to the body for the manipulator.
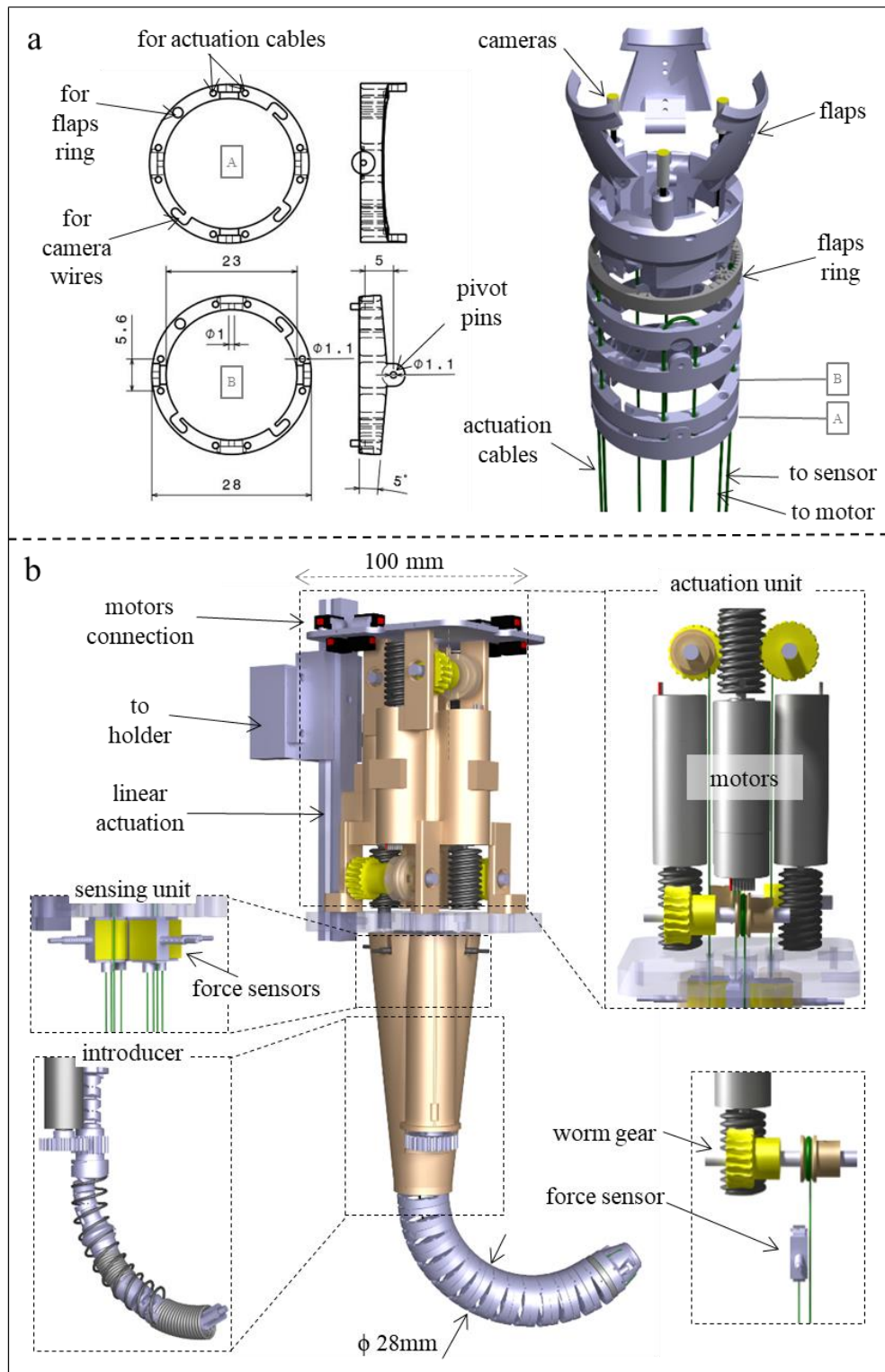
Figure 3-3 Manipulator design (schematics). a) Articulated/continuum structure based on links (with pin joints). Passages for actuation cables, flaps and camera wires are also annotated (by overstepping the distal link for ease of representation). b) Overview showing both the actuation unit and the sensing unit; key related components are annotated like coil spring (whereas the cap is omitted for ease of representation).

As for fabrication, pulleys and secondary casing structures (e.g. for the motors and for the sensing unit) were 3D printed (ProJet MJP3600, 3D systems, USA and VisiJet M3 crystal), whereas stainless steel (17-4ph) links were obtained by metal sintering (DMLS/SLM by ZARE srl, Italy) leading to a robust yet lightweight (< 2 kg) prototype (the manipulator is shown in **Figure 3-6**a).

3.5 Controller design overview

As regards control, we termed leading cables (LCs) those driving bending and following cables (FCs) the others which keep tension. As illustrated in Figure 3-5a, for general bending there are two LCs and two FCs.

During positioning the surgeon tele-operates the manipulator by means of a joystick 1 (Figure 3-2a). Its directional input is used by the controller (ATMega 1284P, ATMEL) to identify the LC(s) and the FCs, based on a registration between the 2D reference frame of the joystick and that one identifying the manipulator bending direction. The controller shortens the LC(s) by directly commanding PWM signal based on joystick angles of the bending direction. Meanwhile, the controller keeps the FCs tension to a set value by PID closed-loop control (Figure 3-5b). The set value is small enough (0.6 N) for the FCs to oppose a small resistance to the LC(s), while preventing them to become slack. To gain stiffening in the manipulator the set value for cables can be increased by surgeon's command. Thus causing a light displacement. Then, it can be compensated by joysticks so as to recover the manipulator pose up to a chosen tolerance.

Joystick 2 is also dedicated for valve translational motion and its rotation. While the button on the top will trigger the expansion (**Figure 3-4**). The same strategy of PWM pulses are used to activate the linear servomotor as before.
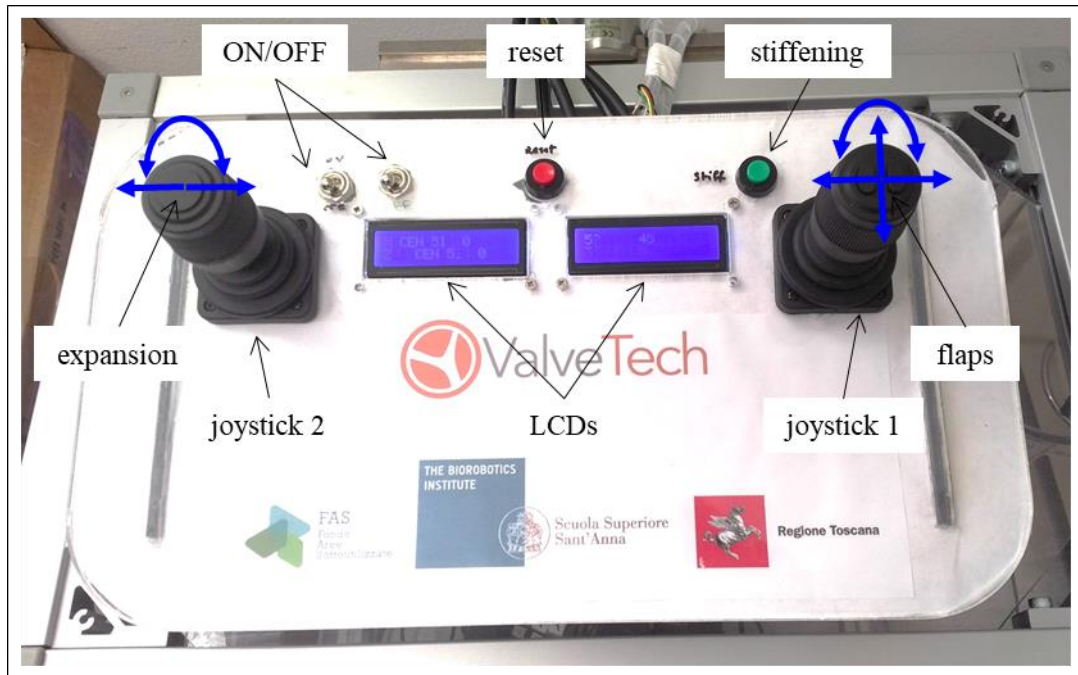
Figure 3-4 Control unit and functions of joysticks. Joystick 1 is dedicated for bending the manipulator (right-left-up-down) and linear insertion of the manipulator (rotation) plus flaps opening/closing (buttons on top). Joystick 2 is dedicated to introducer linear insertion (right-left), valve rotation (rotation) and valve expansion (button on top). The joystick commands are also shown in LCDs.

3.5.1 Safe interaction with tissue

In positioning phase, the manipulator is capturing the cable forces continuously and can react with sudden high forces in the tip. This feature is planned in the microcontroller to release the LC(s) when sensing a sudden high force in corresponding sensor. Meanwhile FC(s) cable lengths are controlled based on the preset forces and can release automatically when they touch an obstacle.
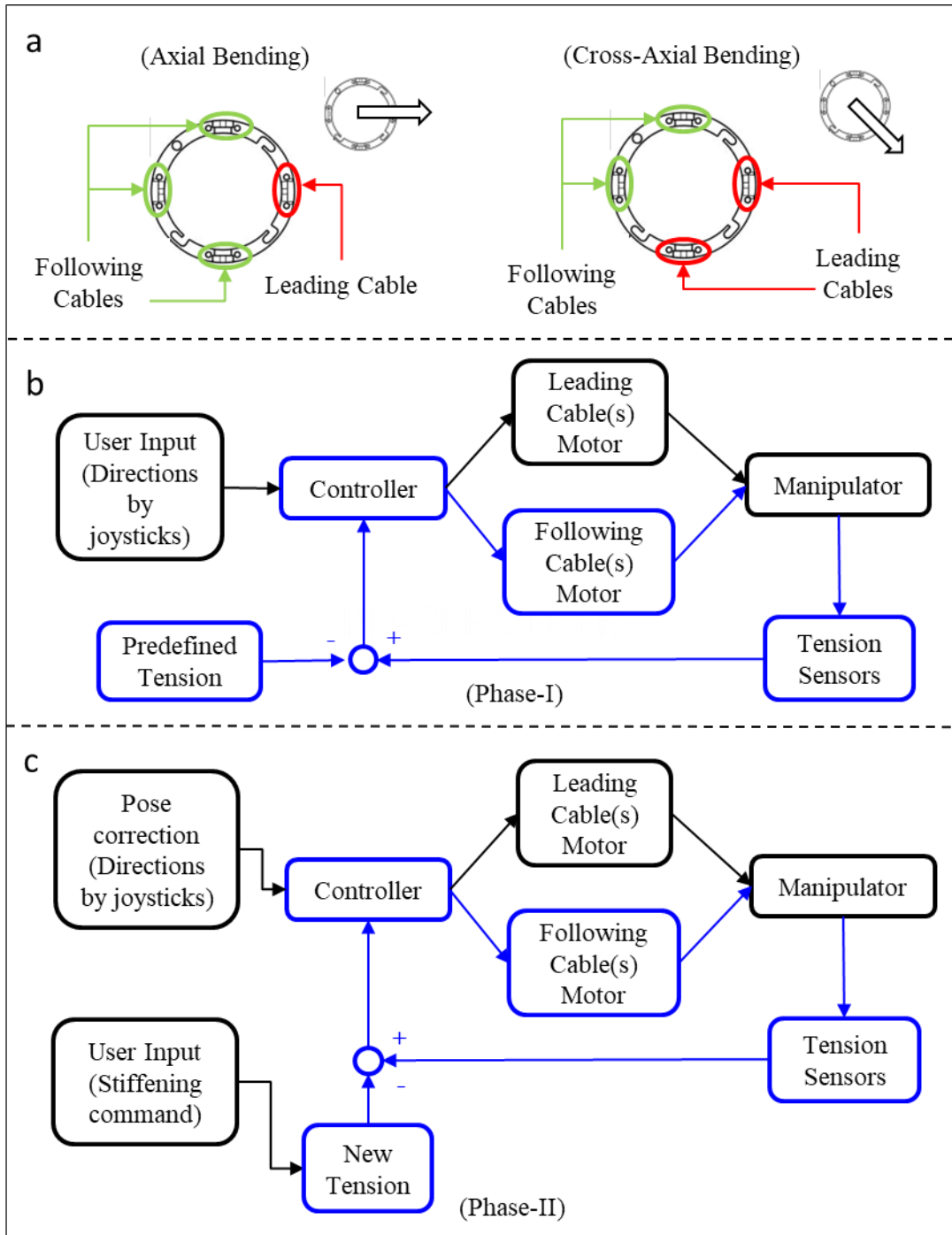
Figure 3-5 Manipulator control (schematics). a) Definition of leading/following cables for both axial and cross-axial bending. b) Control scheme for the positioning phase (closed-loop control is introduced for the following cables, based on direct measurement of the related tension). c) Control scheme for the stiffening phase (pose correction is performed for the cables, to compensate the deviation of the tip from that one defined at the end of the positioning phase).

3.5.2 Experimental assessment phase-I

Once preliminary tests on the joystick-manipulator mapping were performed, we quantitatively assessed the positioning performance by tracking the manipulator tip through the Aurora (NDI Medical, Canada) electromagnetic tracking system (ETS) (**Figure 3-6**). For ease of processing, we connected to Matlab (The Mathworks, MA, US) both the ETS and the Arduino controller (5V TTL serial communication). We thus integrated in a single GUI motor rotations, cable tensions and tip position readings in the ETS Cartesian frame, serving as a unified reference for all the measurements.
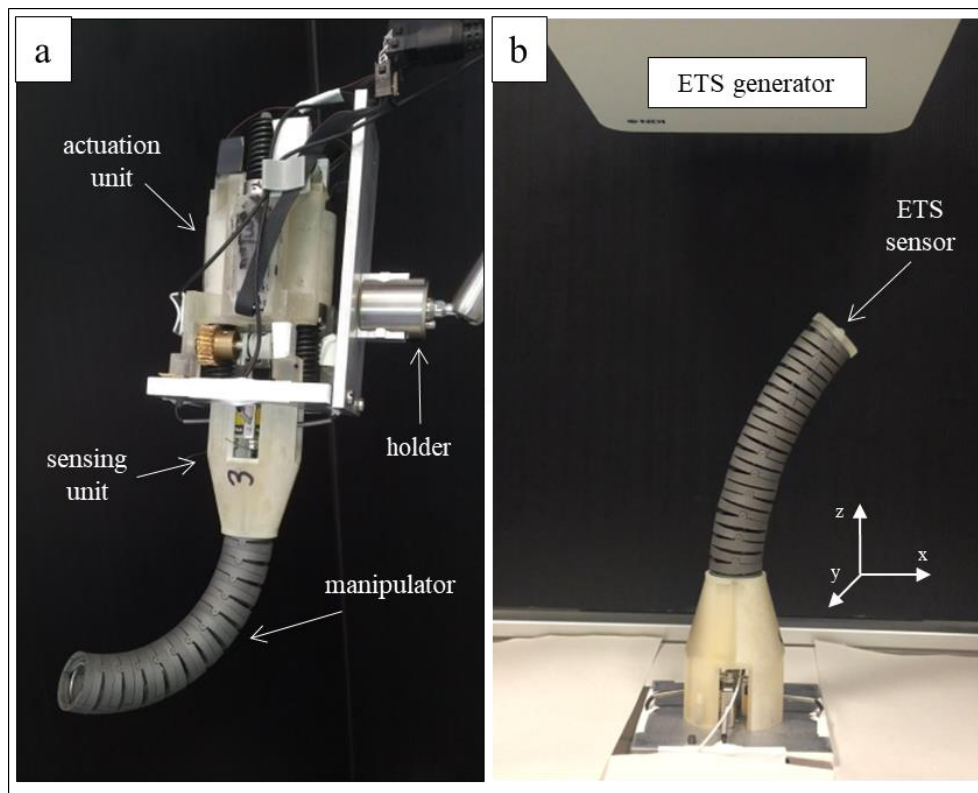
Figure 3-6 Manipulator in a simple form without introducer, flaps, cameras and cartridge. a) Full view also showing the actuation unit. b) Experimental setup for positioning tests also showing the electromagnetic tracking system (ETS).

Starting from an upright pose (manipulator axis coincident with the z-axis), we commanded bending along the four axial directions (i.e., along the x- and y-axis), and the four cross-axial directions (i.e., bisecting the x- and y-axis). For axial bending, we defined as leading tension (LT) that one of the LC; for cross-axial bending we considered the square root of the sum of the squared LCs tensions. For each direction we pulled the LCs up to the aforementioned LT threshold value, so

as to reach the workspace boundary (through the complete compacting of all involved joints). We recorded tip trajectory (four repetitions to assess potential data dispersion) and we quantified its distance (mean ± std over the trajectory points) from that one obtained through a classical constant-curvature model (recalled in Appendix I). Furthermore, we assessed reversibility by commanding a round-path along two selected directions, one axial and one cross-axial, and we computed the distance (mean ± std) between corresponding points (based on encoder steps) along the forward and the backward branch. Finally, we also repeated the positioning experiments after removing the coil spring (thus reducing to an articulated manipulator), with the deliberate aim of assessing the spring effect (**Figure 3-7**). As shown in **Figure 3-7**c,d, the curvature of the resulting trajectory was almost constant: for axial bending (while the spring is included, **Figure 3-7**a) the resulting deviations (over nearly 200 trajectory points) were 3.1 ± 3.1, 1.9 ± 1.0, 3.3 ± 2.8 and 2.1 ± 1.4, whereas for cross-axial bending (nearly 400 points) they were 4.2 ± 2.1, 3.1 ± 2.5, 4.1 ± 2.2 and 4.3 ± 3.1 mm. All of them are suitably smaller than the manipulator characteristic size (even when considering the diameter) and definitely smaller than the workspace span (around 200 mm as shown in **Figure 3-7**). For the round-path experiments we've selected the bending directions labeled by (A) and (CA) in **Figure 3-7**: as shown by **Figure 3-7**a-b, for both axial and cross-axial bending we recorded the same behavior along the considered directions, so that no bias was introduced by making the above choice. The resulting deviation between corresponding points along the forward and the backward branch (**Figure 3-7**c-d) were 2.7 ± 1.9 and 3.2 ± 1.5 mm for axial and cross-axial bending, respectively. We thus observed good reversibility for both bending modalities, and this was due to the presence of the spring. Indeed, by comparing the snapshots in **Figure 3-7**c-d and **Figure 3-7**g-h, it is clear that by removing the spring a less regular behavior was observed (namely less reversible tip trajectories, double-curvature bending configurations leading to a hysteretic behavior over the round-path).
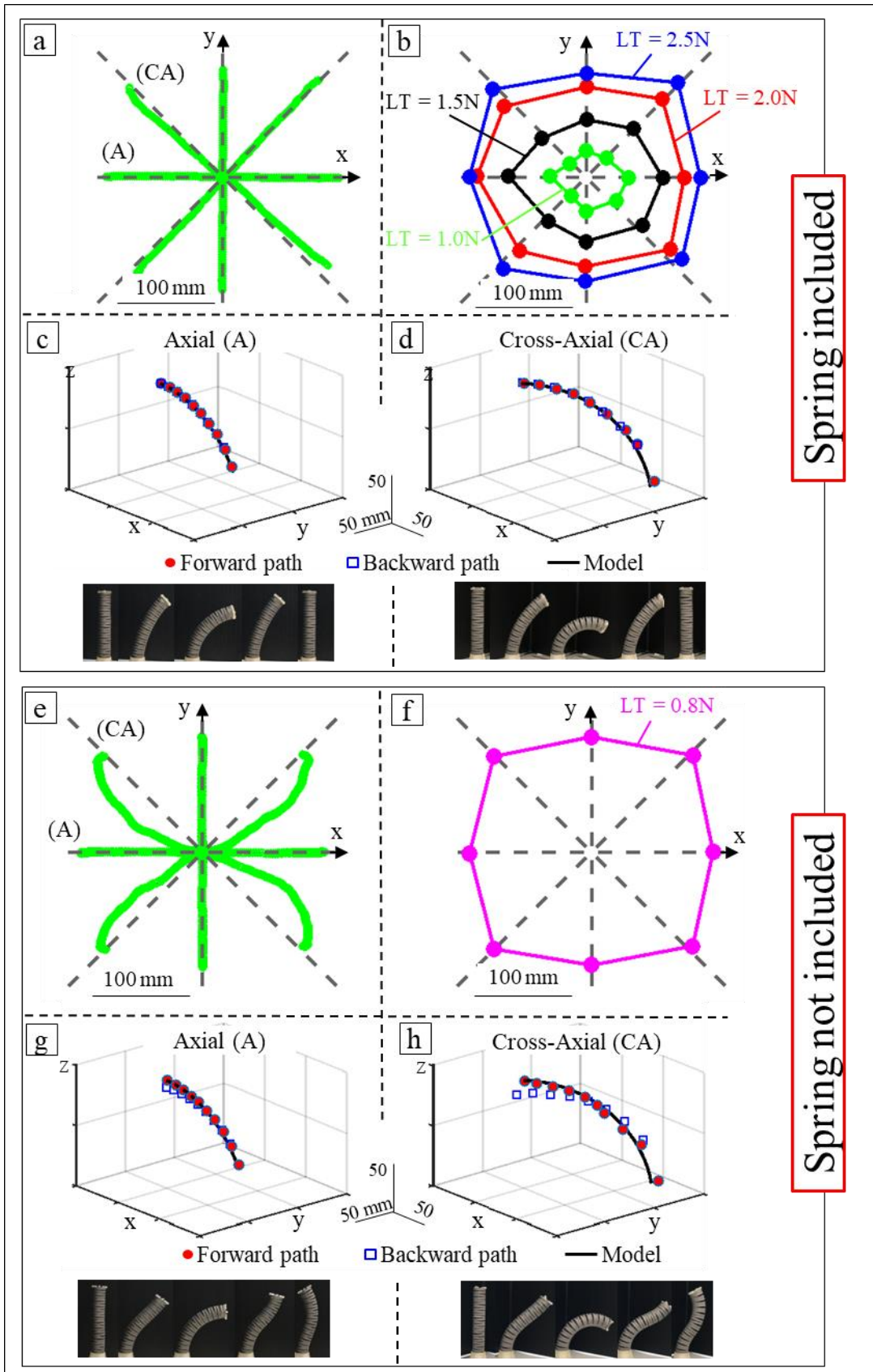
Figure 3-7 Positioning test results. a) Top-view of the tip trajectories (solid) with superimposed the nominal bending directions (dashed). b) Tip positions (top-view) achieved for selected values of the leading tension (LT). c.) Reversible axial bending: forward/backward experimental points and fitting constant-curvature model; selected snapshots (bottom). d.) Reversible cross-axial bending: experimental points along a round-path and fitting constant-curvature model; selected snapshots (bottom). Results from auxiliary positioning tests carried out after removing the coil spring (exactly the same experiment as when including the spring) is reported in e. f. g. h. Selected snapshots showing that also reversibility was lost: hysteretic effects typical of cable-driven articulated systems were recorded.

3.6 Stabilizing flaps

The normal diameter of the ascending aorta is influenced by several factors, including body size, age, gender and blood pressure but usually is less than 40 mm [76]. To match this range of diameters at the distal end of the manipulator, 3 flaps are designed to keep the aorta open and fit the manipulator in the center. They also stabilize the manipulator during the procedure with small delivery vibration. In fact, in the case of aortic valve replacement, flaps are necessary to enhance the view provided by the cameras and preventing the collapse of the aorta wall on cameras. In the closed state, flaps help to protect the valve inside the manipulator and provide gradual increase for tip diameter. Once at the intervention site, the flaps can open and help the manipulator to stay in the middle of aorta which is one of the advantages of the robot in comparison to other manipulators [77]. Flaps are designed to operate without hindering the bending radius of whole manipulator or produce extra disturbance on the tip orientation. For this purpose, a flexible shaft (braided steel cable, usually used in bicycle brake system, φ = 1.6 mm) is used to open/close the flaps. The shaft is passing through the manipulator joints (Figure 3-3a) and transfer a DC gear motor torque to a pinion gear. The pinion gear is engaged with a ring that is partially machined like an internal gear. Each flap is connected to the ring by two fishing cables (φ = 0.18 mm) for opening and closing. Thus, by clockwise rotating the ring; all flaps can actuate simultaneously for opening and counterclockwise for closing. Actuation commands are sent by two buttons on the first joystick. Need to remark that the DC motor can freely slide in dedicated channel for compensation of different bending curvatures (placed on the side of sensing unit, opposite to introducer servomotor).

In order to validate the performance of the manipulator and to study the manipulator's ability in aorta to push the surroundings, a simple experiment has been organized to measure the flaps force on the vessels. The experimental set-up is shown in Figure 3-8. We measured forces in the distal section of the flaps by

means of a 3-axis force sensor (Nano 17 ATI Industrial Automation, NC, US) mounted on an industrial robot (MELFA S-series, by Mitsubishi Electric, Japan). More precisely, we pushed the sensor three times and by recording the corresponding forces we obtained the (mean ± std) point then the Mitsubishi robot moved 1 mm back and we repeated the same opening test. By mapping the displacements to the flaps angle (range from 83° to 112°) and corresponding force the graph will be completed.
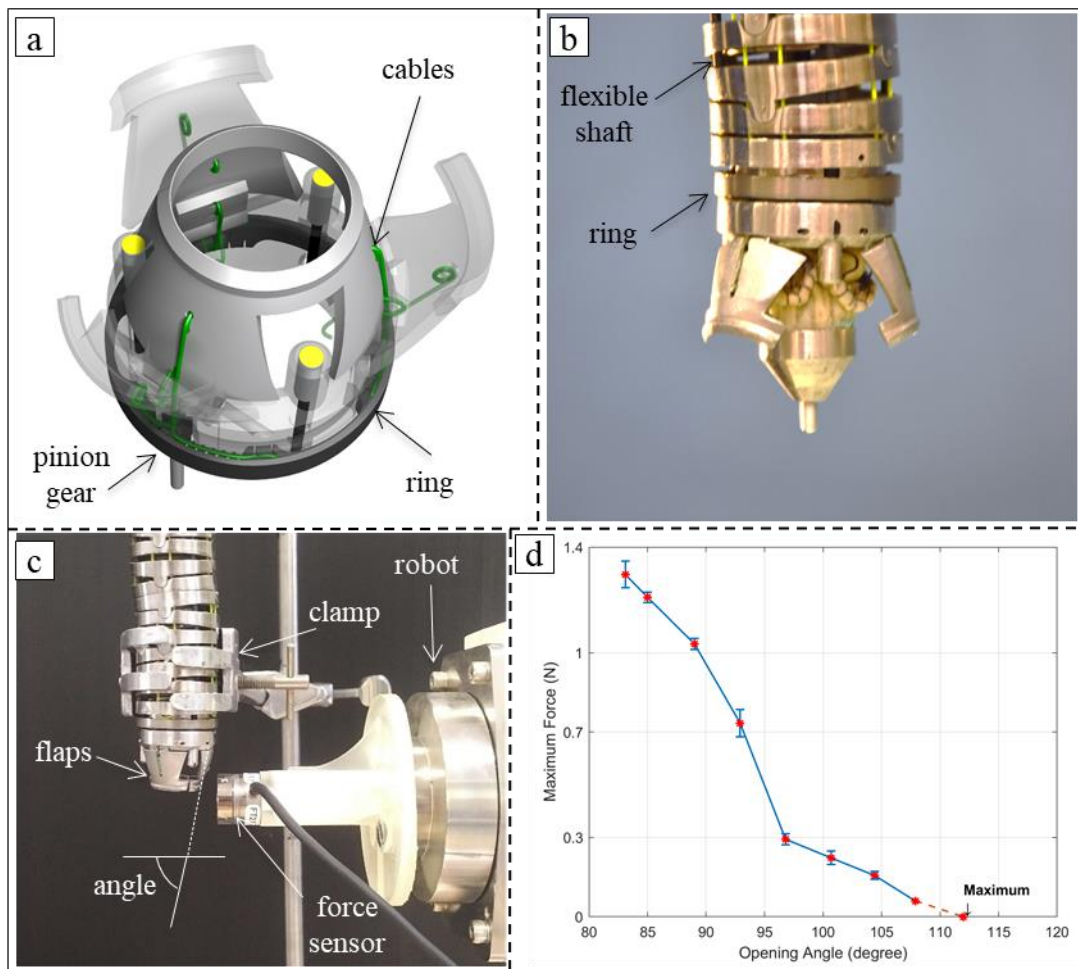
Figure 3-8 Stabilizing flaps. a) Schematics of design and opening/mechanism. b) Real prototype while the flaps are opened. c) The experiment setup to measure opening force of a flap. d) Measured force of one flap while it starts from close to open position.

3.7 Endoscopic vision

The manipulator is designed to provide the surgeons with the possibility to reach and explore the surgical area, and replace the heart valve with the help of endoscopic vision. Three tiny cameras are embedded laterally in top joint of the

manipulator and 120° angular shifted. FISCam[1] (FISBA, Switzerland) cameras have been selected because of their small diameter (less than 2 mm in diameter) and 120° field of view. The visual depth of field is up to 5 cm and provide 400x400 pixel resolution. The cameras include LED fibers which bundle circularly to provide illumination in the aorta. The integrated illumination power is controlled through separate control box out of the system. All wires are passing laterally through specific slots in the manipulator to keep them safe without any need for cutting (Figure 3-3).

To increase the field of view and offer a wider vision of the operative field, some solutions suggest stitching techniques to merge the pairs of images into one [78]. However, traditional methods for stitching images such as the SIFT [79], SURF [80], or ORB [81] algorithms are computationally expensive, because they require the identification of features in each image and the search for correspondences between each image pair. This makes these powerful and effective methods restraining in real time application. Other solutions consist of expanding the surgeon's field of view through dynamic view expansion: in a recent work, images from a single camera are merged using Simultaneous Localization And Mapping (SLAM) to generate a sparse probabilistic 3D map of the surgical site [82]. The problem of visualization in minimally invasive systems is substantial and several companies already provide systems such as the Third Eye Retroscope and Third Eye Panoramic, which allow framing larger areas through auxiliary systems, or the Fuse Full Spectrum Endoscopy, a complete colonoscopy platform including a video colonoscope and a processor. The systems currently on the market, however, are mostly developed for colonoscopy or gastroscopy, and cannot be integrated for use in heart operations due to the different morphology and surgical task.

Three different off-axis viewpoints provide visual information not as usable if compared to the usual endoscopic view, where a single camera is centered on the workspace. This is aggravated by the fact that, in order to maximize the common field of view of the three cameras, their x-y axes are not parallel. As shown in **Figure 3-9**a, the y-axes of the camera reference systems are radially oriented with

---

[1]http://www.fisba.com/expertise/expertise-components/fisba-fiscam

respect to the structure axis, making navigation inside the aorta extremely difficult. The cameras are referenced with numbers from 1 to 3, number 1 being associated with the reference camera.

In order to achieve accurate and reliable image stitching, camera calibration is an essential step. Plane-based camera calibration methods, as the well-known Zhang's method [83], requires the camera to observe a planar calibration pattern at a few unknown orientations. At first, the matches between 3-D world points (corners of a given chessboard) and their corresponding 2-D image points are to be found.

As done in [84], image stitching is performed by applying an appropriate warping of the camera images based on the estimation of the three plane-induced homographies between each camera image and a virtual camera ideally placed at the barycenter of the tree cameras and oriented as the reference camera 1, as shown in **Figure 3-9**b. This allows us to remap each camera view on an ideal and central (on-axis) viewpoint of the annulus plane. Being the aortic annulus the target of the surgical task, ideally should be the homography plane. Yet, since the exact position and orientation of the annulus plane cannot be estimated in advance, the homography is calculated considering a plane oriented parallel to the virtual camera.
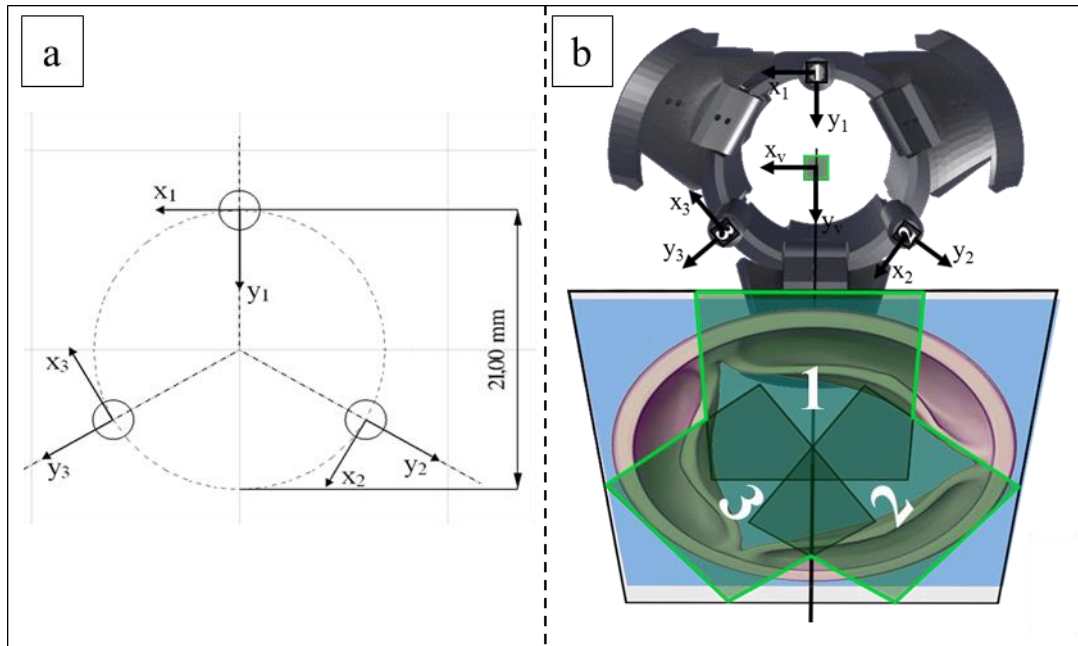
Figure 3-9 Camera configuration. a) The reference systems of the three cameras are oriented radially with respect to the manipulator axis. Camera 1 is the reference camera. b) Image stitching of virtual camera (in green) are shown. The homographic plane is highlighted in blue and the contributions of the three views, merged and captured by the virtual camera, are distinguished.

3.8 Stiffening

As a matter of fact, controllable-stiffness mechanisms are receiving growing attention, and different strategies were proposed based on the variation of the geometrical/material properties of the manipulator (involving, e.g., material phase transition, or structural interactions between system components, such as for jamming), or on actuation-related aspects (including, e.g., pressurization and variable-impedance mechanisms) [85]. Cable tensioning, which falls within the latter class, may be regarded to as a popular strategy, yet it still poses issues, e.g. for joint design [86]. To the best of our knowledge, manipulator stiffening based on cable tensioning was quantitatively addressed by a limited number of studies. Among them, a model was introduced in [87] for the stiffening of a catheter composed by a series of bead-shaped vertebras connected by ball-socket joints and containing four pull wires. More in detail, the model related wire tension to the frictional moment occurring at the spherical joint contact, and permitted to estimate the stiffness of the catheter in the straightened pose. Furthermore, the stiffening of an articulated manipulator was considered in [88]. Its links, profiled to also vary the neutral line based on the pose, contained two couples of pulling wires, and the

stiffness of the manipulator in the straightened pose was studied as a function of the wire tension. Additional stiffness measurements were performed in [89], by considering the effect of cable shortening on a pneumatically actuated soft-material manipulator. The same tensioning was applied to all the cables, thus introducing some pose variation (namely shortening) already when considering the straightened pose because of the intrinsic manipulator compliance. The same tension variation was imposed on all the wires when also stiffening the hard-material articulated systems in [87] and [88]: besides being functional to analytical derivations, that stiffening strategy was allowed by the straightened manipulator pose specifically considered therein. Indeed, thanks to symmetry, no pose deviations were induced by simultaneously shortening all the wires. This does not occur, however, for generic manipulator configurations, and pose-preserving stiffening (namely stiffening without movements causing pose deviations) is a sought manipulator feature for which, however, a clear strategy seems to be missing.

The stiffening command that ignites phase-II is characterized by a total shortening Δl to be applied to the LC(s) through a sequence of N_s steps. At the beginning of each step, the controller shortens the LC(s) at a given count rate (as described above), thus causing a light manipulator displacement. Then, it simultaneously shortens all the FCs (still by the same strategy) so as to recover the manipulator pose up to a chosen tolerance. To the purpose, closed-loop control based on tip displacement is introduced (Figure 3-5). In the carried out experiments we derived tip displacement from an auxiliary external sensor, for ease of development.

I then assessed the stiffening performance for selected manipulator poses along the two aforementioned axial and cross-axial bending directions. In particular, we chose four configurations (A1 - A4) along the axial, and four configurations (CA1 - CA4) along the cross-axial direction. They were respectively associated with the following values of the leading tension: 1.0, 1.5, 2.0 and 2.5 N. These values were chosen, also based on the positioning tests results (see Figure 3-7b), to span the workspace: A1 and CA1 were close to the straightened pose, whereas A4 and CA4 were close to the workspace boundary, thus corresponding to strongly bended

configurations (Figure 3-10). We excluded both the straightened and the maximally bent configurations because of their relative minor interest in the applicative scenario. For each configuration we then proceeded as follows. We recorded the tip position and the leading tension, labelled as LT_0. We then displaced the manipulator distal section by means of a 3-axis force sensor (Nano 17 ATI Industrial Automation, NC, US) mounted on an industrial robot (MELFA S-series, by Mitsubishi Electric, Japan). More precisely, we pushed the said distal section by 1, 2 and 3 mm along the x-axis, by recording the corresponding forces through the external sensor, and we obtained the stiffness along the x-axis (k_{x0}) by linearly fitting the corresponding trend. We repeated the same procedure for obtaining the stiffness along the y-axis (k_{y0}) and the z-axis (k_{z0}); however, we halved the displacements when probing along the z-axis, since the manipulator structure was responsible for an increased stiffness for most of the considered poses. We thus archived the stiffness (k_{x0}, k_{y0}, k_{z0}) associated with the starting cable tension (LT_0). We then issued the stiffening command, namely a shortening Δl =1.7-3.4 mm (smaller values were adopted for the poses close to the workspace boundary) to be applied in a single step ($N_s = 1$, for simplicity). In particular, reading tip displacement versus the recorded position from the ETS, we fed it back to the controller, and ceased pose recovery for displacements below 1 mm. We then measured the current leading tension (LT_1) and stiffness (k_{x1}, k_{y1}, k_{z1}) as described above. We issued three additional stiffening commands so as to obtain in total four sets of measurements, i.e., up to LT_4 and (k_{x4}, k_{y4}, k_{z4}). Finally, we assessed the stiffening trend by linearly fitting the points on the stiffness/LT plane thus obtained.

The manipulator configurations adopted for the stiffening tests are illustrated in Figure 3-10, whereas the results for axial and cross-axial bending are shown in Figure 3-11. For ease of readability, the latter figures also remind the stiffness-probing directions (through the corresponding forces F_x, F_y and F_z), and they feature a non-dimensional representation of the stiffness-LT trend in order to focus on the stiffening effect produced by cable tensioning.

The poses Aj and CAj (j = 1,...,4) in Figure 3-10 correspond to the points appearing along the directions (A) and (CA), respectively, in Figure 3-10, In particular, A1 and CA1 were associated with $LT_0 = 1.0$ N, and so on up to A4 and CA4, which corresponded to $LT_0 = 2.5$ N. Consistently with physical intuition, higher LT_0 values corresponded to configurations with a higher initial stiffness along the x- and y-axis. Indeed, for A1-A4 we respectively obtained [0.04, 0.07, 0.08, 0.09] N/mm for k_{x0}, and [0.04, 0.05, 0.08, 0.1] N/mm for k_{y0}, with the enhanced k_{x0} in A4 due to the directly opposing reaction of the metallic manipulator structure. Moreover, for CA1-CA4 we respectively obtained [0.05, 0.07, 0.14, 0.31] N/mm for k_{x0}, and [0.04, 0.08, 0.12, 0.21] N/mm for k_{y0}. Still based on physical intuition, we expected k_{z0} to be ruled by the manipulator structure (rather than LT_0), with a stronger opposing reaction in A1 and CA1, i.e. closer to the straightened configuration. The recorded values, namely [4.01, 3.01, 2.24, 0.99] N/mm for A1-A4 and [4.52, 3.80, 2.03, 1.41] N/mm for CA1-CA4, supported our physical understanding (and the subsequent stiffening results were not affected by the fact that k_{z0} was only weakly related to LT_0).
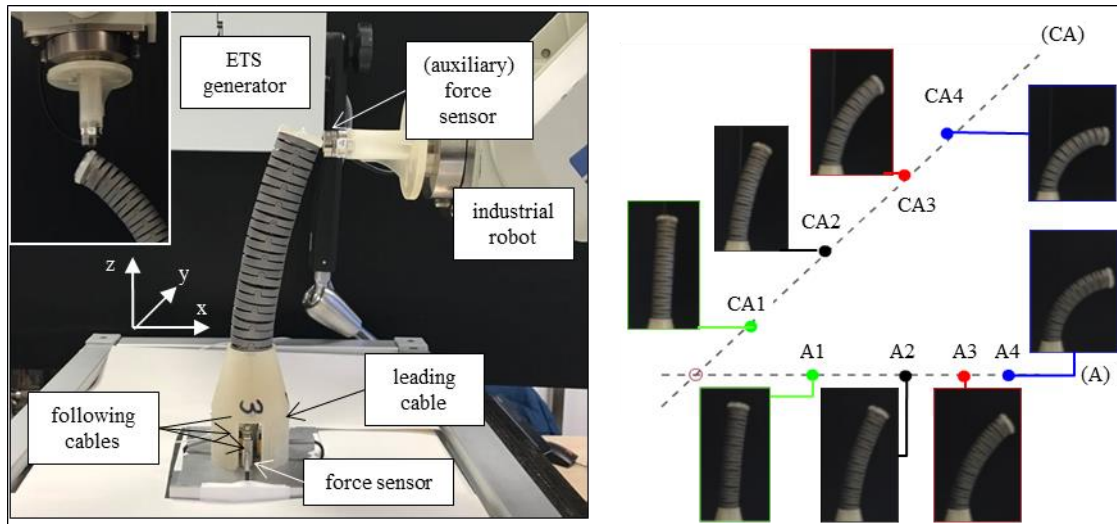
Figure 3-10 Left) Experimental setup for stiffening tests also showing the auxiliary force sensor mounted on the industrial robot. The arrangement shown in the main frame of the subfigure was used for the x-stiffness (the y-stiffness would be obtained by a simple rotation); the arrangement in the inset was used for the z-stiffness. Right) Manipulator selected poses for the stiffening tests. They correspond to those in **Figure 3-7**b along the axial (A) and the cross-axial (CA) bending direction. In particular: poses A1 and CA1 are associated with a leading tension LT0 = 1.0 N; A2 and CA2 with LT0 = 1.5 N; A3 and CA3 with LT0 = 2.0 N; A4 and CA4 with LT0 = 2.5 N.

The results of the stiffening tests are summarized in **Figure 3-11**. Each point in **Figure 3-11** was obtained by linearly fitting a series of force-displacement

experimental points (see *Sec.* 3.5.2): the related goodness-of-fit (R^2) was 0.93 ± 0.08 for axial bending, and 0.92 ± 0.07 for cross-axial bending. Please notice that the LT/LT_0 span in **Figure 3-11** decreases when passing from A1 (CA1) to A4 (CA4) due to the trivial scaling effect of LT_0, and because of the increasingly reduced margin with respect to the workspace boundary. Noticeably, the resulting stiffening trends in **Figure 3-11** could be suitably approximated by linear fitting (see also the R^2 values therein), featuring some deviations just close to the workspace boundary. Let us remark that we obtained similar trends for the x- and y-stiffness in cross-axial bending, as expected by symmetry. Furthermore, as for the x-stiffness, we observed a more pronounced trend in axial bending, consistently with the fact that the whole tensioning action contributed to stiffening (whereas for cross-axial bending only a component of the tensioning effort acted along the x-axis, owing to the definition of LT). In addition, the relatively pronounced trend observed for the y-stiffness in axial bending was due to the fact that, for that specific loading condition, the probing force was elongating all the tendons, whereas some of them were partially unloaded for the other loading conditions. Finally, the relatively less pronounced trend observed for the z-stiffness was trivially due to the fact that the z-stiffness, in dimensional terms, was systematically the highest one, because of the dominating contribution to stiffness brought by the manipulator structure.

Overall, these results show the positive contributions brought by the articulated/continuum design in terms of smooth and accurate positioning capabilities.
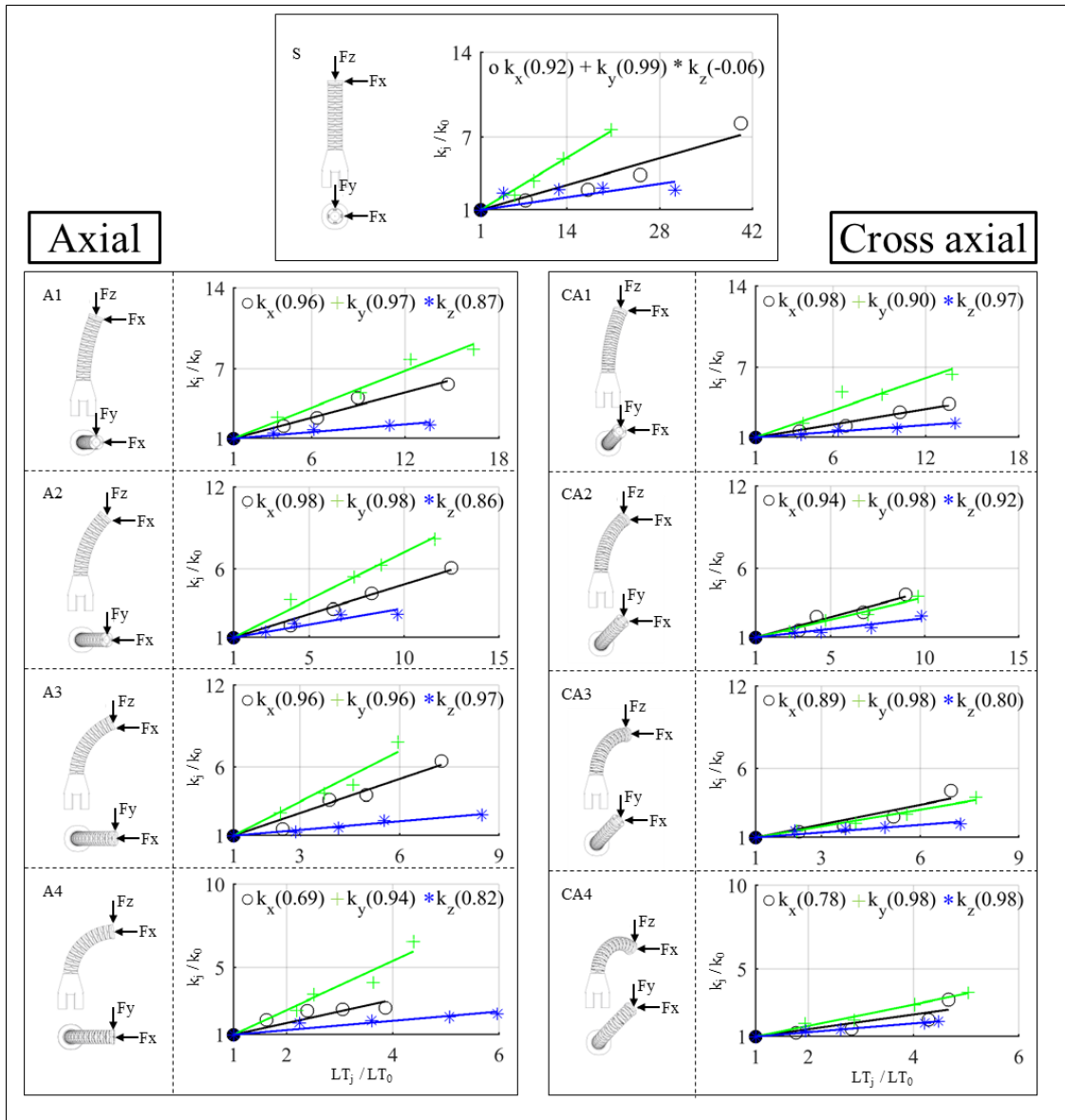
Figure 3-11 Stiffening test results for axial bending (Left) and cross-sectional bending (Right) (the selected configurations also appear in **Figure 3-10**). The stiffness trend versus leading tension trend is shown (the non-dimensional form aims to highlight the stiffening effect). Symbol kj shortly represents (kxj, kyj, kzj), namely all the measures at step j (the specific stiffness value being identified by the legend marker). The figure reported in parentheses close to each marker denotes the goodness (R2 value) of the corresponding linear fit.

3.9 Valve introducer

The introducer is inserted in the central passage of the manipulator and it includes a stainless steel coil spring (ϕ = 21.6 mm, ϕ_{coil} = 1.6 mm, by Metersprings srl, Italy) and two DC gear motors (RS PRO, 951D Series, Italy) for valve rotation and expansion (**Figure 3-12**). Let us remark that I introduced the spring for two reasons: to enhance controllability (discussed in experimental assessment phase-I) and to support valve deployment by a corkscrew movement. A simple illustration

of this mechanism is shown in **Figure 3-12** that by rotation of the spring coil (through gear engagement) the internal components translate forward/backward. In this configuration, the internal components have a slider in its tail and cartridge connection on distal tip. Between each segments of the introducer a stainless steel tension spring (ϕ = 17 mm, ϕ_{coil} = 1.6 mm, by Metersprings srl, Italy) is placed to satisfy the flexibility of the system. Also the ultimate tension spring constrains the introducer to follow the proper orientation of head plane when it comes out of the manipulator. The distal tip is designed by special pin hole connections for attaching the cartridge and a connector to transfer motion for expansion. The motion required to expand the cartridge is transferred by a flexible shaft actuated by ultimate DC motor. While the lower DC motor is actuating the whole segment to provide rotation of the valve. The commands for translational movements are captured by the second joystick (see Figure 3-2) and actuated by a servomotor placed on the side of sensing section (see Figure 3-3). Valve rotation can be done by joystick rotation and expansion will start by the button on the second joystick.
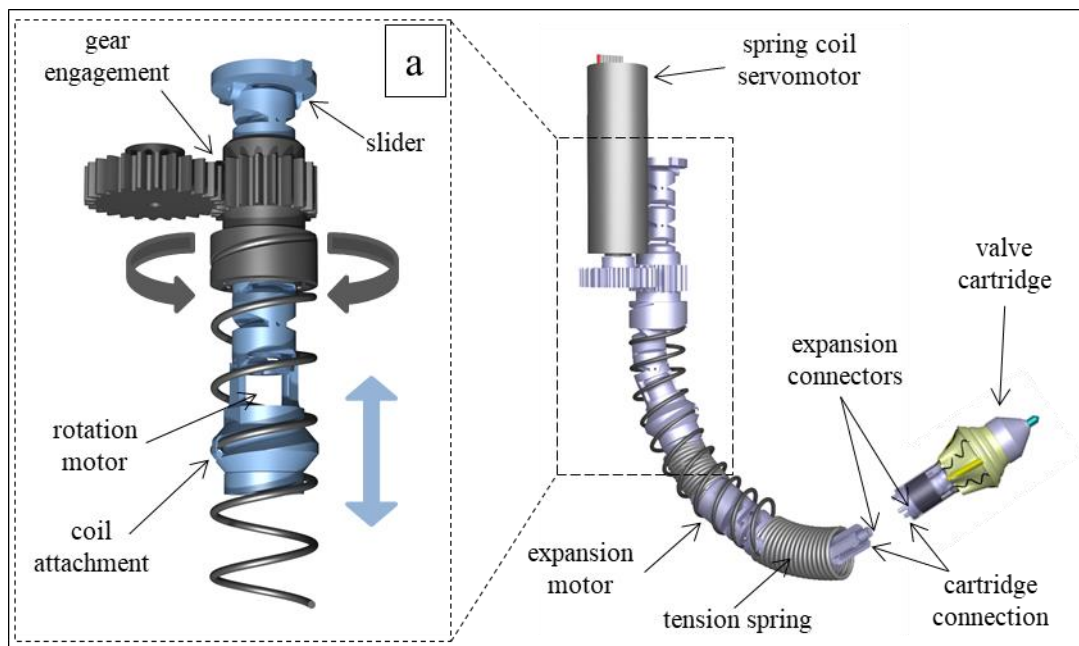
Figure 3-12 Introducer mechanism for valve translation, rotation and expansion. DC motors are also positioned in the middle and pin holes for cartridge connection is designed on distal tip. a) Simple illustration of the translational movement by arrows.

97

3.10 Valve cartridge

The valve cartridge is designed to keep the collapsed valve secure and make the system suitable for different prosthesis sizes just by changing the cartridge. The focus of this study is based on 23 mm diameter one which is the most usable prosthesis in surgeries. Anyhow, the cartridge can easily scale up to keep bigger diameters without any changes in the introducer and manipulator. The expansion is actuated by rotating a central screw which is fabricated partially in M3 left hand and right hand (**Figure 3-13**). In this scenario, just one way rotation of the central screw is needed to move the skirt cap out in the first stage. The strategy to expand the valve in two stages guarantees proper anchoring and safe expansion of the frame without minimum chance of dislocation. By pressing again the button on the second joystick, the second stage of expansion will start and frame tube sheath moves in opposite direction. Finally, by removing two constrains on the skirt and frame the valve releases in aorta. To provide a separate motion in skirt and frame (satisfying expansion stages with one actuator), the threated lengths are different. So firstly the cap will move and after traveling the same length the nut will be in contact with the sheath and make it move back while the cap is already out of contact.
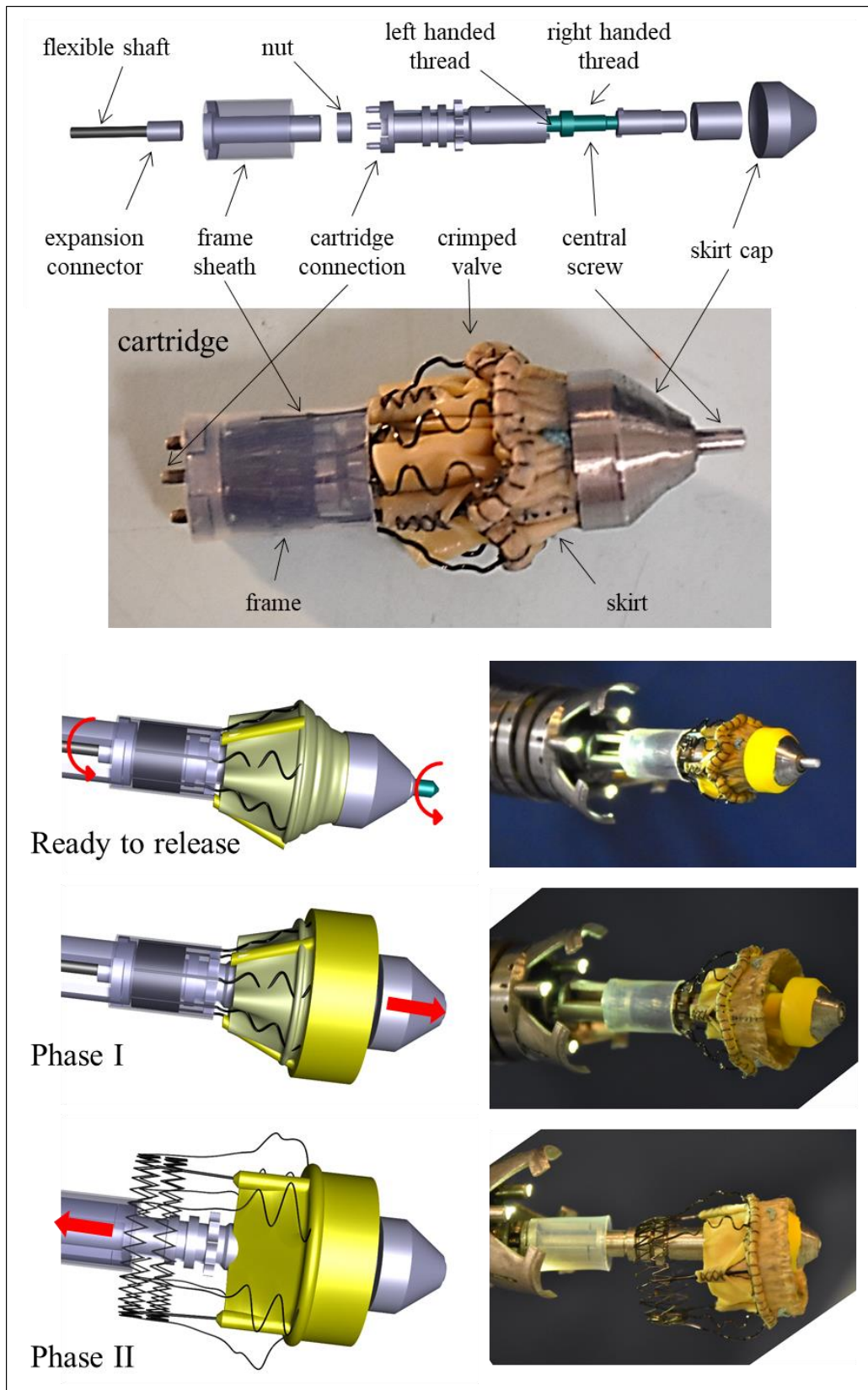
Figure 3-13 Valve cartridge and expansion phases

99

In the next two sections, two cases in which the proposed robotic manipulator has been tested will be described with the aim to verify its proper functioning and successful delivery.

3.11 Case Study: Valve delivery validation with simulator

The mini thoracotomy location can be defined preoperatively using patient specific surgical simulators [90]. The simulator allows moving a virtual replica of the manipulator in the patient virtual anatomy, in order to evaluate the best location of the mini thoracotomy.

Before the operation, the cartridge is prepared by surgeons using a dedicated crimping device. The Sorin valve is collapsed with its dedicated crimper inside the cartridge by special key (Figure 3-14b). The crimping process is so similar with the standard one recommended by the company. The central screw moves the skirt part of cartridge and the sheath is forced by hand to fully capture the valve. The introducer should be moved completely out of the manipulator for charging the cartridge by help of the pins holes connection and the flexible central shaft is matched with central screw (Figure 3-14d). When the cartridge is implanted securely, the introducer can be retracted inside the manipulator (Figure 3-14e). By closing flaps, the cartridge is completely secure in the system. At this stage, the preparation stage is finished and it will be ready for intervention (e.g. inserting in the patient's aorta) (Figure 3-14f).
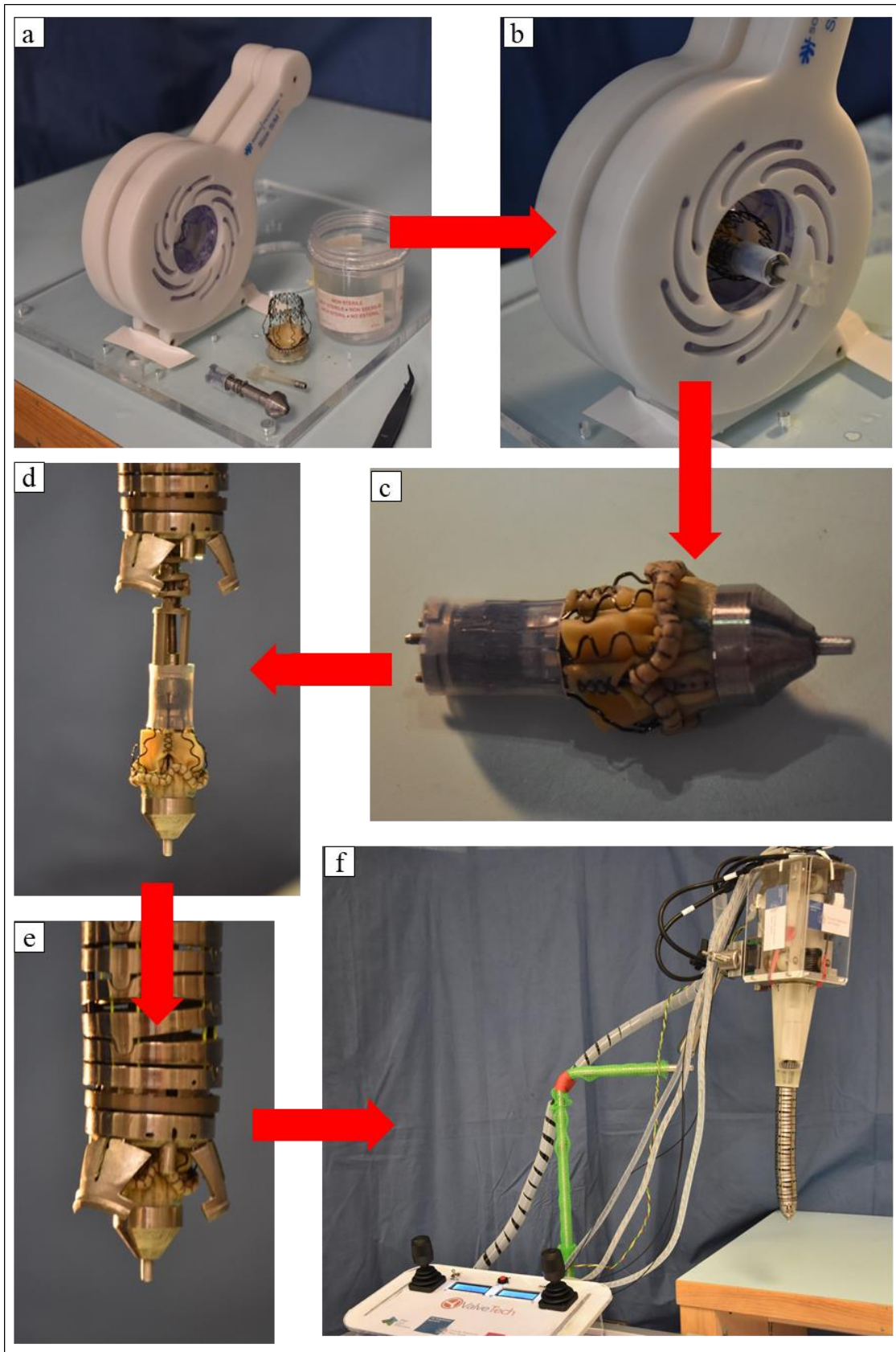
Figure 3-14 Valve/robot preparation stage. a) Collapsing the valve. b) Charging the valve in cartridge. c) Ready cartridge. d) Installing the cartridge to the introducer. e) Retraction of the cartridge inside the manipulator. f) Flaps are closed and the manipulator is ready.

The base of the robot system is then moved into position (by adjusting the Martin arm), in line with the guidance from preoperative scans, to provide sufficient freedom for inserting the manipulator (Figure 3-15a). The manipulator is moved linearly inside the chest while by utilizing the bending ability the manipulator can find the aorta and finally reaches the intervention site (usually 3-4 cm behind the calcified valve). When the manipulator is inside the aorta in the best position/orientation and can see the nadir points by help of cameras, the stiffening procedure can be started by pressing a button on control unit (the stiffening level is optional). Then, flaps are opening for keeping the manipulator in center and preventing the tissue from collapsing on cameras line of sight. The nadir points are now completely recognizable by illumination of cameras and image processing techniques (Figure 3-15d). At this time a small modification is also possible for precise adjustment of the manipulator inside the aorta.

The introducer is commanded to move linearly by following the orientation of the manipulator's tip inside the aorta and adjust its prefect position (forward/backward motion). The suitable site is recognized by camera images and techniques to recognize the nadir points. The introducer is also equipped with rotation mechanism to precisely adjust the valve in accordance with nadir points. So just by axial rotating the joysticks, the surgeons can modify its angular orientation and precisely adjust the valve.

When all the requirements are satisfied and the nadir points fit the valve, the expansion phase can start. By pressing the button in the control unit, the cartridge starts to expand. In this system, the valve is expanded in two phases. First the skirt part will be release for anchoring the valve in the site and in the second phase the frame part will be expanded to completely secure the valve inside aorta (Figure 3-15e).

The empty cartridge (attached with introducer) can pass through inside the manipulator by using backward translational motion as before and flaps are closed. The manipulator is ready for retraction and it can unbend and come out now.
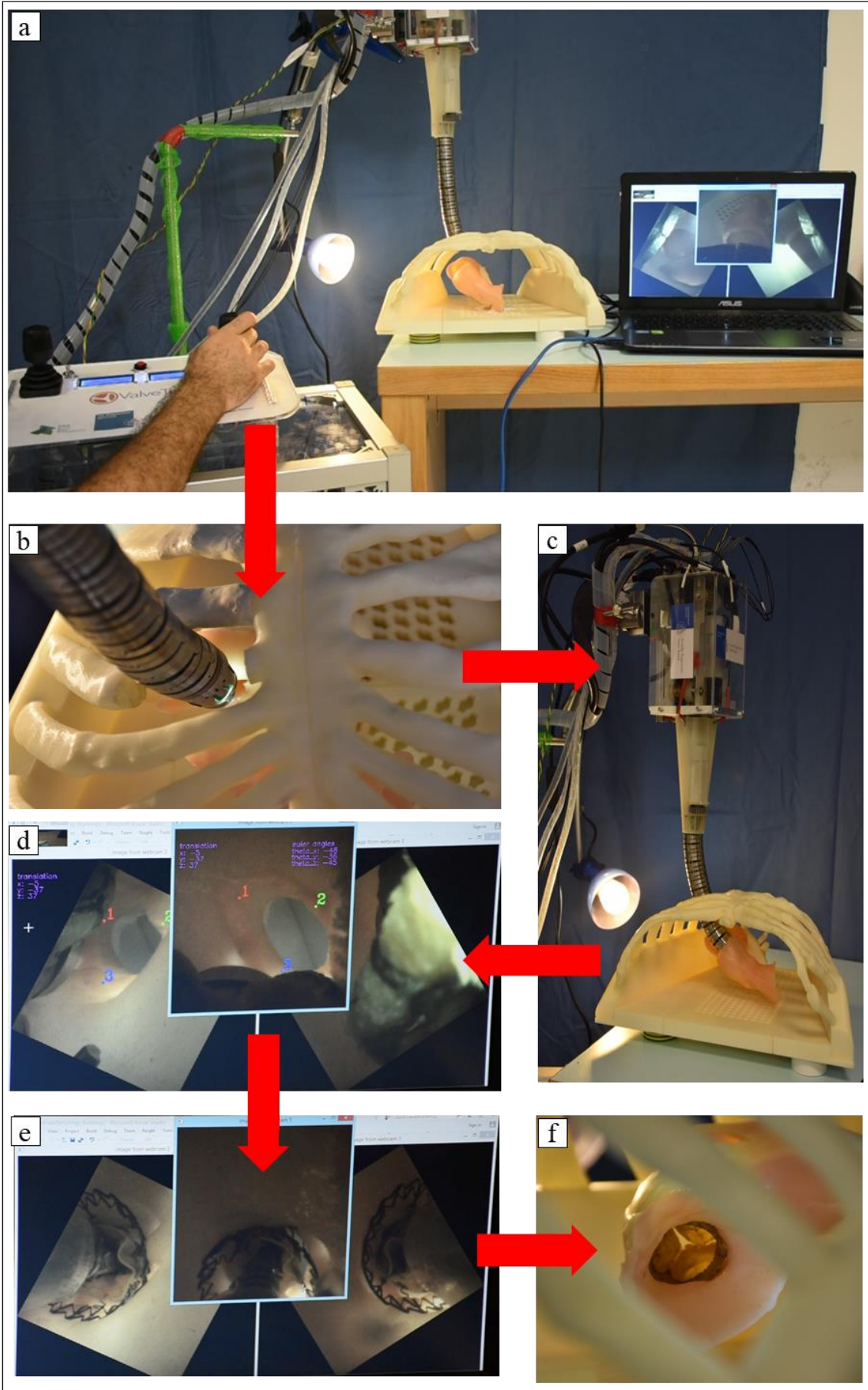
Figure 3-15 Valve delivery procedure. a) The robot is placed on the line of insertion. b) The manipulator is guided to find the intervention site. c) The manipulator is on the intervention site. d) The flaps are opened and the nadir points are recognized. e) The introducer is reached the release site and the valve is expanded. f) The manipulator is out of the simulator and the valve stays inside aorta.

3.12 Perspectives and future work

We introduced a novel cable-driven articulated/continuum manipulator with the ability of pose preserving under stiffening: starting from an articulated structure (which could be functional to deliver a wide class of payloads), we steered design in view of valve surgery applications. In particular, we also integrated a coil spring that, while being devised for valve precise delivery, enhanced the positioning performance of the manipulator. Indeed, it permitted to accurately bend the manipulator also along directions not intrinsically favored by joints constraints (cross-axial bending), and to avoid the hysteretic effects typically observed when reversibly operating articulated cable-driven systems, which were also reported in this study for completeness.

Moreover, we introduced a simple cable tensioning strategy based on the leading tension concept, and we effectively achieved pose-preserving stiffening by considering a variety of starting poses. The maximum stiffening factor was in between 2 (e.g., k_z in CA4) and 9 (e.g., k_y in A1), based on relevant margins from the initial pose to the workspace boundary, and on potential contributions by the structure itself. More importantly, the resulting stiffening trend was almost linear with cable tensioning, for all the considered poses. This extends, e.g., the observations in [88], which were based on a straightened pose only. Furthermore, despite its simplicity, the proposed tensioning strategy permits to circumvent a detailed modelling of frictional effects that, being complex already for simple contact geometries [87], poses challenging issues in general and sensibly depend on the specific manipulator [91].

The proposed introducer is functioning with minimum disturbance on the manipulator's position while it is able to bend in all directions together with the articulated manipulator. Also, the motors inside the introducer provide extra benefit to the surgeons by rotation of the valve that will help to match the valve

precisely. Two stage valve expansion is also a privilege of our design in compare with the robotic delivery in state of the art.

However, we are aware of the limitations affecting the present study. Primarily in stiffness tests, to keep the developmental burden commensurate with the scope and the main aim of this study, we used an auxiliary external sensor. A stronger demonstration should be based on image-processing, by leveraging the tip cameras integrated in the manipulator. Moreover, even if we studied many manipulator configurations, a wider characterization should also consider generic 3D poses and more bending planes (not only, e.g., those associated with the bisecting directions). Further miniaturization is also possible with improvements in valve characteristics especially when it's crimped.

References:

1. Osnabrugge RLJ, Mylotte D, Head SJ, et al. Aortic stenosis in the elderly: Disease prevalence and number of candidates for transcatheter aortic valve replacement: A meta-analysis and modeling study. *J Am Coll Cardiol*. 2013;62(11):1002-1012. doi:10.1016/j.jacc.2013.05.015

2. Joseph J, Naqvi SY, Giri J, Goldberg S. Aortic Stenosis: Pathophysiology, Diagnosis, and Therapy. *Am J Med*. 2017;130(3):253-263. doi:10.1016/j.amjmed.2016.10.005

3. Marquis-Gravel G, Redfors B, Leon MB, Généreux P. Medical Treatment of Aortic Stenosis. *Circulation*. 2016;134(22):1766-1784. doi:10.1161/CIRCULATIONAHA.116.023997

4. Kogoj P, Devjak R, Bunc M. Balloon aortic valvuloplasty (BAV) as a bridge to aortic valve replacement in cancer patients who require urgent non-cardiac surgery. *Radiol Oncol*. 2014;48(1):62-66. doi:10.2478/raon-2013-0078

5. Mohr FW, Holzhey D, Möllmann H, et al. The German Aortic Valve Registry: 1-year results from 13 680 patients with aortic valve disease. *Eur J Cardio-thoracic Surg*. 2014;46(5):808-816. doi:10.1093/ejcts/ezu290

6.   Thourani VH, Suri RM, Gunter RL, et al. Contemporary real-world outcomes of surgical aortic valve replacement in 141,905 low-risk, intermediate-risk, and high-risk patients. *Ann Thorac Surg*. 2015;99(1):55-61. doi:10.1016/j.athoracsur.2014.06.050

7.   Grigorios T, Stefanos D, Athanasios M, et al. Transcatheter versus surgical aortic valve replacement in severe, symptomatic aortic stenosis. *J Geriatr Cardiol*. 2018;15(1):76-85. doi:10.11909/j.issn.1671-5411.2018.01.002

8.   Iribarne A, Easterwood R, Chan EY, et al. The golden age of minimally invasive cardiothoracic surgery: current and future perspectives. *Future Cardiol*. 2011;7(3):333-346. doi:10.2217/fca.11.23

9.   Lorusso R, Gelsomino S, Renzulli A. Sutureless aortic valve replacement: An alternative to transcatheter aortic valve implantation? *Curr Opin Cardiol*. 2013;28(2):158-163. doi:10.1097/HCO.0b013e32835da4b2

10.   Boix-Garibo R, Uzzaman MM, Bapat VN. Review of Minimally Invasive Aortic Valve Surgery. *Interv Cardiol Rev*. 2015;10(3):144. doi:10.15420/ICR.2015.10.03.144

11.   Vernick W, Atluri P. Robotic and minimally invasive cardiac surgery. *Anesthesiol Clin*. 2013;31(2):299-320. doi:10.1016/j.anclin.2012.12.002

12.   Balkhy HH, Lewis CTP, Kitahara H. Robot-assisted aortic valve surgery: State of the art and challenges for the future. *Int J Med Robot Comput Assist Surg*. 2018;14(4):e1913. doi:10.1002/rcs.1913

13.   Vola M, Maureira P, Kassir R, et al. Robotic total endoscopic sutureless aortic valve replacement: proof of concept for a future surgical setting. *Int J Med Robot Comput Assist Surg*. 2016;12(3):370-374. doi:10.1002/rcs.1694

14.   Rodriguez E, Nifong LW, Bonatti J, et al. Pathway for surgeons and programs to establish and maintain a successful robot-assisted adult cardiac surgery program. *J Thorac Cardiovasc Surg*. 2016;152(1):9-13. doi:10.1016/j.jtcvs.2016.05.018

15. Folliguet TA, Vanhuyse F, Konstantinos Z, Laborde F. Early experience with robotic aortic valve replacement. *Eur J Cardio-thoracic Surg*. 2005;28(1):172-173. doi:10.1016/j.ejcts.2005.03.021

16. Suri RM, Burkhart HM, Schaff H V. Robot-assisted aortic valve replacement using a novel sutureless bovine pericardial prosthesis: Proof of concept as an alternative to percutaneous implantation. *Innov Technol Tech Cardiothorac Vasc Surg*. 2010;5(6):419-423. doi:10.1097/IMI.0b013e318202c8e5

17. Shemin RJ. The future of cardiovascular surgery. *Circulation*. 2016;133(25):2712-2715. doi:10.1161/CIRCULATIONAHA.116.023545

18. Li M, Kapoor A, Mazilu D, Horvath KA. Pneumatic actuated robotic assistant system for aortic valve replacement under MRI guidance. *IEEE Trans Biomed Eng*. 2011;58(2):443-451. doi:10.1109/TBME.2010.2089983

19. Yeniaras E, Lamaury J, Navkar N V, et al. Magnetic resonance based control of a robotic manipulator for interventions in the beating heart. *2011 IEEE Int Conf Robot Autom*. 2011:6270-6275. doi:10.1109/ICRA.2011.5980459

20. Merk DR, Holzhey D, Burgert O. Image-Guided Transapical Aortic Valve Implantation. 2011;6(4):231-236.

21. Karar ME, Merk DR, Falk V, Burgert O. A simple and accurate method for computer-aided transapical aortic valve replacement. *Comput Med Imaging Graph*. 2016;50:31-41. doi:10.1016/j.compmedimag.2014.09.005

22. Fishman EK, Ney DR, Heath DG, Corl FM, Horton KM, Johnson PT. Volume Rendering versus Maximum Intensity Projection in CT Angiography: What Works Best, When, and Why. *RadioGraphics*. 2006;26(3):905-922. doi:10.1148/rg.263055186

23. Peters TM. Image-guidance for surgical procedures. *Phys Med Biol*. 2006;51(14):R505-R540. doi:10.1088/0031-9155/51/14/R01

24. Willaert W, Aggarwal R, Bicknell C, et al. Patient-specific simulation in carotid artery stenting. *J Vasc Surg*. 2010;52(6):1700-1705.

doi:10.1016/j.jvs.2010.08.015

25. Bersvendsen J, Beitnes JO, Urheim S, Aakhus S, Samset E. Automatic measurement of aortic annulus diameter in 3-dimensional Transoesophageal echocardiography. *BMC Med Imaging*. 2014;14(1):31. doi:10.1186/1471-2342-14-31

26. Calleja A, Thavendiranathan P, Ionasec RI, et al. Automated Quantitative 3-Dimensional Modeling of the Aortic Valve and Root by 3-Dimensional Transesophageal Echocardiography in Normals, Aortic Regurgitation, and Aortic Stenosis. *Circ Cardiovasc Imaging*. 2013;6(1):99-108. doi:10.1161/CIRCIMAGING.112.976993

27. Zheng Y, John M, Liao R, et al. Automatic aorta segmentation and valve landmark detection in C-arm CT: application to aortic valve implantation. *Med Image Comput Comput Assist Interv*. 2010;13(Pt 1):476-483. http://www.ncbi.nlm.nih.gov/pubmed/20879265.

28. Cerillo AG, Mariani M, Glauber M, Berti S. Sizing the annulus for transcatheter aortic valve implantation: more than a simple measure? *Eur J Cardio-Thoracic Surg*. 2012;41(3):717-718. doi:10.1093/ejcts/ezr050

29. Kempfert J, Van Linden A, Lehmkuhl L, et al. Aortic annulus sizing: echocardiographic versus computed tomography derived measurements in comparison with direct surgical sizing. *Eur J Cardio-Thoracic Surg*. 2012;42(4):627-633. doi:10.1093/ejcts/ezs064

30. Binder RK, Webb JG, Willson AB, et al. The Impact of Integration of a Multidetector Computed Tomography Annulus Area Sizing Algorithm on Outcomes of Transcatheter Aortic Valve Replacement. *J Am Coll Cardiol*. 2013;62(5):431-438. doi:10.1016/j.jacc.2013.04.036

31. Schwarz F, Lange P, Zinsser D, et al. CT-Angiography–Based Evaluation of the Aortic Annulus for Prosthesis Sizing in Transcatheter Aortic Valve Implantation (TAVI)–Predictive Value and Optimal Thresholds for Major Anatomic Parameters. Moretti C, ed. *PLoS One*. 2014;9(8):e103481.

doi:10.1371/journal.pone.0103481

32. Stortecky S, Heg D, Gloekler S, Wenaweser P, Windecker S, Buellesfeld L. Accuracy and reproducibility of aortic annulus sizing using a dedicated three-dimensional computed tomography reconstruction tool in patients evaluated for transcatheter aortic valve replacement. *EuroIntervention*. 2014;10(3):339-346. doi:10.4244/EIJV10I3A59

33. Elattar MA, Wiegerinck EM, Planken RN, et al. Automatic segmentation of the aortic root in CT angiography of candidate patients for transcatheter aortic valve implantation. *Med Biol Eng Comput*. 2014;52(7):611-618. doi:10.1007/s11517-014-1165-7

34. Moore JT, Chu MWA, Kiaii B, et al. A Navigation Platform for Guidance of Beating Heart Transapical Mitral Valve Repair. *IEEE Trans Biomed Eng*. 2013;60(4):1034-1040. doi:10.1109/TBME.2012.2222405

35. Manenti A, Colasanto D, Morandi C. Computed Tomography in Aid to Direct Aortic Access. *Ann Thorac Surg*. 2013;95(3):1137. doi:10.1016/j.athoracsur.2012.08.113

36. Ionita CN, Mokin M, Varble N, et al. Challenges and limitations of patient-specific vascular phantom fabrication using 3D Polyjet printing. In: Molthen RC, Weaver JB, eds. ; 2014:90380M. doi:10.1117/12.2042266

37. Walther T, Blumenstein J, van Linden A, Kempfert J. Contemporary management of aortic stenosis: surgical aortic valve replacement remains the gold standard. *Heart*. 2012;98 Suppl 4:iv23-9. doi:10.1136/heartjnl-2012-302399

38. Andersen HR, Knudsen LL, Hasenkam JM. Transluminal implantation of artificial heart valves. Description of a new expandable aortic valve and initial results with implantation by catheter technique in closed chest pigs. *Eur Heart J*. 1992;13(5):704-708. http://www.ncbi.nlm.nih.gov/pubmed/1618213.

39. Cribier AG. The Odyssey of TAVR from Concept to Clinical Reality. *Texas Hear*

Inst J. 2014;41(2):125-130. doi:10.14503/THIJ-14-4137

40.   Kourkoveli P, Spargias K, Hahalis G. TAVR in 2017—What we know? What to expect? *J Geriatr Cardiol*. 2018;15(1):55-60. doi:10.11909/j.issn.1671-5411.2018.01.005

41.   Webb JG, Wood DA. Current status of transcatheter aortic valve replacement. *J Am Coll Cardiol*. 2012;60(6):483-492. doi:10.1016/j.jacc.2012.01.071

42.   Cosgrove DM, Sabik JF. Minimally invasive approach for aortic valve operations. *Ann Thorac Surg*. 1996;62(2):596-597. doi:10.1016/0003-4975(96)00418-3

43.   Zubair MH, Smith JM. Updates in Minimally Invasive Cardiac Surgery for General Surgeons. *Surg Clin North Am*. 2017;97(4):889-898. doi:10.1016/j.suc.2017.03.002

44.   Estrera AL, Reardon MJ. Current approaches to minimally invasive aortic valve surgery. *Curr Opin Cardiol*. 2000;15(2):91-95. http://www.ncbi.nlm.nih.gov/pubmed/10963145.

45.   Kaczmarczyk M, Szałański P, Zembala M, et al. Minimally invasive aortic valve replacement - Pros and cons of keyhole aortic surgery. *Kardiochirurgia i Torakochirurgia Pol*. 2015;12(2):103-110. doi:10.5114/kitp.2015.52850

46.   Svensson LG, D'Agostino RS. Minimal-access aortic and valvular operations, including the "J/j" incision. *Ann Thorac Surg*. 1998;66(2):431-435. doi:10.1016/S0003-4975(98)00462-7

47.   Johnston DR, Atik FA, Rajeswaran J, et al. Outcomes of less invasive J-incision approach to aortic valve surgery. *J Thorac Cardiovasc Surg*. 2012;144(4):852-858.e3. doi:10.1016/j.jtcvs.2011.12.008

48.   Aris A, Cámara ML, Montiel J, Delgado LJ, Galán J, Litvan H. Ministernotomy versus median sternotomy for aortic valve replacement: a prospective, randomized study. *Ann Thorac Surg*. 1999;67(6):1583-1587. doi:10.1016/S0003-4975(99)00362-8

49. Korach A, Shemin RJ, Hunter CT, Bao Y, Shapira OM. Minimally invasive versus conventional aortic valve replacement: a 10-year experience. *J Cardiovasc Surg (Torino)*. 2010;51(3):417-421. http://www.ncbi.nlm.nih.gov/pubmed/20523293.

50. Brinkman WT, Hoffman W, Dewey TM, et al. Aortic Valve Replacement Surgery: Comparison of Outcomes in Matched Sternotomy and PORT ACCESS Groups. *Ann Thorac Surg*. 2010;90(1):131-135. doi:10.1016/j.athoracsur.2010.03.055

51. Flameng W, Herregods M-C, Hermans H, et al. Effect of sutureless implantation of the Perceval S aortic valve bioprosthesis on intraoperative and early postoperative outcomes. *J Thorac Cardiovasc Surg*. 2011;142(6):1453-1457. doi:10.1016/j.jtcvs.2011.02.021

52. Folliguet TA, Laborde F, Zannis K, Ghorayeb G, Haverich A, Shrestha M. Sutureless Perceval Aortic Valve Replacement: Results of Two European Centers. *Ann Thorac Surg*. 2012;93(5):1483-1488. doi:10.1016/j.athoracsur.2012.01.071

53. Santarpino G, Pfeiffer S, Schmidt J, Concistrè G, Fischlein T. Sutureless Aortic Valve Replacement: First-Year Single-Center Experience. *Ann Thorac Surg*. 2012;94(2):504-509. doi:10.1016/j.athoracsur.2012.04.024

54. Miceli A, Santarpino G, Pfeiffer S, et al. Minimally invasive aortic valve replacement with Perceval S sutureless valve: Early outcomes and one-year survival from two European centers. *J Thorac Cardiovasc Surg*. 2014;148(6):2838-2843. doi:10.1016/j.jtcvs.2014.02.085

55. Aymard T, Kadner A, Walpoth N, et al. Clinical experience with the second-generation 3f Enable sutureless aortic valve prosthesis. *J Thorac Cardiovasc Surg*. 2010;140(2):313-316. doi:10.1016/j.jtcvs.2009.10.041

56. Martens S, Sadowski J, Eckstein FS, et al. Clinical experience with the ATS 3f Enable® Sutureless Bioprosthesis☆☆☆. *Eur J Cardio-Thoracic Surg*. February 2011. doi:10.1016/j.ejcts.2010.12.068

57.   Weymann A, Konertz J, Laule M, Stangl K, Dohmen PM. Are Sutureless Aortic Valves Suitable for Severe High-Risk Patients Suffering from Active Infective Aortic Valve Endocarditis? *Med Sci Monit*. 2017;23:2782-2787. doi:10.12659/MSM.902785

58.   Modi P, Rodriguez E, Hargrove WC, Hassan A, Szeto WY, Chitwood WR. Minimally invasive video-assisted mitral valve surgery: A 12-year, 2-center experience in 1178 patients. *J Thorac Cardiovasc Surg*. 2009;137(6):1481-1487. doi:10.1016/j.jtcvs.2008.11.041

59.   Gao C, Yang M, Xiao C, et al. Robotically assisted mitral valve replacement. *J Thorac Cardiovasc Surg*. 2012;143(4):S64-S67. doi:10.1016/j.jtcvs.2012.01.045

60.   Falk V, Walther T, Autschbach R, Diegeler A, Battellini R, Mohr FW. Robot-assisted minimally invasive solo mitral valve operation. *J Thorac Cardiovasc Surg*. 1998;115(2):470-471. doi:10.1016/S0022-5223(98)70295-8

61.   Reichenspurner H, Damiano RJ, Mack M, et al. Use of the voice-controlled and computer-assisted surgical system zeus for endoscopic coronary artery bypass grafting. *J Thorac Cardiovasc Surg*. 1999;118(1):11-16. doi:10.1016/S0022-5223(99)70134-0

62.   Francesco S, Stefanos D, Romano M, Tiziano C, Giovanni P, Tiziano M. Aortic Valve Replacement through a Mini Lateral Thoracotomy with High Thoracic Epidural Anesthesia. *Innov Technol Tech Cardiothorac Vasc Surg*. 2006;1(4):160-164. doi:10.1177/155698450600100406

63.   Nifong LW, Chu VF, Bailey BM, et al. Robotic mitral valve repair: experience with the da Vinci system. *Ann Thorac Surg*. 2003;75(2):438-443. doi:10.1016/S0003-4975(02)04554-X

64.   Folliguet TA, Vanhuyse F, Konstantinos Z, Laborde F. Early experience with robotic aortic valve replacement. *Eur J Cardio-Thoracic Surg*. 2005;28(1):172-173. doi:10.1016/j.ejcts.2005.03.021

65.   Poffo R, Pope RB, Selbach RA, et al. Cirurgia cardíaca videoassistida:

resultados de um projeto pioneiro no Brasil. *Rev Bras Cir Cardiovasc.* 2009;24(3):318-326. doi:10.1590/S0102-76382009000400010

66. Bodner J, Wykypiel H, Wetscher G, Schmid T. First experiences with the da Vinci™ operating robot in thoracic surgery☆. *Eur J Cardio-Thoracic Surg.* 2004;25(5):844-851. doi:10.1016/j.ejcts.2004.02.001

67. Maeso S, Reza M, Mayol JA, et al. Efficacy of the Da Vinci Surgical System in Abdominal Surgery Compared With That of Laparoscopy. *Ann Surg.* 2010;252(2):254-262. doi:10.1097/SLA.0b013e3181e6239e

68. Vrooijink GJ, Ellenbroek TTM, Breedveld P, Grandjean JG, Misra S. A preliminary study on using a Robotically-Actuated Delivery Sheath (RADS) for transapical aortic valve implantation. *Proc - IEEE Int Conf Robot Autom.* 2014:4380-4386. doi:10.1109/ICRA.2014.6907497

69. Rosen J, Sekhar LN, Glozman D, et al. Roboscope: A flexible and bendable surgical robot for single portal Minimally Invasive Surgery. In: *2017 IEEE International Conference on Robotics and Automation (ICRA)*. IEEE; 2017:2364-2370. doi:10.1109/ICRA.2017.7989274

70. Berthet-Rayne P, Gras G, Leibrandt K, et al. The i2Snake Robotic Platform for Endoscopic Surgery. *Ann Biomed Eng.* 2018;46(10):1663-1675. doi:10.1007/s10439-018-2066-y

71. Burgner-Kahrs J, Rucker DC, Choset H. Continuum Robots for Medical Applications: A Survey, IEEE Transactions on Robotics. *IEEE Trans Robot.* 2015;31(6)(6):31(6):1261-1280.

72. Kato T, Okumura I, Kose H, Takagi K, Hata N. Tendon-driven continuum robot for neuroendoscopy: validation of extended kinematic mapping for hysteresis operation. *Int J Comput Assist Radiol Surg.* 2016;11(4):589-602. doi:10.1007/s11548-015-1310-2

73. Li Z, Ren H, Chiu PWY, Du R, Yu H. A novel constrained wire-driven flexible mechanism and its kinematic analysis. *Mech Mach Theory.* 2016;95:59-75. doi:10.1016/j.mechmachtheory.2015.08.019

74. Hong W, Xie L, Liu J, Sun Y, Li K, Wang H. Development of A Novel Continuum Robotic System for Maxillary Sinus Surgery. *IEEE/ASME Trans Mechatronics*. 2018;4435(17441903800). doi:10.1109/TMECH.2018.2818442

75. Zhao B, Zhang W, Zhang Z, Zhu X, Xu K. Continuum Manipulator with Redundant Backbones and Constrained Bending Curvature for Continuously Variable Stiffness. In: *2018 IEEE/RSJ International Conference on Intelligent Robots and Systems (IROS)*. IEEE; 2018:7492-7499. doi:10.1109/IROS.2018.8593437

76. Erbel R, Eggebrecht H. Aortic dimensions and the risk of dissection. *Heart*. 2006;92(1):137-142. doi:10.1136/hrt.2004.055111

77. Moustris GP, Hiridis SC, Deliparaschos KM, Konstantinidis KM. Evolution of autnomous and semi-autnomous robotic surgical systems: a review of the literature. *Int J Med Robot*. 2011;7(April):375–392. doi:10.1002/rcs

78. Kim DT, Nguyen VT, Cheng C-H, Liu D-G, Liu KCJ, Huang KCJ. Speed Improvement in Image Stitching for Panoramic Dynamic Images during Minimally Invasive Surgery. *J Healthc Eng*. 2018;2018:1-14. doi:10.1155/2018/3654210

79. Lowe DG. Distinctive Image Features from Scale-Invariant Keypoints. *Int J Comput Vis*. 2004;60(2):91-110. doi:10.1023/B:VISI.0000029664.99615.94

80. Bay H, Tuytelaars T, Van Gool L. SURF: Speeded Up Robust Features. In: ; 2006:404-417. doi:10.1007/11744023_32

81. Rublee E, Rabaud V, Konolige K, Bradski G. ORB: An efficient alternative to SIFT or SURF. In: *2011 International Conference on Computer Vision*. IEEE; 2011:2564-2571. doi:10.1109/ICCV.2011.6126544

82. Mountney P, Guang-Zhong Yang. Dynamic view expansion for minimally invasive surgery using simultaneous localization and mapping. In: *2009 Annual International Conference of the IEEE Engineering in Medicine and Biology Society*. IEEE; 2009:1184-1187. doi:10.1109/IEMBS.2009.5333939

83.   Zhengyou Zhang. A Flexible New Technique for Camera Calibration. *IEEE Trans Pattern Anal Mach Intell.* 2000;22:1330-1334.

84.   Cutolo, F., U. Fontana and VF. Perspective Preserving Solution for Quasi-Orthoscopic Video See-Through HMDs. *Technologies.* 2018;6(1):9. doi:10.3390/technologies6010009

85.   Blanc L, Delchambre A, Lambert P. Flexible Medical Devices: Review of Controllable Stiffness Solutions. *Actuators.* 2017;6(3):23. doi:10.3390/act6030023

86.   Jeong H, Kang B, Cheong J. Stiffness analysis and experimental validation of modular-type hybrid antagonistic tendon-driven joint systems. *Robotica.* 2018;36(11):1680-1700. doi:10.1017/S0263574718000632

87.   Loschak PM, Burke SF, Zumbro E, Forelli AR, Howe RD. A robotic system for actively stiffening flexible manipulators. *IEEE Int Conf Intell Robot Syst.* 2015;2015-Decem(c):216-221. doi:10.1109/IROS.2015.7353377

88.   Kim Y-J, Cheng S, Kim S, Iagnemma K. A Stiffness-Adjustable Hyperredundant Manipulator Using a Variable Neutral-Line Mechanism for Minimally Invasive Surgery. *IEEE Trans Robot.* 2014;30(2):382-395. doi:10.1109/TRO.2013.2287975

89.   Shiva A, Stilli A, Noh Y, et al. Tendon-Based Stiffening for a Pneumatically Actuated Soft Manipulator. *IEEE Robot Autom Lett.* 2016;1(2):632-637. doi:10.1109/LRA.2016.2523120

90.   Turini G, Condino S, Sinceri S, et al. Patient Specific Virtual and Physical Simulation Platform for Surgical Robot Movability Evaluation in Single-Access Robot-Assisted Minimally-Invasive Cardiothoracic Surgery. In: ; 2017:211-220. doi:10.1007/978-3-319-60928-7_18

91.   Kato T, Okumura I, Song SE, Golby AJ, Hata N. Tendon-Driven Continuum Robot for Endoscopic Surgery: Preclinical Development and Validation of a Tension Propagation Model. *IEEE/ASME Trans Mechatronics.* 2015;20(5):2252-2263. doi:10.1109/TMECH.2014.2372635

92. Camarillo DB, Milne CF, Carlson CR, Zinn MR, Salisbury JK. Mechanics modeling of tendon-driven continuum manipulators. *IEEE Trans Robot*. 2008;24(6):1262-1273. doi:10.1109/TRO.2008.2002311

93. Camarillo DB, Milne CF, Carlson CR, Zinn MR, Salisbury JK. Mechanics Modeling of Tendon-Driven Continuum Manipulators. *IEEE Trans Robot*. 2008;24(6):1262-1273. doi:10.1109/TRO.2008.2002311

94. Iii RJW, Jones BA. Design and Kinematic Modeling of Constant Curvature Continuum Robots : A Review. 2010. doi:10.1177/0278364910368147

Appendix I:

Piecewise constant curvature hypothesis demonstrates the kinematics of flexible module to model the bending of manipulator. Based on the simplifications of constant curvature model, this method has frequently been used in continuum manipulators to demonstrate kinematics effectively [72,92,93]. Different formulations to calculate forward kinematics like Denavit–Hartenburg (D-H) parameters, Frenet–Serret (F-S) frames and exponential coordinates [94] arrive at the same final result. In order to describe the kinematics, the global coordinate systems of the manipulator is shown in **Figure 3-16** manipulator pose and Piecewise constant curvature formulation. We consider the z-axis to be tangent to the base of the continuum robot. When $\emptyset = 0$, positive curvature $(k = {}^{1}/_{r}, k > 0)$ produces bending about the +y-axis such that produce arc with radius r in the x-z plane. Referring to **Figure 3-16** manipulator pose and Piecewise constant curvature formulation, we seek to derive mapping with a geometric argument for the arc parameters $(l(q), k(q), \emptyset(q))$ in the manipulator, as a function of $q = [l_1 \, l_2 \, l_3 \, l_4]$ which describe the lengths of four cables. As shown by the geometry in the figure 11, the radius of curvature r measured from the manipulator's radius of curvature for each individual actuator.

$$l(q) = \frac{l_1 + l_2 + l_3 + l_4}{4}$$

$$\emptyset(q) = \tan^{-1}\left(\frac{l_4 - l_2}{l_3 - l_1}\right)$$

$$k(q) = \frac{(l_1 - 3l_2 + l_3 + l_4)\sqrt{(l_4 - l_2)^2 + (l_3 - l_1)^2}}{d(l_1 + l_2 + l_3 + l_4)(l_4 - l_2)}$$
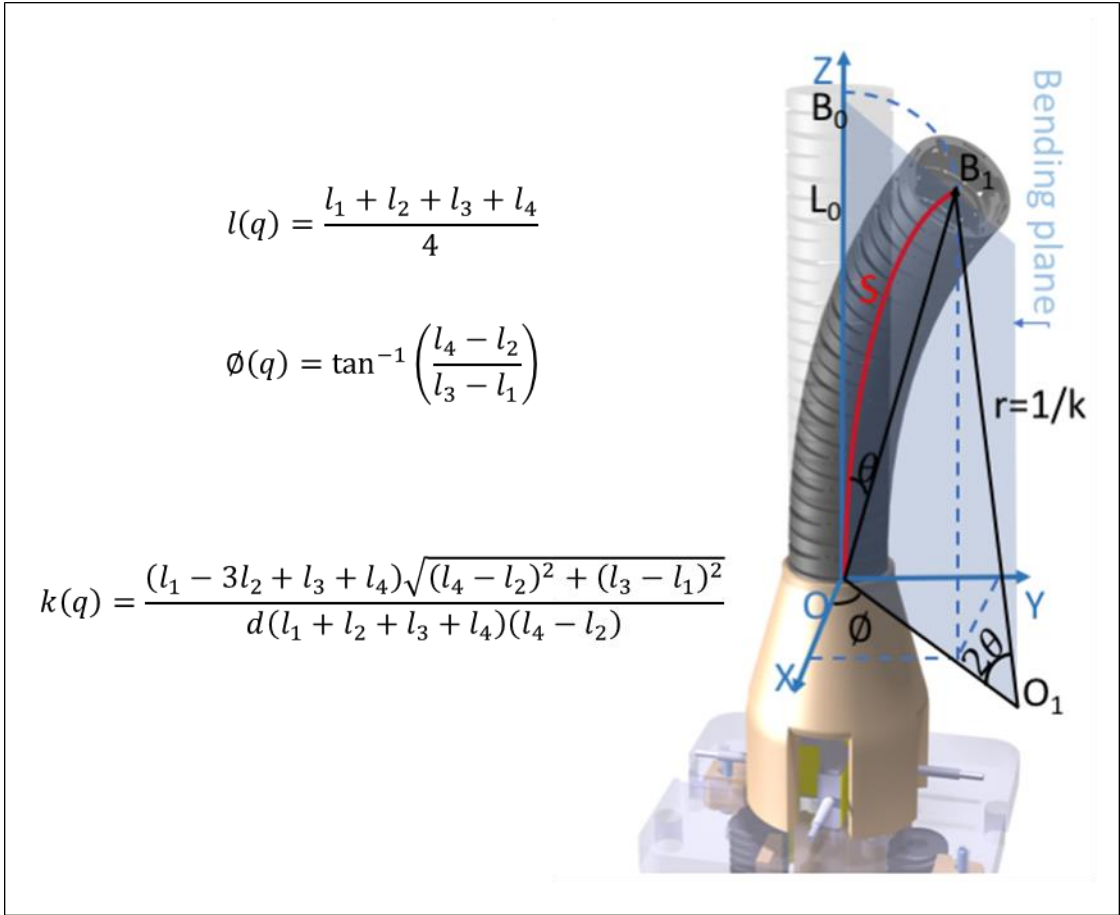

Figure 3-16 manipulator pose and Piecewise constant curvature formulation

4. Implantable artificial pancreas refilled by ingestible capsules

Part of the material reported in this chapter has been published in:

- **I. Tamadon**, V. Simoni, V. Iacovacci, F. Vistoli, L. Ricotti and A. Menciassi "Miniaturized peristaltic rotary pump for non-continuous drug dosing" 41th International conference of the IEEE Engineering in Medicine and Biology Society, (Accepted).

- V. Iacovacci#, **I. Tamadon**#, M. Rocchi, P. Dario, and A. Menciassi "Towards dosing precision and insulin stability in an artificial pancreas system" J. Med. Device., vol. 13, no. 1, p. 011008, Jan. 2019, (#equally contributing authors), **Doi:** 10.1115/1.4042459

- V. Iacovacci, **I. Tamadon**, C. Perri, P. Dario, L. Ricotti, and A. Menciassi "Towards an autonomous fully-implantable artificial pancreas" 6th national congress of bioengineering, June 25th-27nd 2018, Milan, Italy.

- V. Iacovacci, L. Ricotti, **I. Tamadon**, et al. "Towards a fully implantable autonomous artificial pancreas" 44th ESAO (European Society for Artificial Organs) Congress, 6-9 Sep 2017 Vienna, Austria.

In this chapter, the design and fabrication of an advanced prototype of fully implantable artificial pancreas refillable by means of ingestible mechatronic capsules is reported, with a special focus on mechanisms miniaturization. This activity is grounded on a pre-existing patent [1] and consisted of the design of miniaturized systems, choice and integration of actuators and testing, both on bench and ex-vivo.

4.1 Target medical problem and concept

Type 1 Diabetes (T1D) is the result of immune-mediated destruction of the beta-cells in the islets of Langerhans, the site of insulin secretion and production. The World Health Organization (WHO) reports that 347 million people worldwide

suffer from diabetes and that between 2005 and 2030 diabetes deaths are expected to double. In addition, the worldwide diabetes market is expected to reach 55 billion $ by 2019 [2]. Beyond epidemiological and economic issues related to diabetes, this pathology also has a dramatic social and medical impact. Traditional therapies to treat T1D, in fact, are unable to correctly mimic physiological insulin profiles and do not allow diabetic patients to have a normal lifestyle [3].

Current T1D therapy is based on exogenous supply of insulin. It can be performed either with insulin pens, injectiors or continuous subcutaneous insulin pumps, in which the amount of insulin to be released is calculated according to patient-specific rules envisioned by the diabetologist and to multiple daily self-monitoring blood glucose (SMBG) measurements performed by the patient [4]. This therapeutic paradigm implies that diabetic patients are almost slave of their pathology, as they must adhere to the therapy all days of their life and perform several actions per day, to manage the pathology.

An alternative to exogenous insulin injections is represented by Artificial Pancreas (AP) [3]. An AP is a device that aims at substituting the endocrine pancreas through an artificial device able to sense blood glucose levels, to determine the correspondent amount of insulin needed, and to finally deliver an appropriate amount of insulin in the body [5]. It is sometimes defined as a "mechatronic puzzle" made of three main blocks: a glucose sensor [6,7], a control algorithm [8-11] and an insulin pump [12,13]. While results obtained by the SC-SC (subcutaneous glucose sensing and subcutaneous insulin delivery) AP are certainly very promising respect to manual injections [12], especially in terms of glucose control during the night and reduction of number of hypoglycemic events, important limitations are inherently present in this technological route [5]. The major bottleneck is the SC site of insulin delivery which, by introducing a significant delay and variability in insulin appearing in plasma, renders the glucose control extremely difficult, especially after a perturbation, e.g. a meal or an exercise [12].

The intraperitoneal (IP) supply route, which implies the infusion of insulin into the peritoneal cavity, represents a desirable alternative to SC infusion and allows the

direct absorption of the hormone into the portal circulation, thus better mimicking the physiological insulin profiles [14,15] and resulting appealing for implantation as well. AP systems can be classified as wearable or implantable, depending on the exploitation of an external or implanted insulin pump [5]. An example of a commercial wearable AP exploiting the IP supply route is the DiaPort System by Roche Diagnostics, provided with a transcutaneous access allowing direct insulin injection into the peritoneum by using an external portable device [16]. The strong limitation of this kind of systems is that T1D patients are forced to constantly control these devices, avoiding some daily activities (sport activity, showers, etc.) or modifying them. Furthermore, carrying devices (or transcutaneous gate accesses) on the body cause negative feelings of shame and embarrassment. This is also an important factor, especially in children and adolescents [12].

The concept on which this chapter is prepared aims at addressing the limitations of current APs, by developing a series of technologies enabling a fully implantable autonomous and long-term artificial pancreas, constituted of a subcutaneous glucose sensor and an intraperitoneal insulin pump, in a closed-loop control strategy (**Figure 4-1**). Implanted batteries can be charged by using a belt in a wireless fashion, through non- radiative energy transfer [17]. A portable device (e.g. a smartphone or a tablet) can receive wireless data from the central control unit, and show in real-time to the patient the current status of his/her artificial implanted organ (battery, insulin reservoir and blood glucose levels). The complete platform is featured by a novel, high-impact, refilling strategy allowing to fed the totally implanted insulin pump by means of swallowable insulin capsules (so without the need of medical intervention) [17]. This solution, when safely implemented in the system, has the potential to eradicate most of the limitations of traditional artificial pancreas listed above [18]. A prototype for a novel insulin pump is also necessary, by combining microengineering, mechatronics and biochemistry, in order to produce a miniaturized smart device able to maintain insulin stability (avoiding clotting) in the implanted reservoir for a prolonged time period, and preventing catheter obstructions. The pump is expected to be implanted close to the stomach or to the first duodenal loop, and connected to an implanted docking/aspiration system

interfacing with the stomach/duodenal wall. This will allow the use of an ingestible capsules as "insulin carriers", allowing insulin refilling in a completely non-invasive way.
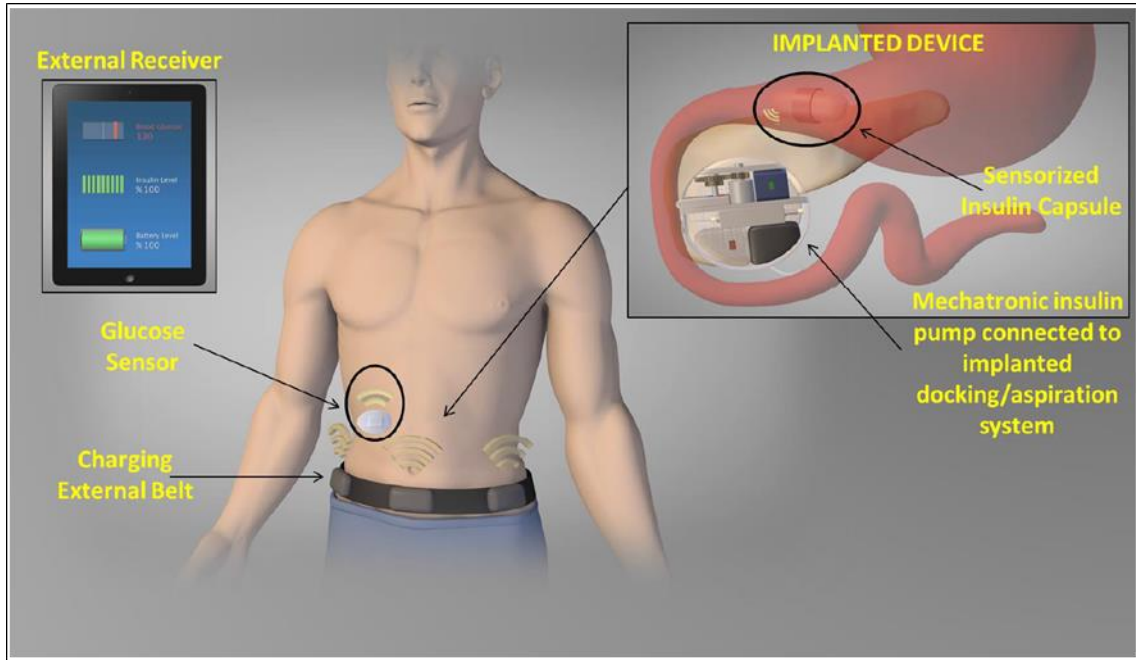
Figure 4-1 Envisioned components of the smart artificial pancreas system [17]

4.2 State of the art in the field of Artificial Pancreas

The development of APs can be traced back 50 years, when the possibility for external blood glucose regulation was established by studies in people with T1D using intravenous glucose measurement and infusion of insulin and glucose. Since the late 1990s, continuous subcutaneous insulin infusion (CSII) has become the common modality of insulin pump therapy worldwide.

- *Glucose sensors*

Since 1999 continuous (or semi-continous) glucose monitoring systems enabling retrospective data analysis of blood glucose profiles are commercially available for short time diagnostic use and treatment optimization. These systems measure glucose concentration in the interstitial fluid of subcutaneous tissue in a minimally invasive way. Main approaches for sampling are subcutaneous insertion of an electrochemical sensor or insertion of an electrochemically micro dialysis catheter.

Sensors like Medtronic's Enlite, Dexcom's G4 Platinum, and GlySens ICGMTM are already available commercially [19,20,21]. However, regular calibration using finger sticks and common glucose meters is still necessary. Most subcutaneous sensors are disposable and last for three to four days. Data on glucose levels, insulin dosing, errors and alarms are stored and can be downloaded afterwards. For glucose monitoring, precision, accuracy, sensitivity and stability are important, as well as calibration requirements, availability of results, longevity and robustness [22,23]. Continuous measurement of the glucose level is not compulsory, measuring every 10-15 minutes seems to be sufficient. Medtronic Minimed, Synthetic Blood International and Dexcom™ have performed significant research in this field. The DexCom system is implanted under the skin in the abdomen and is designed to function for up to one year. Readings are transmitted wirelessly to a hand-held receiver [22].

Other devices based on various technologies have not yet reached the market. They include the use of ultrasound (to increase permeability and transdermal transport), fluorescence, near or middle infrared light (to measure glucose based on absorption, reflection or optical rotation), or 'smart' glucose sensitive gels (that show reversible viscosity change under influence of glucose leading to controlled release of insulin [24].

- ***Algorithm-based dose controllers***

An automated control algorithm is necessary to associate blood sugar level readings and appropriate insulin dosage to administer. This algorithm should mimic the response of the pancreatic ß-cell to glucose levels, which includes different phases [25]. The availability of fast-acting insulin analogues has provided significant improvements in terms of pharmacokinetics and dynamics, as they allow reduction of insulin action variability, related to both the basal rate and the bolus infusion [3]. There are two main categories of control algorithms used for insulin closed-loop systems: proportional-integral-derivative (PID) controllers and model predictive control (MPC) algorithms [26,27]. Tuning of CSII based on subcutaneous glucose sensing and on the application of both MPC and PID, resulted effective for basal "out-of-meal" periods but it was unsuccessful in

addressing insulin needs at meal periods [28]. Partial reduction of these post-meal deviations can be obtained by the handheld programming of a priming bolus around 15 minutes before food intakes [29].

Mimicking the ß-cell response has some open issues:

1. It is complicated to emulate the insulin-secretion profile for meal and exercise;
2. Depending on the type of sensor and its location, different delays and noise in the transmitted signals will affect the system;
3. Glucose monitoring is accompanied by a delay due to glucose diffusion and measurement (subcutaneous or intraperitoneal). Thus, glucose measurements are not completely real-time [23,25,30]. Insulin absorption characteristics and sensor dynamics can vary due to a new placement of the delivery catheter/sensor [27] ,alcohol and caffeine [30];

An interface allowing manual input of information (meal announcement) about these factors into the pump controller by the patient could add to the precision of the system [30]. Meal announcement or "feedforward control" improved results [23,27,30]. APs only use insulin to control blood glucose levels, while the natural pancreas uses both insulin and glucagon. It is difficult to prevent hypoglycemia without glucagon or glucose as an additional manipulated input [27]. Research on the further refinement of control algorithms for an AP is still continuing [31].

- ***Smart insulin pumps***

Depending upon medical needs and expected duration of use, insulin pumps can be located outside the body yet attached to it (subcutaneous) or even fully implanted inside the body.

Current commercial pumps for subcutaneous insulin delivery are small portable devices, usually allowing a wireless-based reception of glycemic parameters from a connected continuous glucose monitoring device. Examples are the IR 1200®, OneTouch®, and Ping® insulin pumps by Animas Corporation, and the MiniMed Paradigm® REAL-Time Revel System by Medtronic. MiniMed paradigm is the market leader in the US (approximately 85% market share). Roche's Disetronic is the market leader outside the US (approximately 15% market share). The latest

manufacturer of insulin pumps is Insulet which produces OmniPod disposable insulin pumps [32,33].

On the other hand, when talking about implantable systems, we refer to the infusion of insulin in the peritoneal cavity that allows the direct absorption of the hormone into the portal circulation, thus mimicking in the best way physiological endogenous insulin secretion [14]. Implanting pumps are, however, more expensive. In addition, experience with implantable pumps is limited [23,34,35]. In 1999 approximately 1000 pumps were implanted [23]. In comparison with SC route, IP bolus administration provide dramatic reduction of severe hypoglycemic events, good reproducibility of insulin absorption and reduced time to peak and return to baseline [15]. Implantable pumps offer advantages for patients who have difficulty in maintaining consistent glycemic control, even using CSII [34]. However, pump pocket infections, catheter blockage, stability of insulin and device failure may necessitate surgical removal. There is only one implantable insulin pump approved and commercialized in the EU (Minimed Medtronic 2007, CE mark). This pump is implanted in the lower left quadrant of the abdomen and a 20-30 cm long catheter is placed such that the tip is in the intraperitoneal cavity. It's equipped with a refillable insulin reservoir; the refilling procedure is rather simple, being based on the transcutaneous access to a refill port by a syringe. Infection risks related to the refilling procedure can be prevented by performing it in a clean room by educated physicians, usually covered by prophylactic antibiotics before transcutaneous puncture. U400-regular insulin is filled across the skin into a pump reservoir every two to three months. Insulin delivery is modulated by the patient using an external programmer and RF telemetry, according to the results of self-blood glucose monitoring. The programmer must be synchronized with only one pump, assuring other implantable devices are not affected. The life span of the pump battery is dependent of the daily insulin delivery, but is suggested to be at least seven years.

Clinical use of implantable, programmable insulin pumps that exploit IP delivery is, however, still limited because of the refiling procedure associated with this technology. The limitations are also related to the device cost itself, but also to the man-time cost needed both to refill the pump reservoir with insulin at hospital

every 6–8 weeks and to maintain reliable insulin delivery. Indeed, it is necessary to take into account surgical burden related to eventual catheter obstructions (5-15 per 100 patient-years) and periodical pump replacement due to battery depletion every 8 years on average. Moreover, insulin aggregation in the reservoir requires specific procedures to get rid of the aggregates as the use of a specific insulin formulation [36].

An alternative option to benefit from IP insulin delivery at a lower cost and with higher patient autonomy is represented by the DiaPort® system developed by Roche Diagnostics. This system consists of a small titanium body implanted into the subcutaneous tissue of the abdominal wall, which is connected on one side to a flexible medication catheter, allowing insulin supply to the IP region, and on the other side to an external insulin pump through a catheter.

The exact location of the DiaPort is chosen individually according to the regular habits and clothing of the patient but most frequently it is implanted into the lower right or left quadrant of the abdomen. Clinical investigations have reported close-to-physiological blood glucose and plasma insulin profiles while using such ports for intraperitoneal insulin delivery [37]. However, high risk of infections due to the transcutaneous access and the need by the patient to take constantly care of theses wearable devices are the main drawbacks.

In 2009 a study was published on the testing of an intravenous glucose monitoring and intraperitoneal insulin delivery. Closed-loop system in four diabetes patients over 48 hours. A long-term sensor system (LTSS) was used, containing a sensor of Medtronic MiniMed, and was combined with an implantable physiological insulin delivery system (iPID). Quantitative information on breakfast, lunch and dinner were given. Two-day closed-loop therapy (except for a 15-min premeal manual bolus) was compared with a 1-day control phase with intraperitoneal open-loop insulin delivery, according to randomized order, in a hospital setting in eight type 1 diabetic patients treated by implanted pumps. The percentage of time spent with blood glucose in the 4.4–6.6 mmol/l range was the primary end point. The mean percentage of time spent with blood glucose in the 4.4–6.6 mmol/l range was

significantly higher (40% vs. 28%), and overall dispersion of blood glucose values was reduced among patients [38].

So far, the advantages of the intraperitoneal route are plasma insulin profiles and insulin action closer to the physiological ones [39], whereas still limited availability of insulin delivery devices using this route and the necessity of implantation represent the main limits for the development of an artificial pancreas using the intraperitoneal route.

4.3 Concept description and overview

An Implantable Artificial Pancreas (IAP) can be considered a complex mechatronic puzzle composed of several blocks. An implanted refillable insulin pump designed in this thesis work is shown in **Figure 4-2**. The proposed implantable device consists of:

- A docking/punching system interfaced with the gastrointestinal (GI) tract, in order to selectively dock insulin capsule-shaped carriers periodically ingested by the patient and to aspirate the insulin in a dedicated implanted reservoir;
- A functionalized reservoir connected to an insulin micropump, ensuring drug stability and clotting avoidance and enabling IP insulin supply when required;
- A dedicated electronics, able to collect data from the sensors, to manage the docking mechanisms activation/deactivation, the insulin aspiration and injection, and to wirelessly transmit data to the portable device (e.g. a tablet).
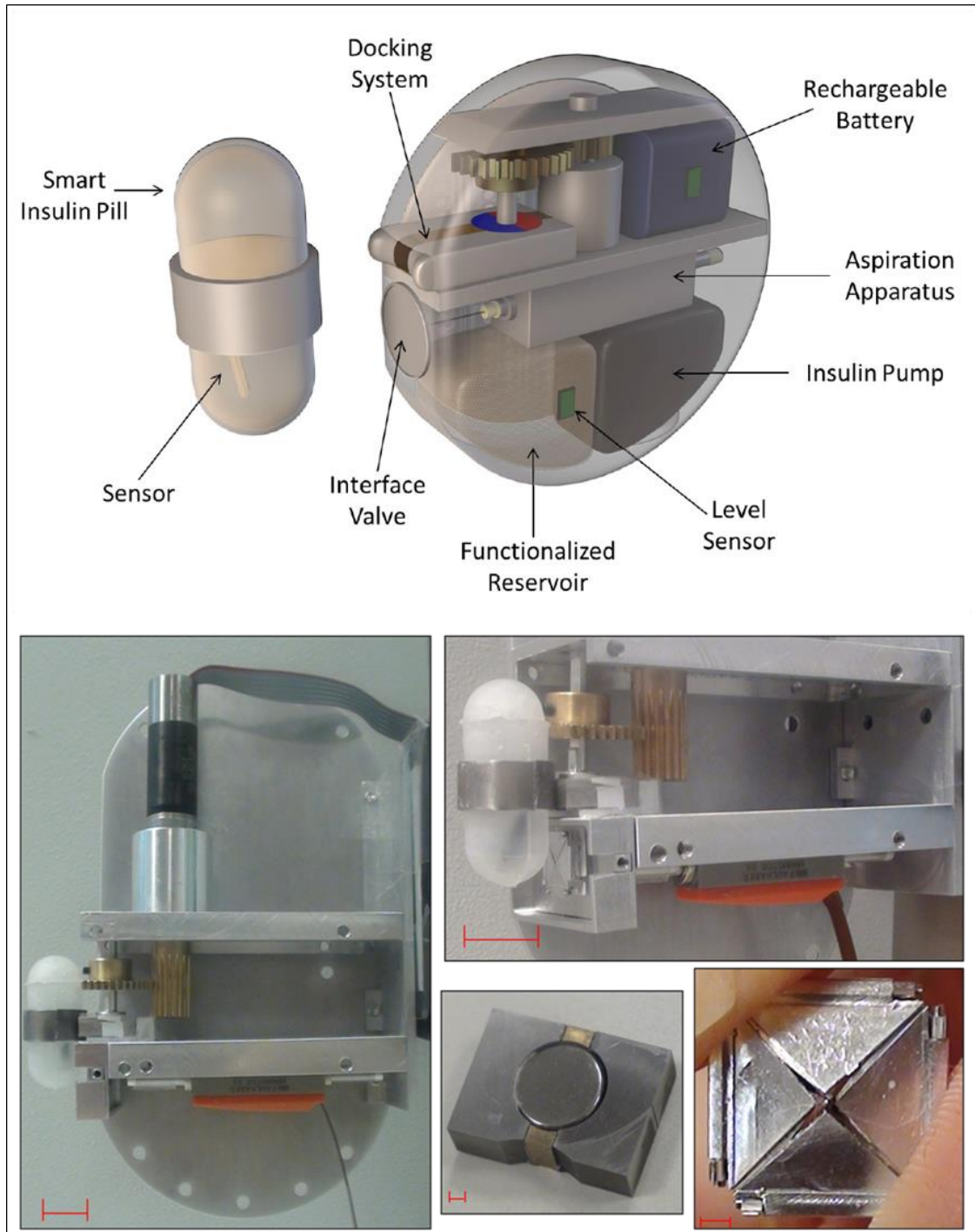
Figure 4-2 IAP concept overview (top) and initial prototype with docking actuator, MSD and capsule for proving the concept (bottom) [17]

The proposed refilling procedure [17,18] can be considered as articulated in the following sequence of actions:

1. The patient ingests the insulin capsule which is passively carried along the GI tract;

2. The reversible docking mechanism is switched on;

3. The capsule is attracted by the implanted device and stably docked (It can be recognized by variation in magnetic field);
4. After a fixed time lapse, a linearly actuated needle punches the capsule;
5. The reservoir is expanded to aspirate the insulin from the capsule;
6. Capsule undocking is commenced and the carrier is naturally excreted (**Figure 4-3**).
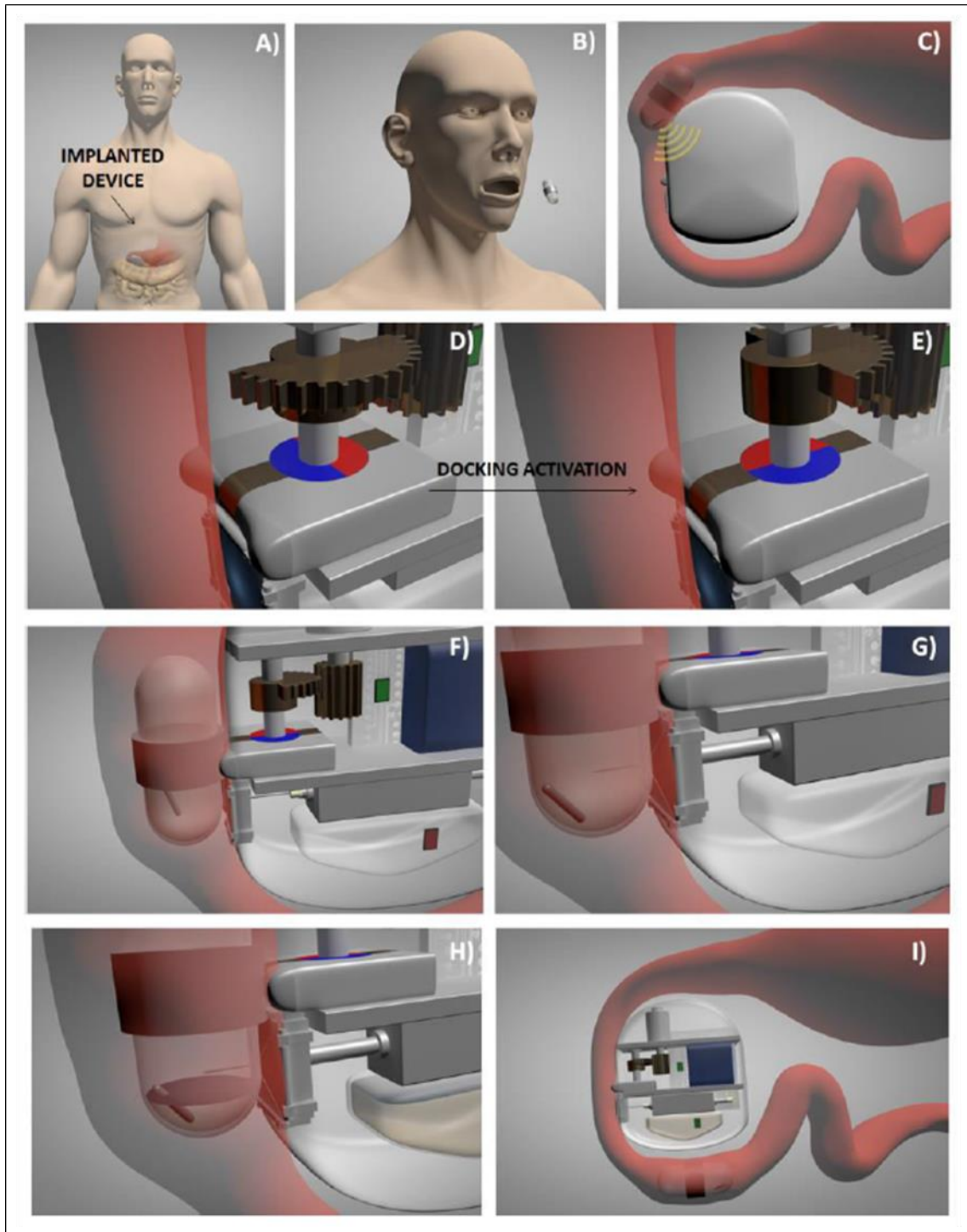
Figure 4-3 Refilling/aspiration sequence in concept [17]

4.4 Device exterior design and units

The mechanical design of the device starts with defining the suitable shape and available space in left anterior abdominal cavity. To reach this goal three shapes were selected and fabricated by 3D printing techniques (ProJet MJP3600, 3D systems, USA and VisiJet M3 crystal) with different dimensions to be placed inside

the body. Preliminary ex-vivo test on cadaver has been performed to finalize the shape and allowable size for the system.
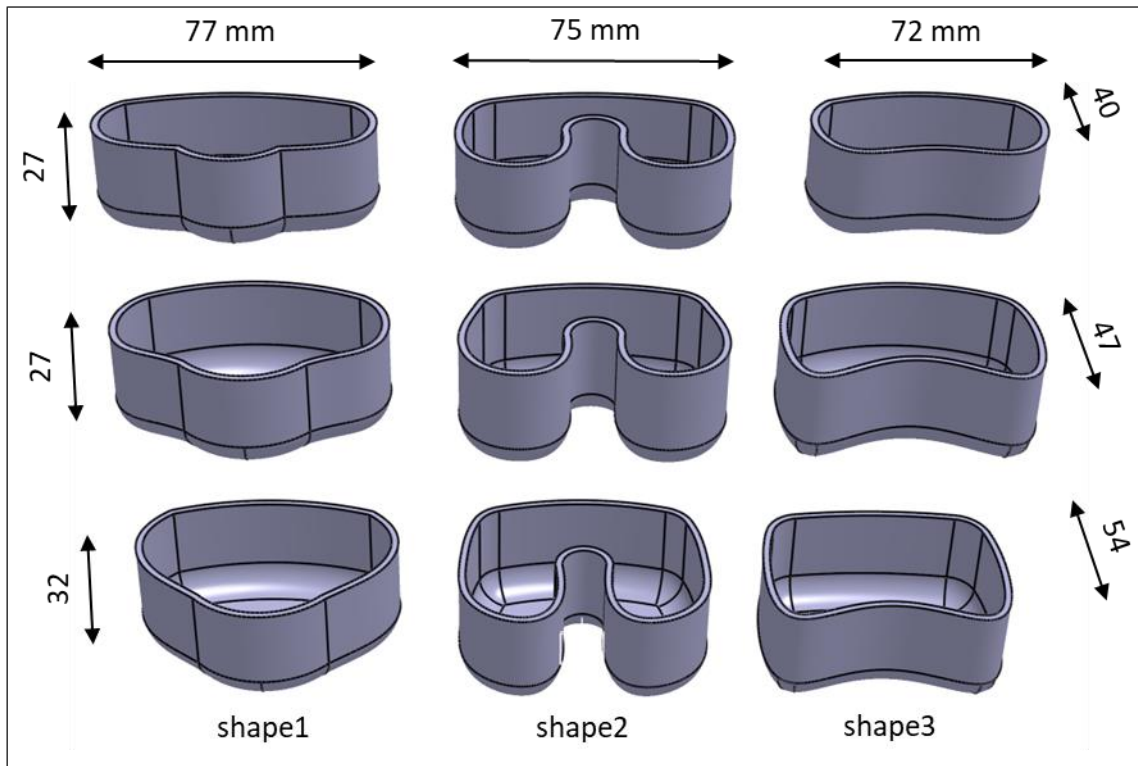
Figure 4-4 Case size and shape considerations

The first results from the surgeons was the proper shape and size. Therefore, shape3 was considered with smallest dimensions and small allowable variation in its height. So, the units described in concept is placed inside the case and electronic board and battery is positioned on top (**Figure 4-5**).

In next sections, the units are described separately and the results are presented after with final goal of reliable working to reach *in vivo* test.
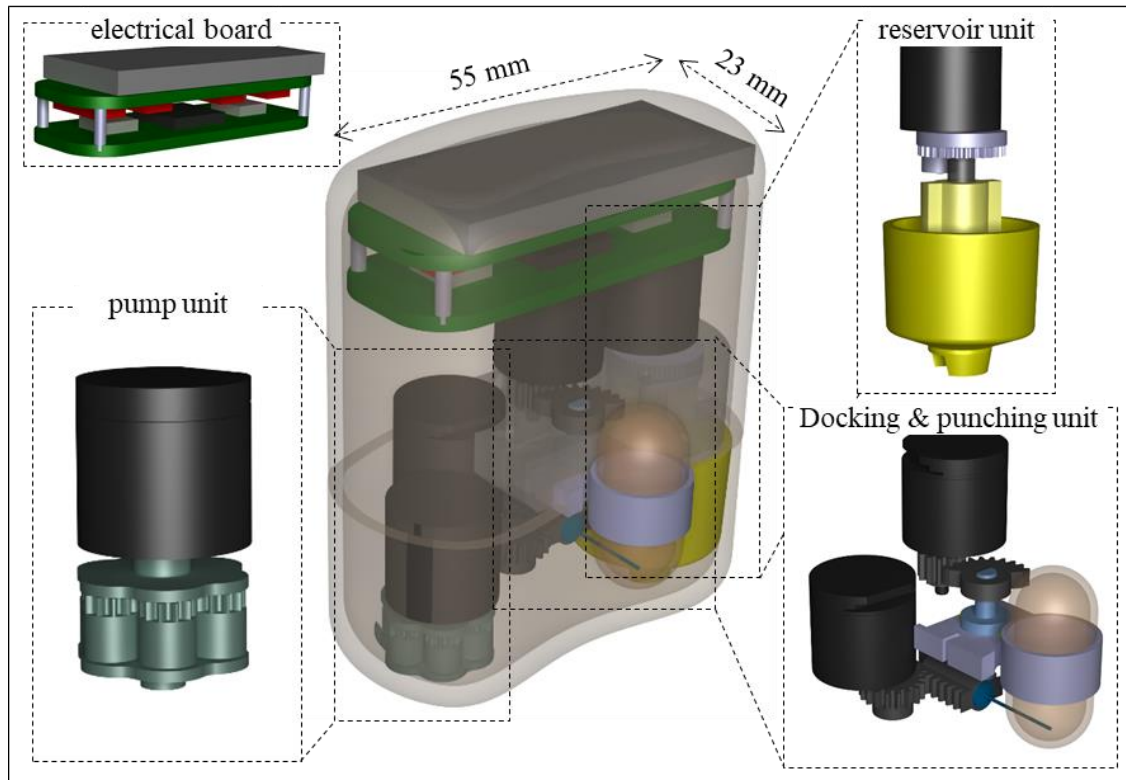
Figure 4-5 System overview and detailed units

4.5 Docking and punching system

A refilling strategy that does not require any periodical surgical procedure is the basis of the concept on which this chapter is focused. This ambitious goal, which would allow to develop a totally implantable long-term artificial pancreas, can be achieved by combining a passive insulin carrier, ingested by the patient when necessary, and an implantable docking system able to dock the carrier and to release it once depleted.

4.5.1 Docking strategy

To realize a docking system it is possible to exploit different physical and engineering strategies, in order to understand which one could represent the best solution for an AP refilling system. One of the simplest docking strategies is based on mechanical systems such as grippers and electromagnetic relays. The main disadvantage of traditional electromagnets, especially in applications in which low power consumption is a key issue, lies in the fact that to maintain an active state, it is necessary to maintain the current flow on, thus requiring high power consumption.

131

A very interesting alternative to mechanical, electromagnetic and permanent-electromagnetic docking systems is represented by Magnetic Switchable Devices (MSDs). An MSD is a ferromagnetic circuit containing central permanent magnets which, depending on the configuration of the circuit, the flux can circulate by following different routes. A rotation or a translation of the permanent magnet can reroute the streamlines in the system forcing or cancelling the flux through specific surfaces, thereby turning *ON* or *OFF* [40].
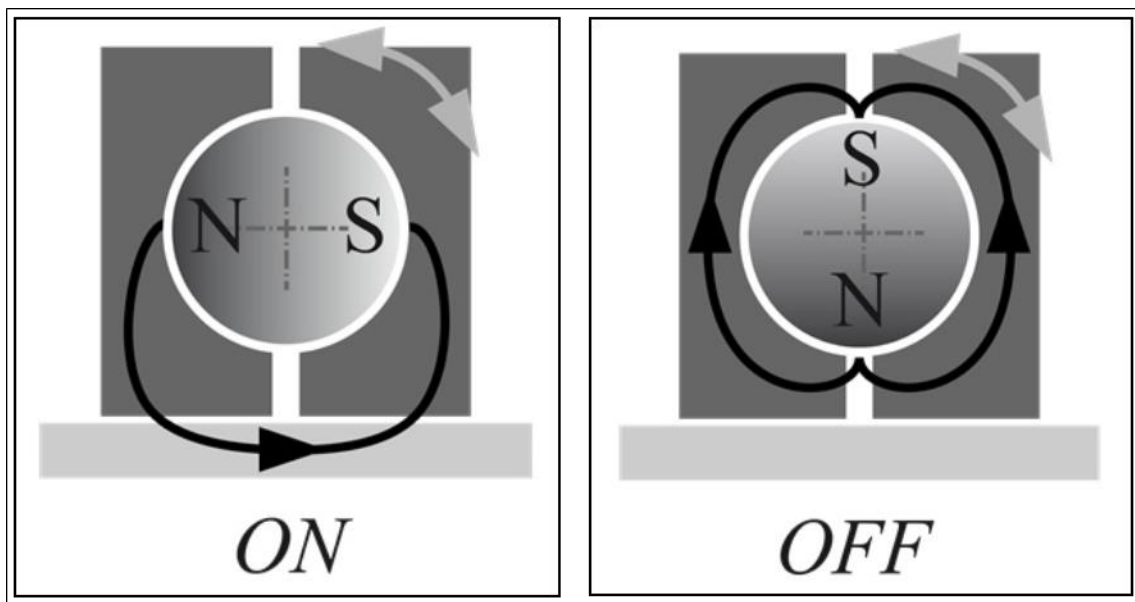
Figure 4-6 Schemes showing the working principles of a MSD. The flux lines represented in black show that in the ON-Mode adhesion accours, whereas it is completely lost in the OFF-Mode

In the MSD configuration, there are several ways to implement the insulation; but the most advantageous one is offered by a bi-metallic structure in which both ferromagnetic parts are soldered together with a diamagnetic material, e.g. brass [41]. As a rule of thumb, the maximum distance for the air-gap should be less than half the distance between the two iron guides for the stator, otherwise flux favors internal leakage from the MSD, decreasing the adhesion force [42].

For the realization of the docking system prototype, our choice has fallen on NdFeB magnets, since they are very strong, characterized by very high magnetic field and easily available in different shapes and sizes as produced through sinterization process (**Figure 4-8**).

The MSD system has to be provided with an actuation system (Faulhaber 1512U003SR324) able to assure a rotation of 90° of the magnet, triggering thus the docking/undocking of the swallowable insulin carrier. This motor was chosen because of its miniature size (ɸ 15, L 15 mm), high torque (30 mNm) and low voltage (3 V). To complete the actuation system, the prototype has been provided with an ATMEGA1284P and DRV8833 chip to drive the actuator towards the execution of the desired task. The actuation task is done by counting the encoder signals through microcontroller and control the motor in precise angular positions. Also, there is a hall sensor on one side of the MSD to track the engagement of the capsule. These data are useful to calculate the timing of the needle punching and understanding the correct alignment of the capsule with MSD (**Figure 4-8**).

To be sure that the system will work correctly, in addition to the 7 mm diameter magnet, a bigger one with diameter of 11.3 mm and a thickness of 5.5 mm, thus a volume of 551.3 mm^3, with a "safety" factor equal to two. The choice to realize also a bigger MSD prototype arises from the wish to ensure correct and stable capsule docking; in case of the small MSD system fails in docking procedure or in case the docking results not sufficiently satisfying, it would be possible, with the same overall design and the same actuators, to exploit a second MSD system that, thanks to a bigger magnet, would surely be able to exert higher adhesion forces.

After the preliminary design phase, it has been necessary to verify if the magnetic behavior of the docking system was suitable for this application so if in passing from ON to OFF configuration, the desired undocking-docking process did effectively take place. To make this check and to see how variations in geometry, magnet and ferromagnetic material could influence system operation, simulations exploiting a Finite Element Method (FEM) software (COMSOL Multiphysics® 4.3), have been carried out.

Simulations have been carried out using Comsol's AC/DC Module and in particular in the Magnetic Fields No Current condition. The system has been studied in stationary condition being the magnetic field generated by a permanent magnet and being the system behaviour stable and stationary.

The whole MSD structure, including both rotor and bimetallic stator, has been imported using the COMSOL Multyphysics CAD Import Module, whereas the swallowable capsule has been represented as a hollow cylinder surrounded by a 7 mm high ferromagnetic ring.

The aim of simulations was to study how magnetic field streamlines oriented themselves into the MSD surrounding, and how they differently intercepted the ferromagnetic target in the two configurations.

In **Figure 4-7** it is evident how in the ON configuration, magnetic field streamlines effectively crossed the ferromagnetic ring surrounding the capsule before closing themselves on the magnet opposite pole; this flux route produced a significant adhesion force on the target probably allowing its docking. On the other hand, in the OFF condition, streamlines do not cross the ferromagnetic target thus not exerting an appreciable adhesion force on it.
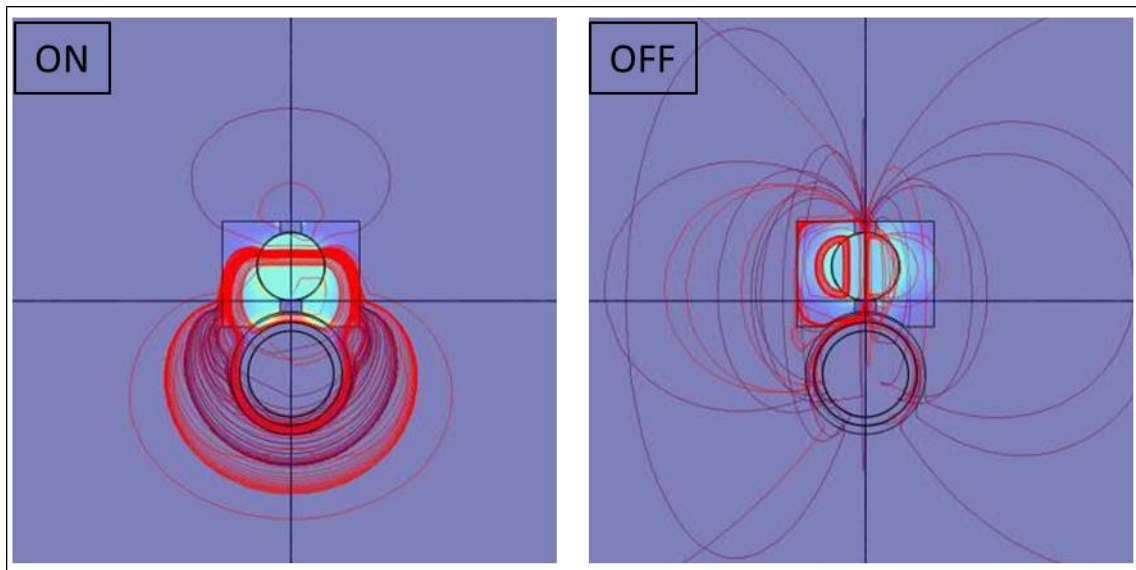
Figure 4-7 MSD in the ON/OFF configuration when capsule attached.

4.5.2 Ingestible insulin capsule

Once described the docking system working principles and design phase, attention has been focused on another fundamental component: the swallowable insulin capsule. The need to have a completely passive carrier arises from the wish to make the insulin capsule low-cost and available on a large scale in pharmacies, as all the other insulin-based products; furthermore, the passive nature of the carrier

allows a strong simplification of the artificial organ which is already both structurally and functionally quite complex. In order to allow geometrical complementarity with MSD ferromagnetic stator and to not compel patients to swallow insulin capsules too frequently, inspiration has not been taken from pharmaceutical capsules, that are typically very small, but from endoscopy capsule. A great advantage derived from the recourse to a "large" capsule is the reduction of the refilling frequency thus of the number of times the system is activated. This allows power consumption decrease and battery lifetime extension.

In particular, attention has been focused on passive endoscopy capsule and their dimensions have been considered as a reference point in the insulin carrier dimensioning phase. It can be seen as most common dimensions are 11-13 mm for the diameter and 24-31 mm for the length.

According to the reported considerations on endoscopic capsules and on GI tract anatomy, it has been decided to provide the system with a polymeric swallowable capsule 30 mm in length and 12 mm in diameter surrounded by a ferromagnetic ring 7 mm high. Capsule prototypes have been realized in polydimethilsiloxane (PDMS-SYLGARD® 184) with a curing agent-monomer ratio 1:10. To realize the hollow capsule, the polymer solution has been prepared in clean room environment and used in conjunction with a custom-made mold (Figure 4-8).

Before designing the mold however it has been necessary to understand a suitable value of thickness for the capsule wall, trying to find out a compromise between the force required to punch a hole into the carrier and the need to have a capsule structure able to maintain its own shape and stability.

In order to asses which was the best carrier wall thickness, PDMS membranes with different thickness values have been prepared and tested through an Instron 4464 with a 10 N static load cell in order to quantify the force required to allow a 21G needle to punch a hole into the membrane.

Table 4.1 Punching force registered for PDMS membranes showing different thicknesses.

MEMBRANE THICKNESS [µm]	MEAN PUNCHING FORCE VALUE [N]

121	0.2327
414	0.2650
613	0.3030
1190	0.9032

On the basis of the force test results, it has been decided to realize a polymeric hollow capsule showing 1 mm-thick walls.

The following step has been to repeat Instron punching force tests (performed on the membranes) on the 1-mm thick capsule in order to verify the accuracy of the interpolation process and to verify the general hypothesis made. Such tests have been carried out both using a 21 G needle, as in the previous tests, and a 31 G one. We would like in fact to exploit this kind of needle in the final system, being a 31 G needle the smallest available in insulin syringes. Mean force values registered through the Instron tests: values of 0.509 ± 0.002 N and 0.44 ± 0.020 N, have been respectively obtained for a 21 and a 31 G needles.

Dimensioned in this way, the swallowable capsule has an internal volume of about 2 cm^3, thus a capacity of 2 ml. The insulin amount that can be carried through this capsule could appear really low but it is not, if we consider that the refilling device is thought to be used in conjunction with an highly concentrated insulin formulation, such as Insuman Basal U-400 by Sanofi-Aventis or Humulin R Regular U-500 by Eli Lilly, which have a concentration of 400 and 500 IU per ml, respectively. Typically the insulin therapy dosage is of 0.5-1 IU per Kg of body weight per day so, considering an average 70 Kg man, the carried insulin would be sufficient for at least two weeks (considering Humulin U-500 insulin and 1IU per kg per day).

It is also important to observe, as already reported in the state of the art, that a too prolonged deposit of insulin into the reservoir can be affected by both insulin interaction with reservoir walls and bubble formation. Consequently, having a restrained carried insulin volume would not be such a disadvantageous issue.
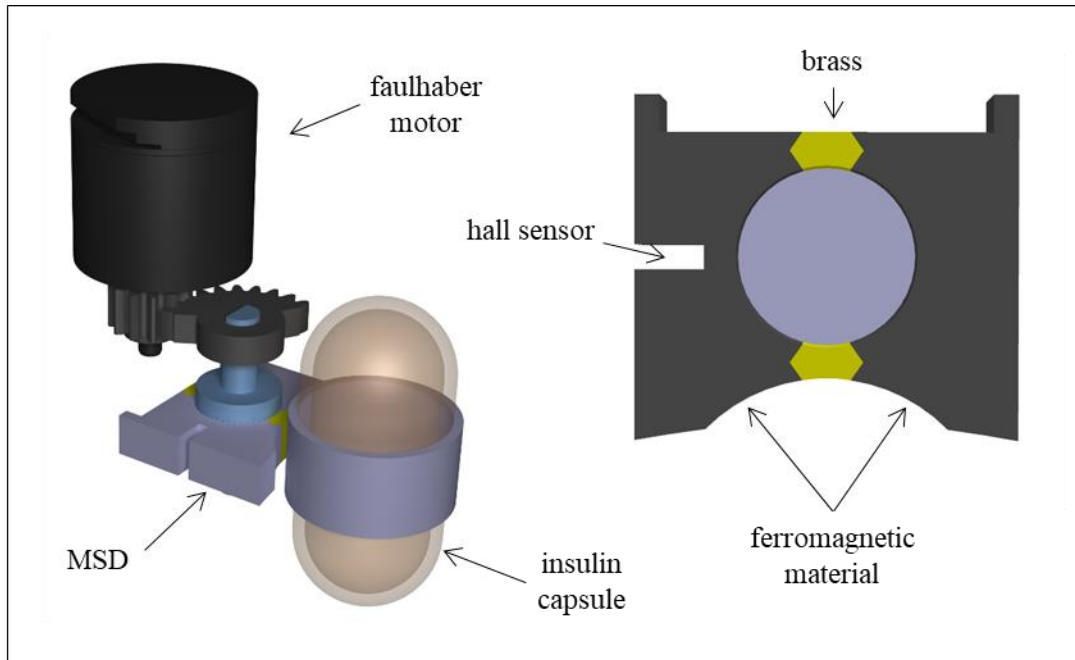
Figure 4-8 Docking unit and actuation mechanism (left), MSD details (right)

4.5.3 Linear needle actuation system

Once we found a way to stably dock the carrier, the following step is to aspirate the insulin contained in it by punching a hole into the PDMS wall. To carry out this task the system has been provided with a linear mechanism, with a needle fixed on its shaft, to punch when the capsule has already been docked, and to retract the needle when all insulin has been sucked. The same motor as docking mechanism was used here and the control unit is as the same as before (i.e. controlling the position of the motor by counting the encoder signal) (Figure 4-9).
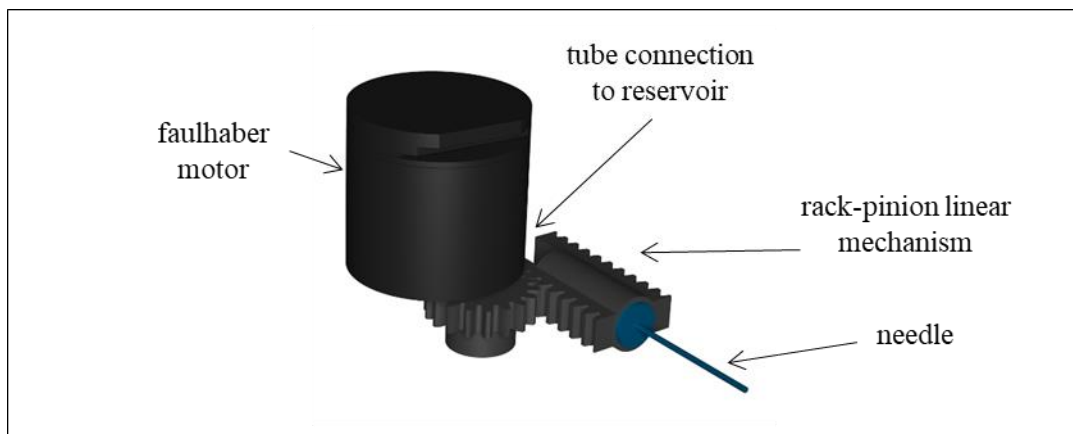
Figure 4-9 linear needle actuation mechanism

137

The docking and punching system has been tested in two configurations (with closed intestine tissue and without) to check the proper working of the system in term of adhesion and punching forces. The capsule was kept with two ropes on upper and lower part to control the capsule approaching the MSD. The lower one can move the capsule close to the MSD while the higher one keeps its weight. By actuating the MSD to ON position the capsule will be attached to the system and the upper rope will be cut. The needle mechanism will move forward and the capsule is punched (Figure 4-10). Very small motion was noticed during the punching without any closing intestine around capsule.

4.5.4 Hall sensor

In order to simplify the capsule components and make the system more robust with its attachments to MSD a Hall Effect sensor is placed in MSD to measure the magnetic fields. The hall sensor is placed in one of the ferromagnetic surroundings of the MSD in proximity of the permanent magnet (Figure 4-8). The data of this sensor is useful to assure the proper attachment of the capsule without any misalignment before and during punching. Also, by removing the RFID tag (the idea was in the concept device), the timing between docking and punching can be recognized. CYSJ106C series Hall-effect element has been selected because of its range (up to 3 T) and Sensitivity (1.8 - 2.4 mV/mT).
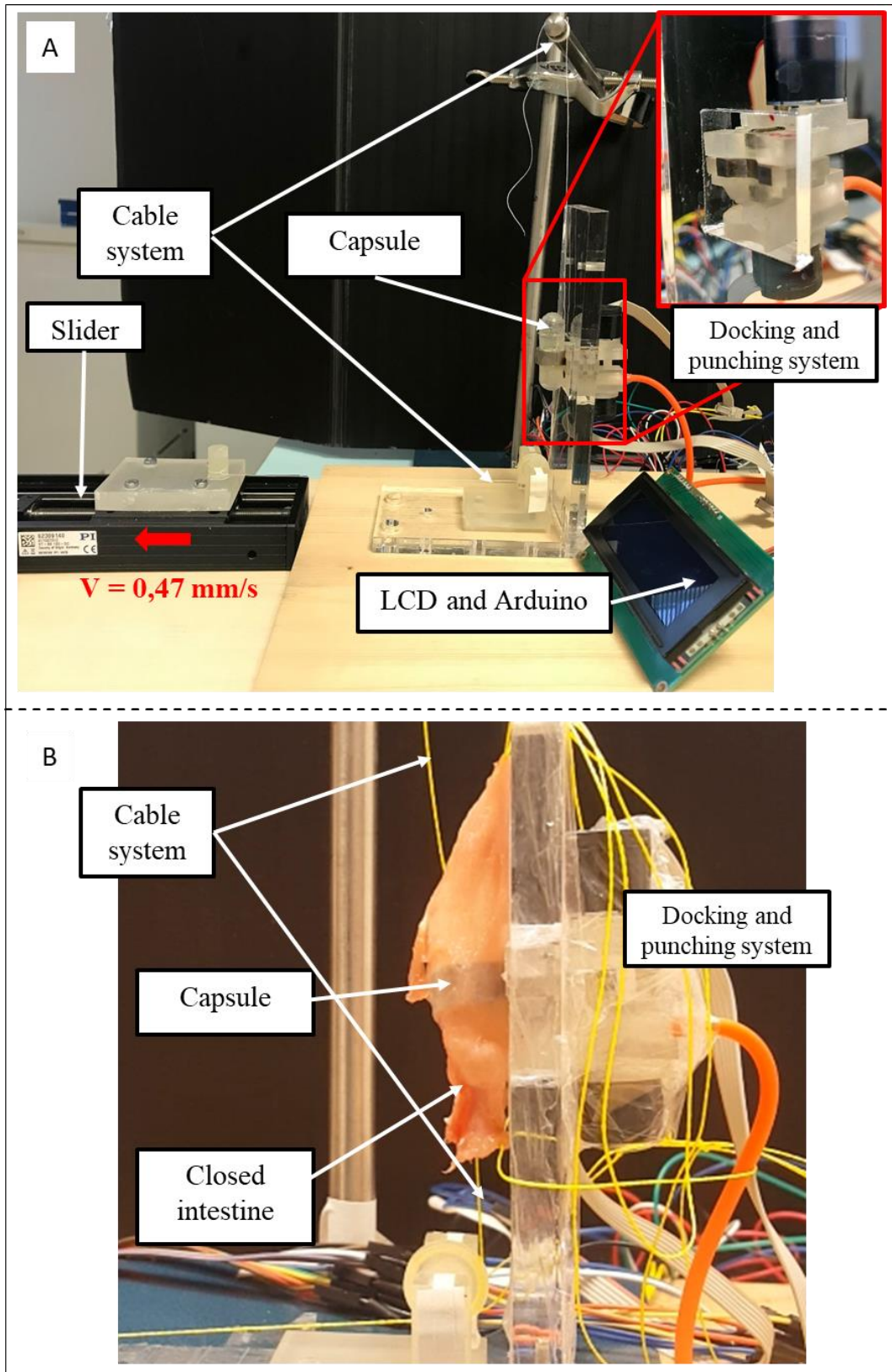
**Figure 4-10** Test experiment with docking and punching mechanism. A) The system while there is no intestine around the capsule and B) while the capsule is approaching inside an intestine.

4.6 Pump and reservoir units

Developing a smart mechatronic system for precise insulin infusion while guaranteeing insulin stability in the long term (1-2 weeks) is a major issue to be faced when designing an implantable artificial pancreas. Insulin can aggregate due to temperature, mechanical stress and contact with air or other hydrophobic interfaces; on the other hand, just few of these factors can be controlled in an implantable system (e.g. temperature is governed by *in body* conditions and cannot be controlled).

To address this challenge, we worked towards the optimization of the overall reservoir-pumping system block to be included in the AP system. Materials selection, processing, characterization and testing with insulin enabled to identify an optimal candidate for reservoir fabrication and to shed the light on the features playing a major role in insulin aggregation. The design of a bi-directional pumping system connected to an air-tight insulin reservoir was pursued to enable AP correct operation, which means both reservoir refilling and insulin precise dosing, without affecting hormone stability. The overall mechatronic block design, characterization and results will be described in the following sections.

4.6.1 Reservoir material selection, processing and surface characterization for insulin stability

It is well established that insulin can aggregate and form fibrils in certain environmental conditions [43]. These fibrils and aggregates show low biological activity and hamper AP correct operation, due to delivery systems (i.e. catheters or pumps) obstructions. Insulin aggregation kinetics is deeply influenced by mechanical agitation, insulin concentration, pH, ionic strength, temperature and interface type [44]. Significant insulin aggregation has been observed in presence of hydrophobic interfaces (e.g. with air) or mechanical agitation [45] and high surface roughness [46]. In an implanted AP, it is almost impossible to control some environmental factors, such as temperature and mechanical agitation since they are determined by in-body conditions. In order to minimize insulin aggregation, two main approaches can be followed: a pharmacological one, aiming at the development of more stable insulin formulations [47], and a technological one, based

on the choice of materials and material features preventing or limiting insulin fibrils formation. This second strategy has been considered in this work.

Many studies correlating insulin aggregation with material chemistry have been reported in literature in the last decades [47,48]. On the other hand, recent studies shed light also on the possible role played by topography [49,50].

The materials to be tested were chosen considering both data on insulin response, partly available from existing literature, and the possibility to process them through different techniques, thus enabling the fabrication of different samples presenting the same chemical composition but different morphological features. However, in all these studies, the contribution of surface roughness was never decoupled from that of material chemistry. Thus, (*i*) identifying a good candidate for reservoir fabrication, avoiding insulin aggregation, and (*ii*) decoupling the effects produced on hormone fibrils formation by surface chemistry from those produced by topography.

Two materials were tested, featured by hydrophilic (Nylon 6) and hydrophobic (Teflon) properties, each processed to obtain two different types of surface (smooth and sprayed), respectively.

Both materials were produced in the desired shapes achieving smooth surfaces, by means of lathe and milling-based manufacturing. Some samples of both materials were then furtherly processed through spray-assisted deposition: a solution of the same bulk material was sprayed on the smooth samples, thus modifying their surface topography. To this aim a Nylon 6 solution prepared by dissolving polymer pellets (7% w/w) in a mixture of formic and acetic acid (4:1 w/w) and a commercial Teflon dispersion (Sigma-Aldrich®, USA), furtherly diluted with deionized water to get a 30% w/w concentration, were employed for spray deposition. Once sprayed the solutions on the smooth substrates, thermal treatment was carried out to enable solvent complete evaporation: Nylon 6 substrates were treated overnight at 37°C whereas Teflon samples underwent a two-step treatment at 120° C (60 min) and 250° C (30 min) to enable the evaporation of water and dispersing agent, respectively.

For both materials, spray deposition was carried out by using an airbrush BD-130 (Fengda®, Fenghua Bida Machinery Manufacture CO.LTD, China) with a 0.3 mm diameter nozzle. The deposition processes were carried out at room temperature, using a 345 kPa pressure, keeping a 2 cm distance between the nozzle and the sample, and lasting 30 s for each sample.

In order to enable a better understanding of the relationship between insulin aggregation and reservoir chemo-physical properties, Nylon 6 and Teflon samples in both configurations were characterized in terms of wettability and roughness.

Optical profilometer analysis (DCM 3D, Leica, Germany), relying on the combination of confocal microscopy and interferometry techniques, was used to quantitatively assess surface roughness. Smooth and sprayed samples were scanned (1.27 x 0.95 mm^2 scanned area); the Gwyddion software was employed to process the three-dimensional surface profiles acquired.

We derived six surface parameters [51]: (*i*) arithmetic average height parameter (R_a), generally used to describe surface roughness - defined as the average absolute deviation of the roughness irregularities from the mean line; (*ii*) root mean square roughness (R_q) - representing the standard deviation of the surface heights distribution; (*iii*) skewness (Rsk) - defined as the third central moment of profile amplitude probability density function. This parameter quantifies the symmetry of the profile about the mean line, and it shows sensitivity to occasional deep valleys or high peaks. Rsk can be used to discriminate two surfaces showing the same R_a or R_q values but with different profiles; (*iv*) maximum height of peak (R_p); (*v*) maximum depth of valleys (R_v); and (*vi*) maximum height of the profile (R_t).

Insulin aggregation tests

Insulin aggregation tests were performed in dedicated vials, made from Nylon 6 and Teflon both in the smooth and sprayed configurations. In order to reduce as much as possible the risk of insulin aggregation, the vials were designed (*i*) by avoiding the presence of air, since the occurrence of a hydrophobic interface, such as the air-liquid one, could favor the formation of clots, and (*ii*) by avoiding the

presence of sharp edges, featured by a high risk to trap air bubbles, thus acting as starting seeds for insulin fibrils formation.

Aggregation tests were carried out by incubating the dedicated vials, filled with 1 ml of properly diluted Insulin (Humalog 100 UI, Ely Lilly, USA), at 37° C to resemble in-body conditions, and under continuous shaking (150 rpm). Mechanical agitation, representing one of the most influent factors in insulin aggregation, was used to test the materials in the "worst case" condition. A shaking frequency well above the one typically reachable in the body due to the subject's daily activities was chosen for the experimental evaluation. In this way, the obtained results, recorded on a time span of 14 days, could be considered reliable also foreseeing reservoir operation in a real biological environment and for a much longer period.

Material surface characterization

By comparing the two materials, in both the smooth and sprayed configurations, it was observed that Nylon 6 showed a higher mean roughness than Teflon [52]. The two materials showed comparable Rsk values in the smooth configurations, whereas the skewness was significantly lower for sprayed Teflon compared with sprayed Nylon 6.

Results

Insulin fibrils formation was evaluated through turbidimetry measures, in particular by considering absorbance values in correspondence to the 350 nm wavelength (A_{350}). The first step was the identification of a suitable insulin solution concentration that would avoid the saturation of the UV-VIS spectra, in order to efficiently carry out aggregation tests and turbidimetry measures. Several concentrations in the range 0.0125-0.4 mg/ml were tested, thus revealing that for concentrations over 0.2 mg/ml, spectra saturation occurred. Insulin solution concentration was consequently set at 0.1 mg/ml in aggregation tests.

A comparison in terms of ability to avoid or at least limit insulin fibrils formation was carried out between sprayed and smooth samples made of Nylon 6 and Teflon,

in order to shed light on the role played by surface chemistry and topography on insulin stability, respectively.

By comparing Nylon 6 and Teflon in the smooth configuration, the ability of hydrophilic materials to favor insulin stability, as already reported in the literature [48], was confirmed. After 14 days, insulin aggregation was significantly lower for Nylon 6 than for Teflon. Interestingly, insulin aggregation kinetics in Nylon 6 vials was more rapid, but it reached a plateau at day 7. Aggregation kinetics did not reach a plateau in the case of Teflon vials, either after 14 days of incubation, thus suggesting a worse long-term behavior of this material.

Samples made of the same material were then compared in the smooth and sprayed configurations. For both the tested materials, it can be observed that the spray treatment introduces a delay in the formation of the first aggregates, thus producing an extension of the initial lag phase. For both Nylon 6 and Teflon, in fact, sprayed samples were featured by a lower amount of insulin aggregates, in comparison with the smooth counterparts, at day 1. However, this trend was inverted at day 5, with significantly higher A_{350} values for the sprayed configurations in comparison with the smooth ones, for both materials. At day 14, sprayed Nylon 6 still showed a significantly higher insulin aggregation in comparison with smooth Nylon 6. Similar results, although not statistically significant, were found for Teflon.

This cross-comparison between a hydrophobic and a hydrophilic material, both in smooth and sprayed configurations, allowed to draw some conclusions and to select Nylon 6 in the smooth configuration as constitutive material for the insulin reservoir to be integrated in the AP. From our analysis, we derived that the spray treatment worsened insulin stability, independently on the material physio-chemical properties. This behavior can be explained with the increase of the number of valleys, and with the decrease of surface skewness: such valleys on vials surface may represent trapping sites for air bubbles, thus working as triggering points for insulin aggregation.

144

4.6.2 Rotary pump and variable volume reservoir

The insulin pump is one of the main components constituting an AP. A precise and reliable injection system is fundamental to properly close the loop and to avoid hypo- and hyperglycaemia episodes.

In this specific case, the micropump should be designed to guarantee an injection resolution of 1 µL. When considering a 100 IU insulin formulation, this value guarantees an accuracy equal to 0.01 IU. This is compliant with insulin infusion systems currently available on the market and exploited also for intraperitoneal insulin supply (e.g. in the AccuCheck DiaPort System by Roche [37]).

Rotary gear pumps have shown great performances in dosing systems [53–56]: they can run in low voltage with bi-directional pumping flow, thus resulting optimal candidates for the foreseen application. Pumping in a gear pump starts with rotor movement. As rotation continues, the volume progresses through the pump to a point where can escape from the chamber.

The flow rate (Q) of a rotary pump is the net quantity of fluid delivered by the pump per unit of time through its outlet port under any given operating condition. When the fluid is incompressible, the flow rate (Q) is numerically equal to the total volume of liquid displaced by the pump per unit of time (Q_d) minus the slip (Q_s).

$$Q = Q_d - Q_s \qquad (1)$$

The theoretical displacement D per revolution (where $Q_d = ND$ and N is the number of revolutions per unit time) is the amount of fluid pumped in one revolution and can be acquired by integrating the differential rate of a net volume transfer over one shaft revolution. Equation 2 shows the relation between pump displacement (D) and gears size (Z is the gear thickness, R_2 is the maximum radius of gears and R_1 is the radius of pitch circles) [54]:

$$D = \int_{\emptyset=0}^{\emptyset=2\pi} \int_{r=R_1}^{r=R_2} \int_{z=0}^{z=Z} r d\emptyset dr dz = 2\pi Z (R_2^2 - R_1^2) \qquad (2)$$

In order to reach given displacements with small and low power actuators, the power loss in the system due to fluid and mechanical friction should be minimized. On the overall, the power loss is related to the viscosity of the liquid, gaps and

speed. Increasing the gap in a pump reduces the shear stress in the liquid and the torque required to actuate the rotor. The resulting efficiency η can be defined as:

$$\eta = \frac{Q-Q_s}{Q} \qquad (3)$$

An accurate prediction of pump displacement based on its geometry is not straightforward due to difficulties in calculating the loss contribution. To derive the precise pump output, experimental validation is thus required. Usually, beyond a certain gap value threshold, which varies from case to case, performances start to deteriorate rapidly. For this reason, two gear pump designs (Figure 4-11) featured by different dimensions were conceived and dimensioned for deriving reliable guidelines for further pump refinement (Table 4.2). Experimental validation enabled to quantify the lost flow rate component and the effective pump output, thus allowing to select the best design and the driving parameters towards an optimized dosing.
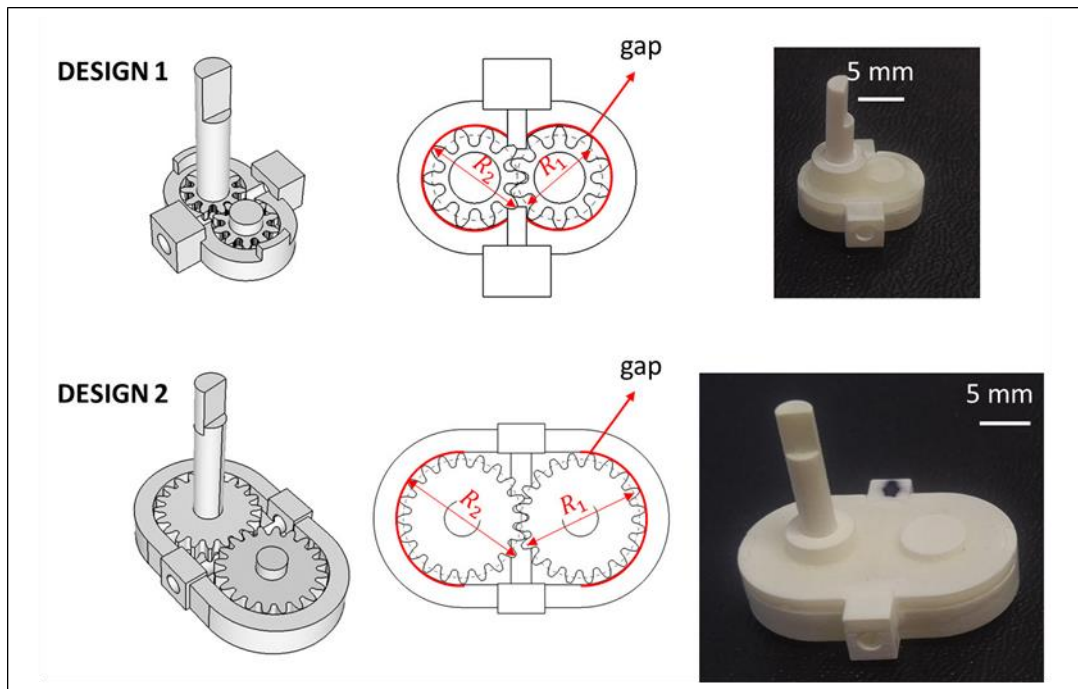

Figure 4-11 Gear pump with two different designs features: CAD design (left) and prototype (right).

Table 4.2 Rotary gear pump dimensional characteristics. D is calculated from Eq. (2).

Max radius (R_2)	Pitch radius (R_1)	Thickness (Z)	Gap	D

	[mm]	[mm]	[mm]	[mm]	[μL/rev]
Design1	3	2.5	1	+0.1	17.2
Design2	5.5	5	2	+0.1	66

A stepper motor (Faulhaber, AM1524) with 24 steps per revolution represented a good compromise between output torque and encumbrance, and it was selected to actuate the gear pump, acting as a dosing system. An integrated microprocessor (LM293 and Atmega32) was used to drive the actuator for controlling the pump output. The system was powered with 3.7 V, 220 mA/h battery. The pump was connected to a computer through a serial communication protocol to enable the transmission of inputs to the motor.

Preliminary validation was performed to assess pump resolution: optical analysis was carried out to quantify liquid meniscus advancement in a tube (1 mm in diameter) due to pump steps.

Validation performed for both gear sizes allowed to measure pump effective output due to losses and to assess the number of steps required to obtain the desired output. Once established the relationship between motor steps and pump output, it was possible to design and dimension the mechanism connecting the reservoir, the pump and the actuator. In order to favor insulin stability, an air-tight reservoir featured by variable volume should be developed: the reservoir plunge was connected to the aforementioned mechanism thus enabling to change its position, and consequently reservoir volume, according to insulin content. With the aim to increase device compactness, the insulin infusion system was designed to enable insulin injection and reservoir refilling through the same mechanism, thanks to a switch placed at the pump output and to the reverse operation of the actuation system (Figure 4-12).
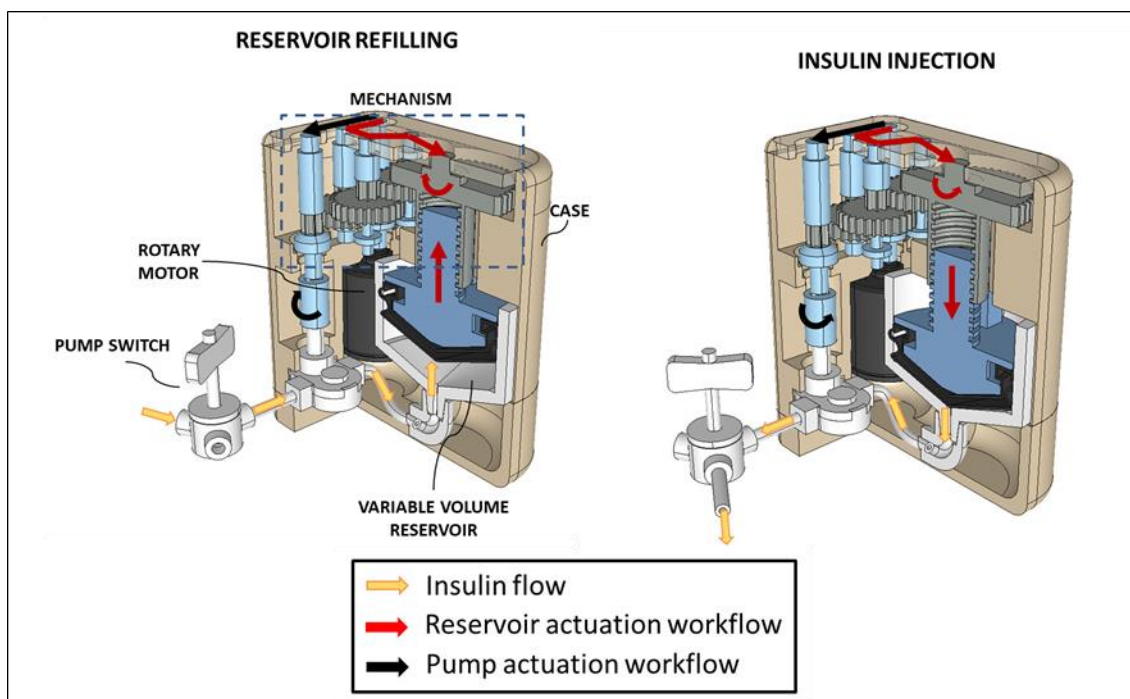
Figure 4-12 Reservoir refilling and insulin injection mechatronic block in the two operating modalities, namely for reservoir refilling through insulin aspiration (left) and for insulin controlled injection (right).

The entire mechatronic block including reservoir, mechanism, motor and gear pump was tested both to validate the reservoir refilling procedure (through mechanism reverse activation) and to perform controlled delivery. Pumping resolution and dosing repeatability were evaluated through a digital scale. Pump reliability was evaluated by performing multiple continuous 1 μL bolus ejections. Finally, the bi-directional aspiration-pumping system operation was tested during an entire reservoir refilling and emptying cycle. In this case, discrete measurements every 10 pump cycles (corresponding ideally to 10 μL ejections) were performed through a digital scale.

In order to assess the adequacy of the designed pumping system, dosing precision and repeatability were evaluated both optically and through a digital scale. The first objective was establishing the number of steps required for 1 μL injections. Both pump designs were tested and their output was quantified as a function of motor steps.

Despite theoretical calculations suggested a significant output difference between the two designs (**Table 4.2**) due to the increased gap and low rotation speed (the

148

gap is required to minimize the friction between components while using miniature stepper motors with low power), the output produced by the two designs were comparable, especially for a number of steps less than 20. This can be ascribed to the fact that in a gear pump the gap strongly influences the output, once fixed the working fluid and the chamber pressure [54]. Due to a more compact design with comparable performances in terms of desired output, Design 1 was selected for further integration: it enables to produce a 1 µL output for 18 steps of the selected actuator (**Figure 4-13**A, B).
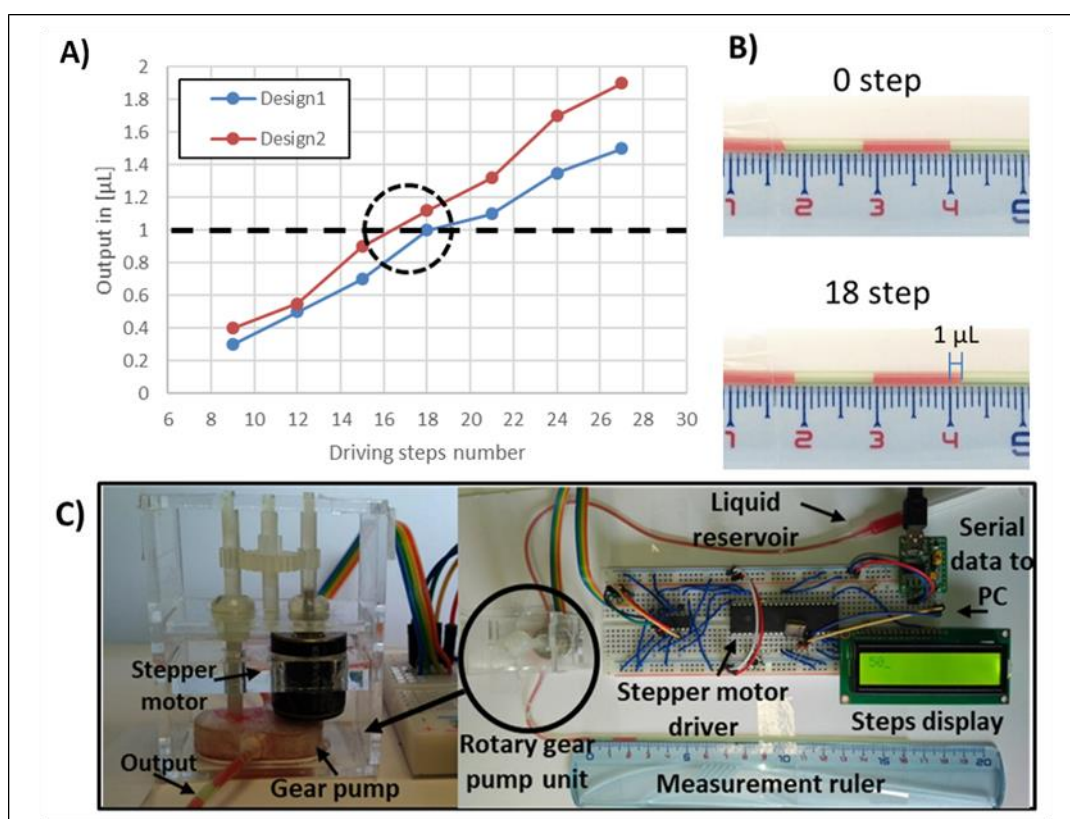
Figure 4-13 (A) Gear pumps output as a function of motor steps; (B) optical evaluation of pumping resolution; (C) experimental setup.

The reservoir was designed and fabricated from Nylon 6, which resulted the best candidate in terms of insulin stability. The reservoir was featured by a conical terminal part favoring hormone conveyance to the output; a complementary plunge provided with a hermetic sealing enabled internal volume changes while avoiding air entrance.

A 1/512 (**Figure 4-14**A) compound gear train mechanism in three stages was designed and fabricated by 3D-printer to connect the reservoir to the stepper motor and the rotary pump. This reduction ratio resulted from calculations based on reservoir cross-section (433.7 mm^2) and on the pitch of the designed power screw (1.5 mm) (**Figure 4-14**B).
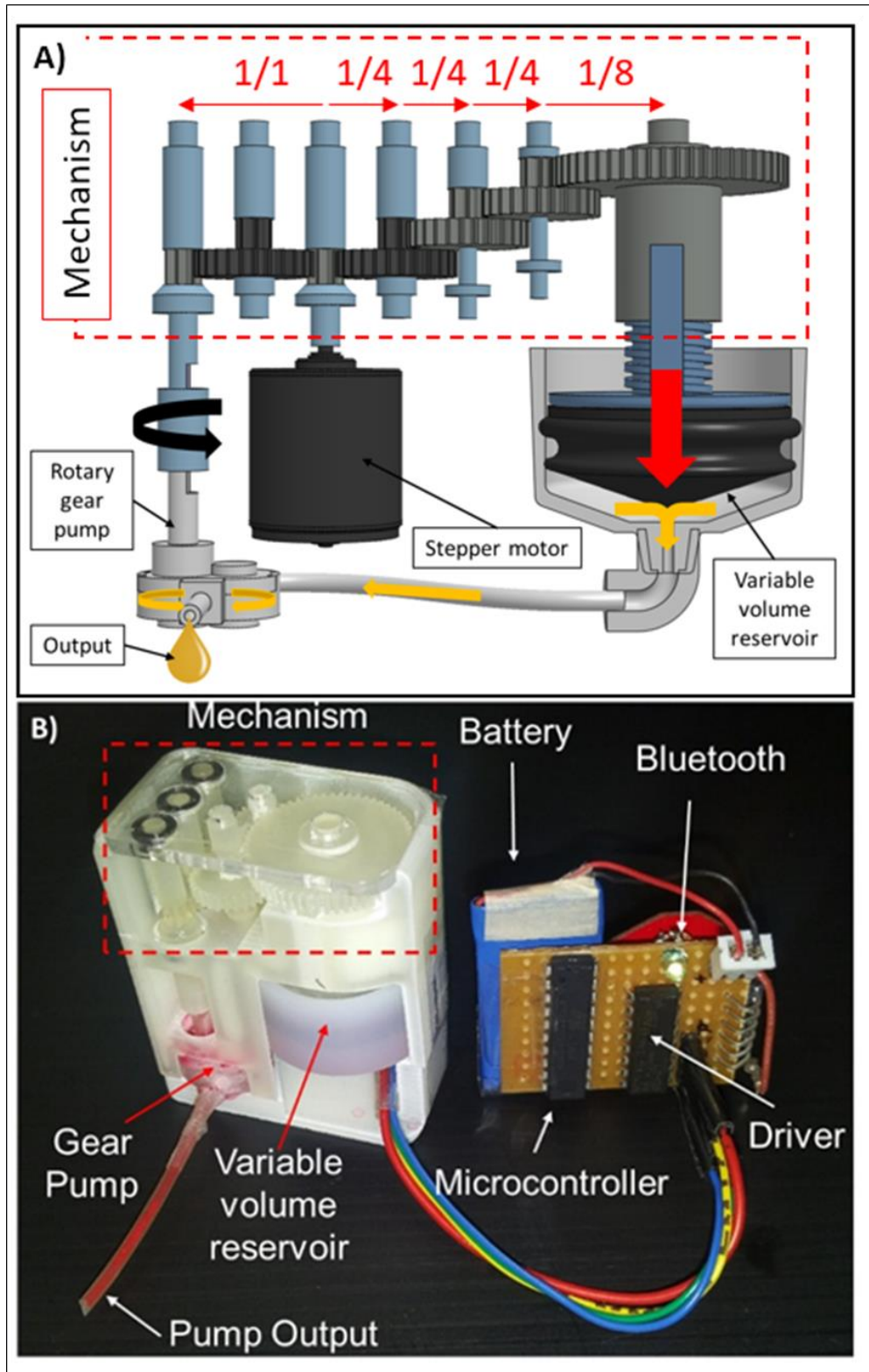
Figure 4-14 Proposed system with rotary gear pump, gear train and variable volume reservoir; B) Pump, mechanism and variable volume reservoir prototype. A Bluetooth module was integrated foreseeing future development and integration of the system.

The performances of the reservoir – pumping block were evaluated for the first 20 pump cycles after refilling, resulting in average 0.97±0.07 µL output for each cycle (**Figure 4-15**A) (each cycle is defined by considering 18 motor steps of the Design 1 pump).

The performances of the system were then assessed in the overall reservoir working range (from 3 mL to the empty configuration) by recording data every ten pump cycles. Three tests were performed to assess pump operation. Average pump 10-cycles output resulted 9.31±1.74 µL when evaluating pump operation along the overall pump range (**Figure 4-15**B, C). The possibility to switch the mechanism to enable reservoir refilling was demonstrated as well, thus confirming the ability of the designed pumping mechanism to work in reverse mode, thus ensuring system bi-directionality. The possibility to employ the same mechanism both for dosing and for aspiration allows for a significant reduction in encumbrances. Tailoring high precision and resolution in a mechanical dosing system implies a slow operation of the overall device. If this is not a major concern in dosing, this can be one issue when considering the reverse operation mode for insulin aspiration and reservoir refilling. Experimental validation of the proposed dosing system revealed that the time interval required for reservoir refilling is about 20 minutes for 3 mL insulin aspiration.

Anyhow, the limitations on the fabrication technique to reach precise gears and tolerances for proper working is one of the limitations of this pump. Also, they might need high torque for rotating and increasing gap will decrease their efficacy. Moreover, sealing of the gear case with minimum interference with material is limiting their application with fluid contamination and low power motors.
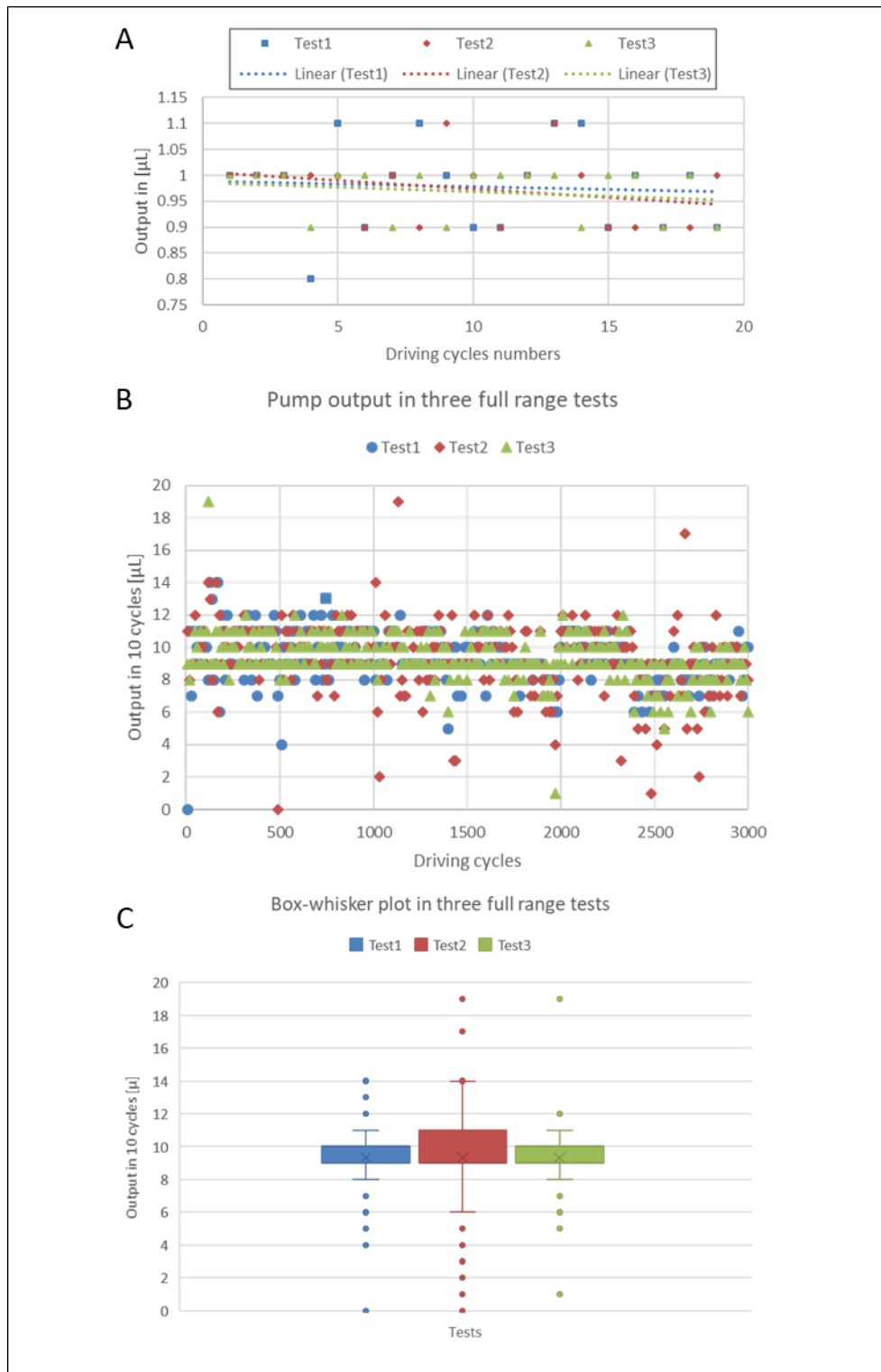
Figure 4-15 Pump output. A) The output for each cycle was measured (evaluated for 20 pump cycles); B) Three full injecting tests (Overall pump range when performing discrete measures every 10 pump cycles); C) Mean value and STD in three tests.

4.6.3 Peristaltic rotary pump in non-continuous drug dosing

Recently, innovative solutions have been proposed to minimize pump dimensions or to remove batteries, thus making them more suitable for implantable systems. Lee et al. designed a novel implantable insulin infusion system actuated by a magnetic pen [57]. However, the control loop was not closed through any digital sensors, thus limiting the potential autonomy of the device. Piezoelectric actuators [58] show a high potential in micro scale pumping, due to their miniature size and low volumetric output. However, the operating voltage of piezoelectric pumps is typically well above the powering ranges supported by batteries suitable for implantable medical devices [59,60]. Peristaltic rotary pumps can fill this gap by ensuring low voltage actuation, ease of sealing, low impact on fluid properties and precise delivery [61]. Although peristaltic rotary pumps have been widely used since 1930's in medical applications as continuous delivering pumps [62,63], their intermittent behavior and thus their ability to work as dosing systems have been not investigated and characterized, yet. In this section, a small scale peristaltic rotary pump working as a dosing system and suitable for inclusion in implantable devices, *e.g.* artificial pancreas, is proposed. Two pump designs, based on four and five rollers, were made. Both systems were characterized to assess their maximum dosing resolution. Both pumps were actuated precisely in order to rotate the rollers by a specific angle and to perform precise intermittent injections. Pump performances were characterized when varying operating speed and operation timing.

Peristaltic pumps are positive displacement pumps used for a variety of fluids including sterile and aggressive ones [64]. The fluid travels in a flexible tube that is fitted between a circular housing and a rotor including a certain number of rollers. The rollers normally compress the tube and occlude the flow [65]. As the rotor turns, *e.g.* by means of a rotational motor, the portion of fluid interposed between consecutive rollers advances through the tube producing dose ejection. Additionally, as the tube opens again when the roller moves on, the fluid is aspirated from a reservoir. Typically, depending on the application, the pump includes two or more rollers transporting the fluid towards the pump outlet. The

rollers can be installed in constant occlusion, as in the simplest designs, or can be spring-loaded to maximize tube lifetime. Generally peristaltic pumps have simple designs without any valves, O-rings or seals that might limit the compatibility with fluids [57]. The tube is the only component entering in contact with the fluid and should be made of a material chemically compatible with the target drug. Furthermore, the tube should be featured by specific mechanical properties combining at the same time high elasticity (to favor occlusion by the rollers) and high resistance to mechanical stresses, to keep the circular cross section stable upon repeated pump cycles.

The performance of peristaltic pumps is mainly affected by the entity of tube compressed between the rollers and the housing. Low compression can cause slip back or leakage to the output whereas high compression leads to a reduced tube lifetime, so an optimal level of compression should be pursued. The term occlusion is used to indicate the minimum gap in the pump based on the flexibility of the tube. In order to properly design the pump, the gap can be calculated based on tube thickness (t) and expected tube occlusion:

$$\text{occlusion} = \left(\frac{(2t\text{-gap})}{2t} \right) *100 \qquad (4)$$

The occlusion is typically 10-20%, with a higher value for softer tubes and lower for a harder ones. Pursuing an optimal occlusion, thus selecting the proper carrying tube, is very important for both guaranteeing the proper operating principle and to avoid fluid leakage when the pump is stopped.

Peristaltic pumps may run continuously, or they may be rotated through partial revolutions to deliver small amounts of fluid in non-continuous (i.e. intermittent) mode. The flow rate during partial rotation is determined by tube internal diameter, housing dimensions and number of rollers. The fluid volume trapped between two adjacent rollers determines the volumetric output. Typically, the dimension of the housing is constrained by available space in implantable device, so the other geometrical entities are dimensioned consequently.

In this device, we imposed a maximum volume of 12 cm^3 for the overall pump to guarantee integration in an implantable device. We imposed a diameter of 18 mm for the external housing (Figure 4-16). A relatively large thickness tube (external diameter: 3 mm, internal diameter: 1 mm - Primasil Silicones Ltd., UK), made of medical grade silicone (material ref: PR 410/40) with shore 40A hardness, was selected as the best compromise to extend tube lifetime. With reference to Figure 4-16, a 10 % tube occlusion was pursued to get maximum tube lifetime and optimal sealing. The rollers were provided with gears (10 teeth, module 0.4) on the bottom side to be engaged with a pinion gear (12 teeth, module 0.4). All rollers were caged together by the rotor, to enable their engaging with the pinion and their rotation with the same speed. The proposed pump was actuated by a DC micromotor (Faulhaber 1512U003SR 324:1) provided by a high reduction gear ratio and with an embedded optical encoder.

As mentioned, in the intermittent mode, the dose delivered through a partial rotation corresponds to the fluid volume trapped between consecutive rollers. The pump output (*dose*) can be thus calculated as:

$$dose=AR(a-2s) \qquad (5)$$

Where *A* is the internal cross section of the tube (=0.785 mm^2), *R* is the tube curvature inside the housing (=6.9 mm), *a* is the angle between two adjacent rollers and *s* is the angle that a deformed tube will form around each roller (=$2\pi/14.4$). By considering a uniform tube compression and a constant tube curvature around the rollers, *a* and theoretical pump doses can be calculated (Table 4.3).
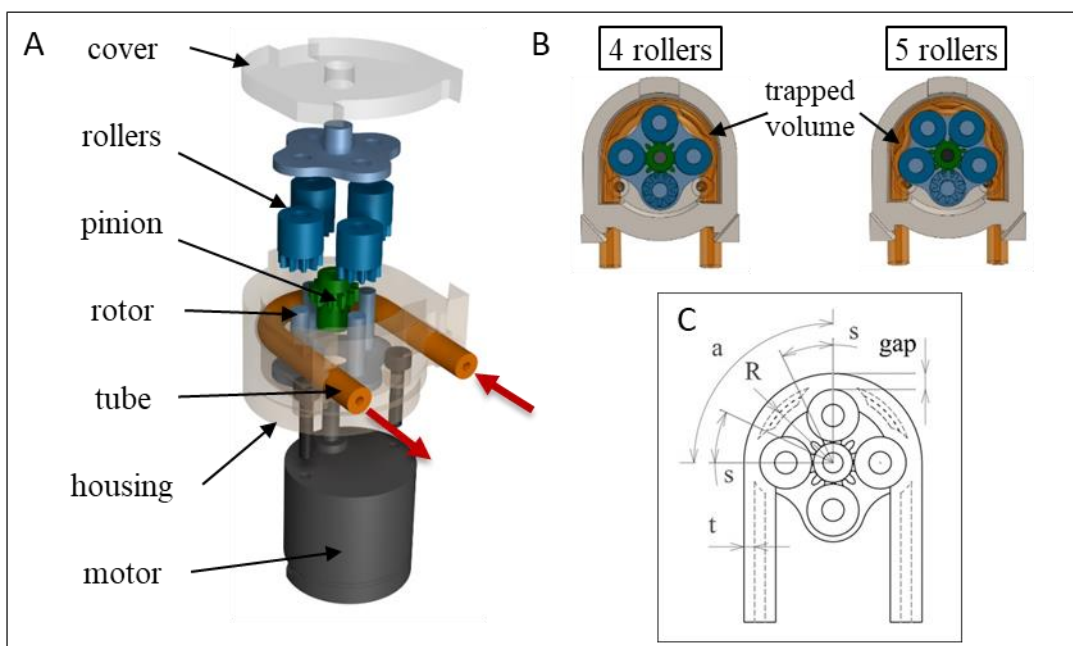
Figure 4-16 The proposed rotary peristaltic pump. A) The components inside the pump (red arrows indicate flow direction). B) Geometrical parameters featuring the pump.

Table 4.3 Theoretical dose volume

Pump type	*a [rad]*	*Dose [μL]*
4 rollers	$\pi/2$	3.78
5 rollers	$2\pi/5$	2.08

To control the pump operation, the motor was connected to a low voltage driver IC (DRV8833, Texas Instrument) and Arduino Uno (Arduino, IT). The motor's encoder was wired to Arduino's counter to precisely control the pump angular displacement. Also, for fully characterizing pump performances, the output was evaluated for both pumps designs when varying operating speed and dose delivery timing (*i.e.* by varying the delay between consecutive infusion periods). In order to modulate the pump speed, pump driving was performed through 100%, 50% and 25% duty cycle PWM signals. By this elaboration, the effects of different battery conditions (fully charged or depleted) were considered. For the four rollers pump, such an input variation corresponded to a pump speed of 15.8, 12.5 and 7.4 rpm, respectively. On the other hand, for the five rollers pump, corresponded to 15.4,

11.3 and 6.5 rpm, respectively. This small difference can be ascribed to the higher resistance load on the motor produced by the five rollers pump.

The Arduino program provided different delays between consecutive releases. This aimed at characterizing the pump in a non-continuous operation mode simulating real on demand drug delivery working scenarios which require intermittent release (e.g. a certain amount of doses followed by a certain lag time). In particular, five intermittent release conditions were evaluated to evaluate the impact of the lag time on dosing precision: continuous rotation (without any lag time), 5, 10, 20 and 60 s of lag time between each release task. Lag time was introduced every 90° for the four rollers pump and every 72° for the five rollers pump, to let advance precisely the amount of volume comprised between consecutive rollers.

Experiments were performed for both pump designs by varying the driving parameters and by measuring correspondingly the fluid amount transferred by the pumps from a 4 mm^3 cylinder reservoir to a Petri dish. The Petri dish was placed on a laboratory precision balance (Entris, Sartorius, DE) featured by a resolution of 1 µL. The laboratory scale was connected through a serial communication (rate 5 Hz) with a PC to receive the data recorded, as in **Figure 4-17**. Thirty 90° rotations and thirty 72° rotations were performed, by varying both rotation speed and lag time between each rotation, and by recording the volume of liquid released. Data were processed by using the Matlab software (MathWorks, USA).
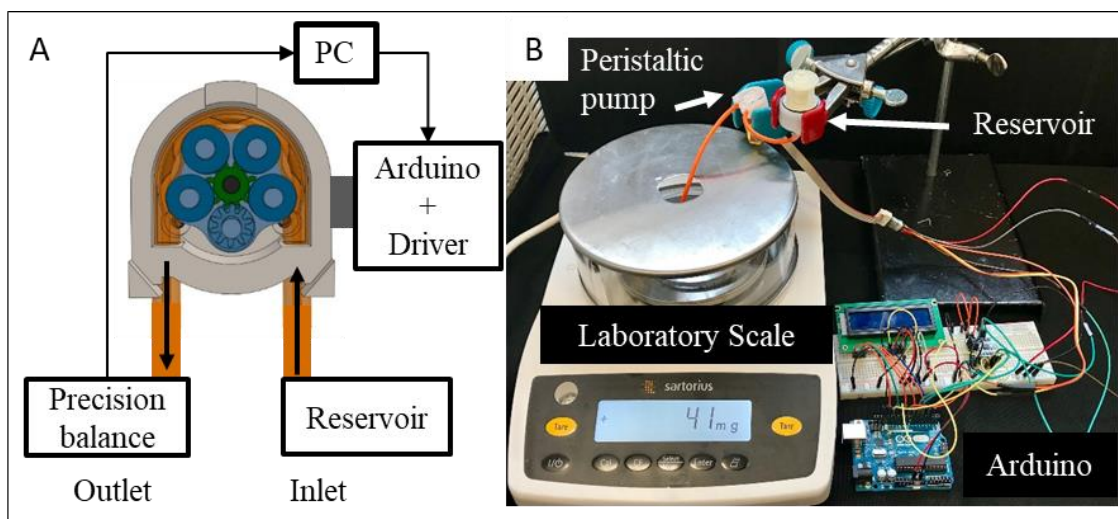
Figure 4-17 Experimental setup for testing the pumps: A) schematic representation (the five rollers pump is shown, as an example) and B) photo.

Pictures of the fabricated miniature peristaltic rotary pumps are reported in Figure 4-18. These prototypes were tested through the procedure described in previous paragraphs. Cumulative pump release upon ten pump operation steps was evaluated by varying the lag time (driving input was 100% of duty cycle PWM) and the rotation speed (with the pump running in continuous mode).
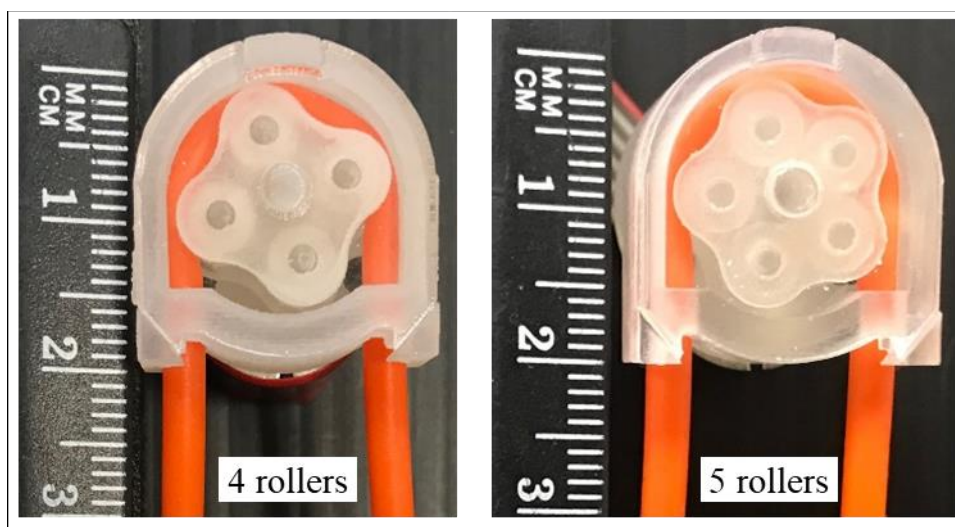
Figure 4-18 Prototypes of the proposed peristaltic rotary pumps with four rollers (left) and five rollers (right).

Figure 4-19A, B show the results in terms of volume released for the four rollers pump, while **Figure 4-19**C, D show the results obtained for the five rollers pump.

159
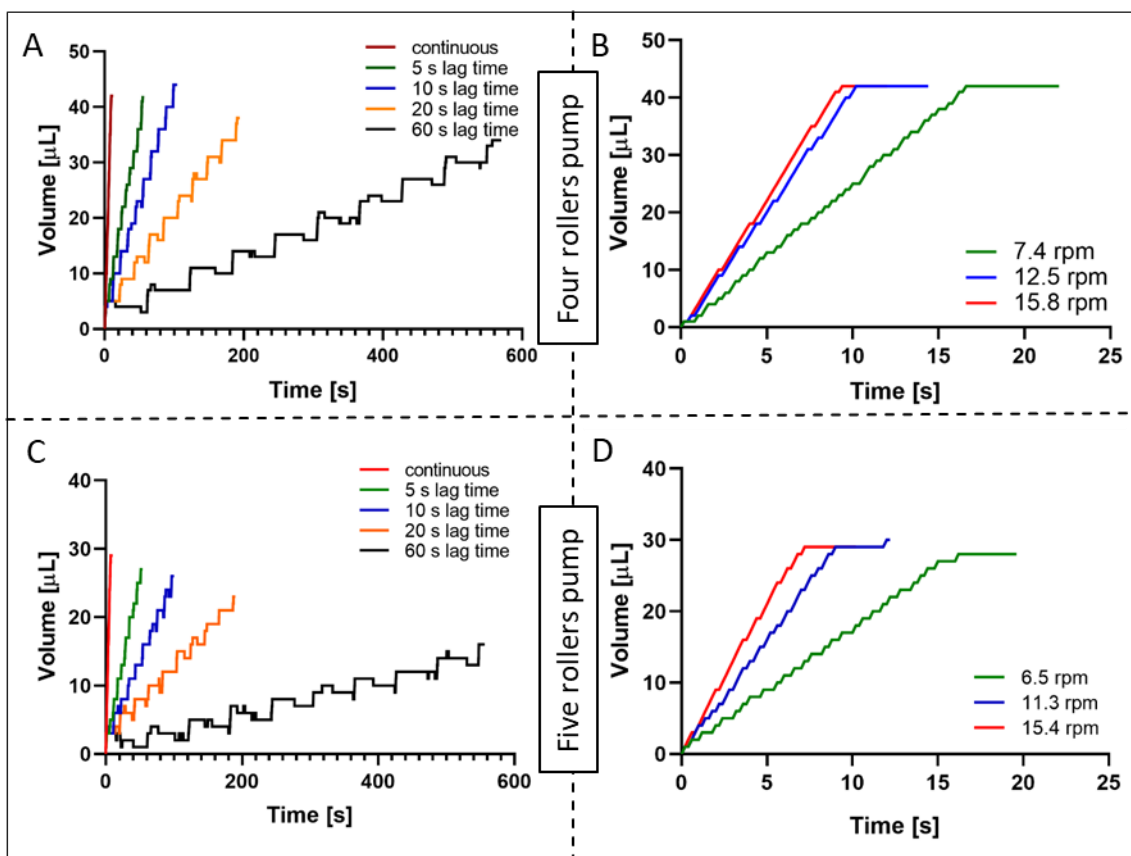
Figure 4-19 Peristaltic pump performances: A) Four rollers cumulative release over ten pump operation steps when varying lag time (at 15.8 rpm) and B) rotation speed (continuous rotation). C) Five rollers cumulative release over ten pump operation steps when varying lag time (at 15.4 rpm) and D) rotation speed (continuous rotation).

Processed data enabled to calculate pumps resolution to be compared with theoretical doses. Single step output results were grouped based on lag time and plotted as boxplot for both pump designs (Figure 4-20). Multiple coupled t-tests highlighted the absence of statistically significant differences (p-value > 0.01) when varying operating speed and lag time.
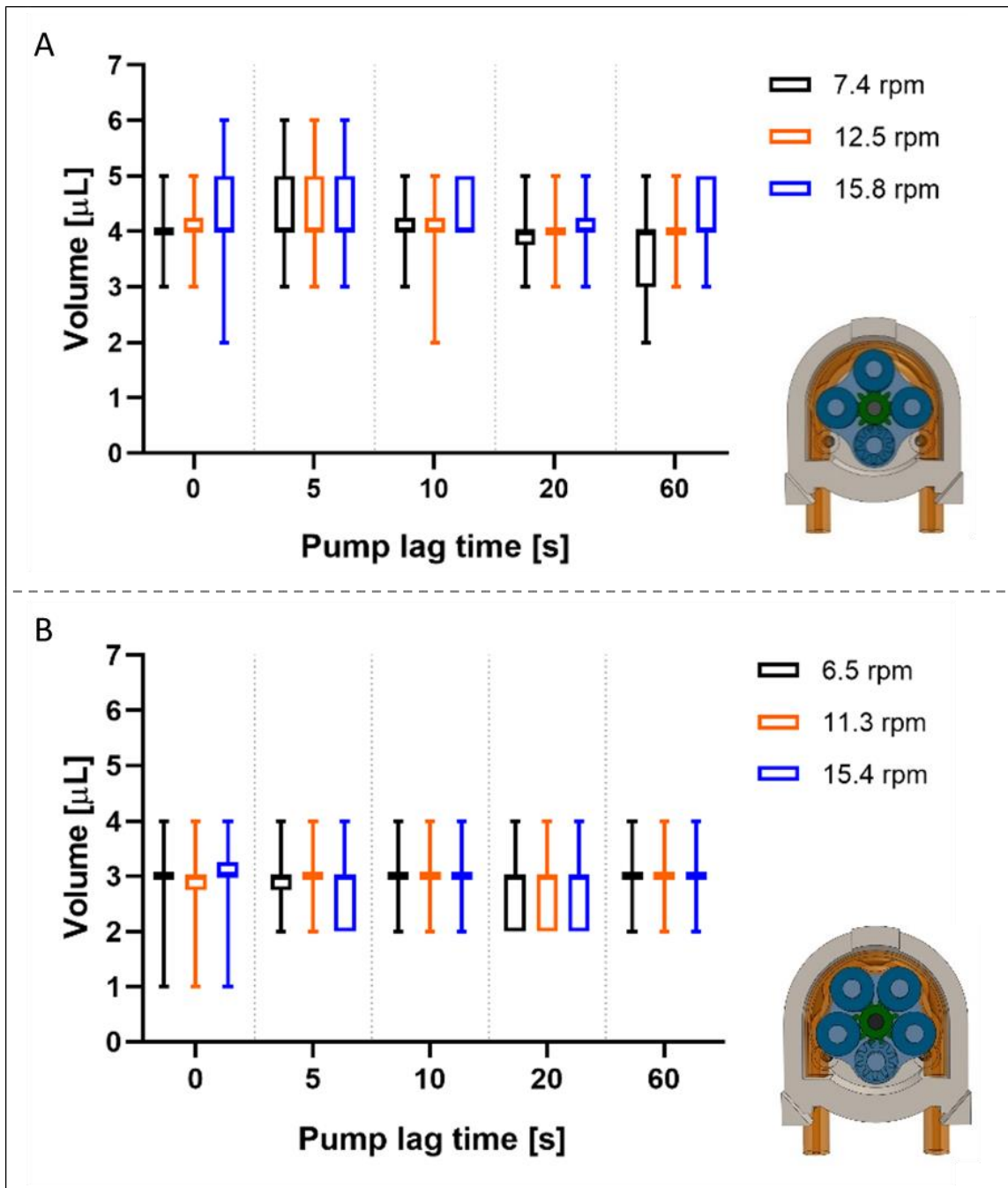
Figure 4-20 Peristaltic rotary pump in single step release for the four (A) and five (B) rollers pump. No statistically significant differences emerged (P-value > 0.01).

Based on the cumulative results in continues mode Figure 4-19B, D it can be observed that speed variation did not significantly affect the release. However, by looking at the single step release (Figure 4-19A, C), the output variance increases for both pumps when operating in continuous mode. Interestingly, the presence of a lag time between consecutive steps led to a greater output stability, especially for the five rollers pump.

For the four rollers pump, the experimental average dosing volume for a single step release resulted 4.11 µL (median value: 4 µL). For the five rollers pump, the experimental average dosing volume for a single step release was 2.88 µL (median value: 3 µL). These experimental outputs resulted in good agreement with theoretical predictions, shown in **Table 4.3**. The difference between the theoretical and the experimental output was +8% for the four rollers pump and +27% for the five rollers pump. This discrepancy can be ascribed to mechanical tolerances associated with the prototyping steps, leading to suboptimal tube compression.

The performance of the proposed dosing systems was poorly affected by speed and lag time variations. In addition, the median and average values of the dosing resolution resulted in good accordance with theoretical calculations. This confirms the reliability and precision of the proposed pumps and their suitability to intermittent operation and various rotational speed conditions. In this framework, we successfully report about the employment for the first time of small size rotary peristaltic pumps operated in non-continuous mode, in contrast with traditional peristaltic pumps with continuous operation.

These pumping system can solve the issue of the contact between fluids and pump mechanisms, thus avoiding leakages and fluid contaminations. Furthermore, the use of a simple rotary actuator enables to reduce powering and driving issues, which are always crucial in wearable and implantable medical devices. The results can lead to an effective use of peristaltic pump systems in intermittent mode in a wide variety of medical applications, including the integration in implantable devices for a precise and temporized release of drugs and hormones.

4.6.4 Smart reservoir and aspiration

In order to reach the finalized design for the implanted artificial pancreas, the only remaining block is a variable volume reservoir as discussed in section 4.6.2 for actively actuation with rotary pump. But in that strategy, the refiling time is a little high to aspirate the insulin from the capsule and this issue is not trivial when considering the real working scenario. This refiling time is lowered by help of another actuator in reservoir block and volume expanding once the needle is

punched the capsule. Moreover, the reservoir will compress the liquid as a result of injection in accordance with pump resolution (acquired by non-continuous tests) after several releases (Figure 4-21). The aspiration time is reduced to 30 seconds by adding the actuator in the system. Also, organizing the available spaces in the curved shape of the case is easier by removing the gear train and placing them a little far apart.
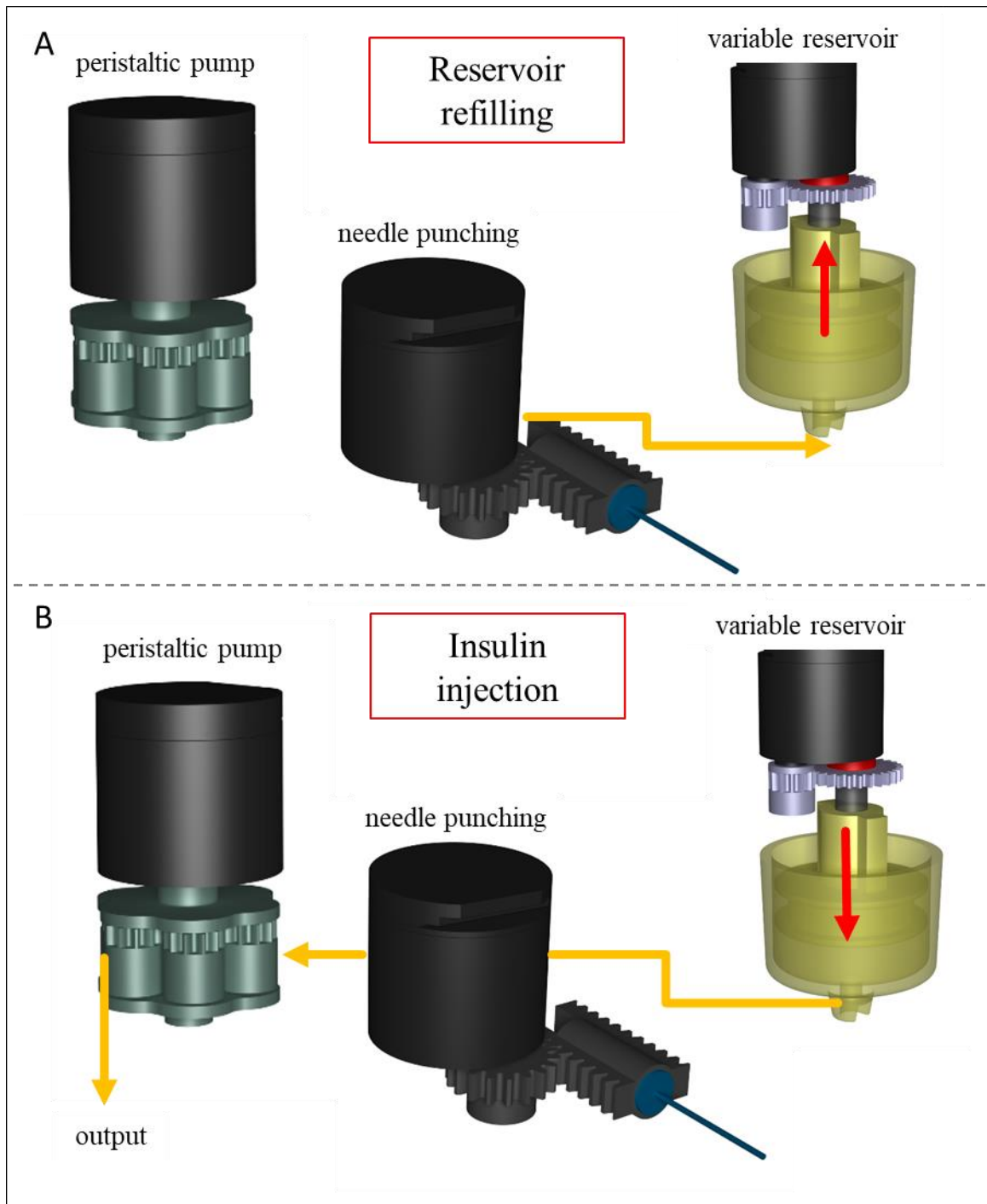
Figure 4-21 Reservoir refilling and insulin injection in two operating modalities, namely for A) reservoir refilling through insulin aspiration and B) for insulin controlled injection.

4. 7 Validation tests on cadaver

Once the prototype blocks are separately 3D printed (ProJet MJP3600, 3D systems, USA and VisiJet M3 crystal) and tested, they assembled together (just the electrical board and battery is missing) and operation tests were carried

out to verify if the system was actually able to perform the desired task (Figure 4-22A). The first complete test was performed ex-vivo on a human cadaver, in collaboration with Dr. Fabio Vistoli and other surgeons from the University of Pisa. The system was successfully implanted in the peritoneal cavity, creating a surgical pouch in which the device was positioned and sutured.

The device was implanted by surgical laparotomy. A xipho-pubic excision on the left anterior abdominal wall enabled to access the abdominal space and to create a peritoneal pouch where to lodge the device. The AP was placed between the peritoneum and the anterior abdominal wall, in a region close to the Morison's pouch. Upon pouch suturing, an intestine loop (first or second jejunal loop) was displaced and fixed to the pouch to enable the capsule-mediated device refilling (Figure 4-22D). The control unit including microcontroller and Bluetooth module is arranged outside the body in separate desk. The capsules are filled with insulin and fed through the device by help of a rope (Figure 4-22E). The magnetic docking mechanism was activated (ON state) and docking of the capsule was recognized by help of hall sensor inside MSD. After successful attachment the punching mechanism is actuated to punch the capsule. Then the reservoir is moved to aspirate the insulin from the capsule. By reaching the position of the piston to the limit, the aspiration sequence is finished and the capsule can detached from MSD (Figure 4-22F shows the collapsed capsule, from which all the insulin was aspirated). At this stage, the device is ready to inject insulin at intraperitoneal level. Every step of peristaltic pump injected 2.5µL out from the catheter (Figure 4-22G). The controller is programmed to move the reservoir every 10 step.
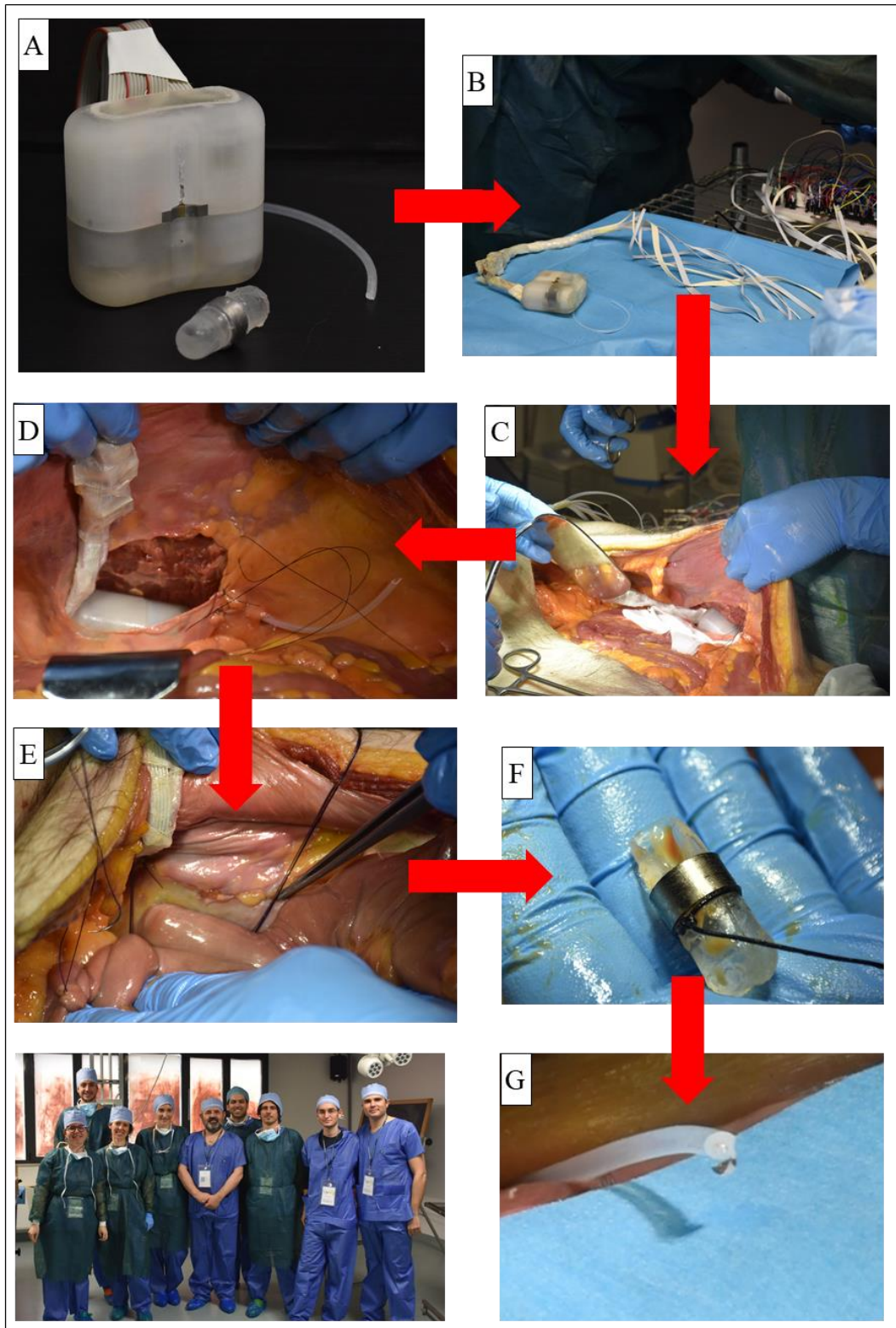
Figure 4-22 Cadaver test to evaluate the device performance. A) 3D printed prototype and capsule. B) The device and separated electronics ready for implantation. C) The device was placed between the peritoneum and the anterior abdominal wall. D) The sutures fixed the device for refilling and injection. E) The capsule is moved by help of a rope in proximity of the docking system and attached to MSD. F) The collapsed capsule when all the insulin is transferred to the reservoir by means of variable reservoir. G) The injection of the insulin by the peristaltic pump.

The actuation commands were sent to the electronic board by Bluetooth communication and a cell phone. **Figure 4-23** shows two screen shots of the terminal program and the communication data with the implant. The commands were just numbers from 1 to 7 with different tasks and the motor positions distinguished by encoder values, were monitoring continuously. Also, the Hall Effect sensor showed the situation of the capsule with MSD. **Table 4.4** shows the commands and each task of the system while **Table 4.5** shows the receiving data and their variation in terminal application for monitoring the tasks.

Table 4.4 User interface and actuation command codes

Command code	1	2	3	4	5	6	7
Task	Docking ON	Docking OFF	Punching Out	Punching IN	Pump Injection	Reservoir Decrease	Reservoir Aspirate

Table 4.5 User interface and monitoring data

Task	Docking ON	Docking OFF	Punching Out	Punching IN	Docking OFF (Hall sensor)	Docking ON (Hall sensor)	Capsule attached (Hall sensor)
Range	10	0	10	0	>415	>401	<400

Figure 4-23 Screenshots of the Bluetooth communication via IAP. First column shows the punching position, Second column is docking position and third one is the raw data of the hall sensor.

4.8 Perspectives and future work

This chapter highlighted the possibility to design and develop a mechatronic device for the refilling of artificial organs, paying particular attention to its application in totally implantable artificial pancreas. It also reviewed the design and characterization of an implantable drug delivery system able to be refilled by ingestible capsules. To reach this goal, a magnetic docking system and a dosing system based on a peristaltic rotary pump were designed and fabricated.

To realize the different components of the system we exploited a merging of competences, ranging from the implantable drug delivery systems in state of the art (whose study was necessary to identify current available systems limitations) to various pumping techniques, endoscopic capsules (for capsule dimensioning

and tracking) until technologies in grippers (in order to find out a docking strategy suitable for miniaturization, easy to implement and low power-consuming).

The system developed demonstrated the feasibility of the application of a MSD for the realization of a docking system to be integrated into a totally implantable, long-term AP and more in general into artificial organs with endocrine functions. This kind of docking allowed, in fact, to obtain a rapid, low power-consuming and miniaturized system able to attract, when necessary, a swallowable polymeric capsule provided with a thin ferromagnetic ring, and to switch off the docking, by a simple 90° magnet rotation, thus allowing capsule detachment and subsequent expulsion. It is possible to exploit a hall sensor to reveal capsule proper attachment. This configuration allow the precise evaluation of capsule position and provide the timing for needle punching.

The proposed rotary peristaltic pump has showed great results to be used inside an IAP as functioning with low voltage and small doses. Performance of the proposed dosing systems was poorly affected by speed and lag time variations. In addition, the median and average values of the dosing resolution resulted in good accordance with theoretical calculations. This confirms the reliability and precision of the proposed pumps and their suitability to intermittent operation and various rotational speed conditions. In this framework, the results successfully report about the employment for the first time of small size rotary peristaltic pumps operated in non-continuous mode, in contrast with traditional peristaltic pumps with continuous operation. These pumping system can solve the issue of the contact between fluids and pump mechanisms, thus avoiding leakages and fluid contaminations. Furthermore, the use of a simple rotary actuator enables to reduce powering and driving issues, which are always crucial in wearable and implantable medical devices. The results shown can lead to an effective use of peristaltic pump systems in intermittent mode in a wide variety of medical applications, including the integration in implantable devices for a precise and temporized release of drugs and hormones.

After having successfully tested all the designed and realized components and having a successful integration, the system will be ready for *in vivo* validations.

In future steps, the system is expected, in order to become effectively part of a totally implantable AP, to be provided also with:

- A miniaturized battery to supply the system with the power required and to exploit non radiative energy transfer that would allow system easy wireless recharge;
- Electronics boards in which Microcontroller, motor drivers, Bluetooth communication and wireless power transmitting would be integrated.

Apart from integration of electronics to make the system ready to perform *in vivo* tests, major attention has to be put on materials biocompatibility and on surgical issues, which arise from the interaction between the device and biological tissues.

References:

1. Ricotti, L.; Assaf, T.; Stefanini, C. and Menciassi A. System for controlled administration of a substance from a human-body-implanted infusion device. 2010. WO2012011132A1.

2. Gregory JM, Moore DJ, Simmons JH. Type 1 Diabetes Mellitus. *Pediatr Rev*. 2013;34(5):203-215. doi:10.1542/pir.34-5-203

3. Cobelli C, Renard E, Kovatchev B. Artificial Pancreas: Past, Present, Future. *Diabetes*. 2011;60(11):2672-2682. doi:10.2337/db11-0654

4. Chertok B, Webber MJ, Succi MD, Langer R. Drug Delivery Interfaces in the 21st Century: From Science Fiction Ideas to Viable Technologies. *Mol Pharm*. 2013;10(10):3531-3543. doi:10.1021/mp4003283

5. Ricotti L, Assaf T, Dario P, Menciassi A. Wearable and implantable pancreas substitutes. *J Artif Organs*. 2013;16(1):9-22. doi:10.1007/s10047-012-0660-6

6. Skyler JS. Continuous Glucose Monitoring: An Overview of Its Development. *Diabetes Technol Ther*. 2009;11(S1):S-5-S-10. doi:10.1089/dia.2009.0045

7.   Oliver NS, Toumazou C, Cass AEG, Johnston DG. Glucose sensors: a review of current and emerging technology. *Diabet Med*. 2009;26(3):197-210. doi:10.1111/j.1464-5491.2008.02642.x

8.   Steil GM, Rebrin K, Janowski R, Darwin C, Saad MF. Modeling β -Cell Insulin Secretion - Implications for Closed-Loop Glucose Homeostasis. *Diabetes Technol Ther*. 2003;5(6):953-964. doi:10.1089/152091503322640999

9.   Magni L, Raimondo DM, Bossi L, et al. Model Predictive Control of Type 1 Diabetes: An in Silico Trial. *J Diabetes Sci Technol*. 2007;1(6):804-812. doi:10.1177/193229680700100603

10.   Patek SD, Magni L, Dassau E, et al. Modular Closed-Loop Control of Diabetes. *IEEE Trans Biomed Eng*. 2012;59(11):2986-2999. doi:10.1109/TBME.2012.2192930

11.   Zarkogianni K, Vazeou A, Mougiakakou SG, Prountzou A, Nikita KS. An Insulin Infusion Advisory System Based on Autotuning Nonlinear Model-Predictive Control. *IEEE Trans Biomed Eng*. 2011;58(9):2467-2477. doi:10.1109/TBME.2011.2157823

12.   Renard E. Insulin Delivery Route for the Artificial Pancreas: Subcutaneous, Intraperitoneal, or Intravenous? Pros and Cons. *J Diabetes Sci Technol*. 2008;2(4):735-738. doi:10.1177/193229680800200429

13.   Klonoff DC. The Artificial Pancreas: How Sweet Engineering Will Solve Bitter Problems. *J Diabetes Sci Technol*. 2007;1(1):72-81. doi:10.1177/193229680700100112

14.   Hanaire-Broutin H, Broussolle C, Jeandidier N, et al. Feasibility of Intraperitoneal Insulin Therapy With Programmable Implantable Pumps in IDDM: A multicenter study. *Diabetes Care*. 1995;18(3):388-392. doi:10.2337/diacare.18.3.388

15.   Selam JL, Raymond M, Jacquemin JL, Orsetti A, Richard JL, Mirouze J. Pharmacokinetics of insulin infused intra-peritoneally via portable pumps. *Diabete Metab*. 1985;11(3):170-173.

http://www.ncbi.nlm.nih.gov/pubmed/3896886.

16. Hofer S, Heidtmann B, Raile K, et al. Discontinuation of insulin pump treatment in children, adolescents, and young adults. A multicenter analysis based on the DPV database in Germany and Austria. *Pediatr Diabetes*. 2010;11(2):116-121. doi:10.1111/j.1399-5448.2009.00546.x

17. Iacovacci V, Ricotti L, Dario P, Menciassi A. Design and development of a mechatronic system for noninvasive refilling of implantable artificial pancreas. *IEEE/ASME Trans Mechatronics*. 2015;20(3):1160-1169. doi:10.1109/TMECH.2014.2327196

18. Ricotti L, Assaf T, Menciassi A, Dario P. A novel strategy for long-term implantable artificial pancreas. In: *2011 Annual International Conference of the IEEE Engineering in Medicine and Biology Society*. IEEE; 2011:2849-2853. doi:10.1109/IEMBS.2011.6090787

19. Bergenstal RM, Tamborlane W V., Ahmann A, et al. Effectiveness of Sensor-Augmented Insulin-Pump Therapy in Type 1 Diabetes. *N Engl J Med*. 2010;363(4):311-320. doi:10.1056/NEJMoa1002853

20. Henry RR, Rosenstock J, Logan DK, Alessi TR, Luskey K, Baron MA. Randomized Trial of Continuous Subcutaneous Delivery of Exenatide by ITCA 650 Versus Twice-Daily Exenatide Injections in Metformin-Treated Type 2 Diabetes. *Diabetes Care*. 2013;36(9):2559-2565. doi:10.2337/dc12-2410

21. Henry RR, Rosenstock J, Logan D, Alessi T, Luskey K, Baron MA. Continuous subcutaneous delivery of exenatide via ITCA 650 leads to sustained glycemic control and weight loss for 48 weeks in metformin-treated subjects with type 2 diabetes. *J Diabetes Complications*. 2014;28(3):393-398. doi:10.1016/j.jdiacomp.2013.12.009

22. Chia CW, Saudek CD. Glucose sensors: toward closed loop insulin delivery. *Endocrinol Metab Clin North Am*. 2004;33(1):175-195. doi:10.1016/j.ecl.2003.12.001

23. Hovorka R. Continuous glucose monitoring and closed-loop systems. *Diabet Med.* 2006;23(1):1-12. doi:10.1111/j.1464-5491.2005.01672.x

24. Tanna S, Joan Taylor M, Sahota TS, Sawicka K. Glucose-responsive UV polymerised dextran–concanavalin A acrylic derivatised mixtures for closed-loop insulin delivery. *Biomaterials.* 2006;27(8):1586-1597. doi:10.1016/j.biomaterials.2005.08.011

25. Steil GM, Panteleon AE, Rebrin K. Closed-loop insulin delivery-the path to physiological glucose control. *Adv Drug Deliv Rev.* 2004;56(2):125-144. http://www.ncbi.nlm.nih.gov/pubmed/14741112.

26. Schaller HC, Schaupp L, Bodenlenz M, et al. On-line adaptive algorithm with glucose prediction capacity for subcutaneous closed loop control of glucose: evaluation under fasting conditions in patients with Type 1 diabetes. *Diabet Med.* 2006;23(1):90-93. doi:10.1111/j.1464-5491.2006.01695.x

27. Bequette BW. A Critical Assessment of Algorithms and Challenges in the Development of a Closed-Loop Artificial Pancreas. *Diabetes Technol Ther.* 2005;7(1):28-47. doi:10.1089/dia.2005.7.28

28. Pickup J, Keen H. Continuous Subcutaneous Insulin Infusion at 25 Years: Evidence base for the expanding use of insulin pump therapy in type 1 diabetes. *Diabetes Care.* 2002;25(3):593-598. doi:10.2337/diacare.25.3.593

29. Weinzimer SA, Steil GM, Swan KL, Dziura J, Kurtz N, Tamborlane W V. Fully Automated Closed-Loop Insulin Delivery Versus Semiautomated Hybrid Control in Pediatric Patients With Type 1 Diabetes Using an Artificial Pancreas. *Diabetes Care.* 2008;31(5):934-939. doi:10.2337/dc07-1967

30. Wolpert HA. A Clinician's Perspective on Some of the Challenges in "Closing the Loop." *Diabetes Technol Ther.* 2003;5(5):843-846. doi:10.1089/152091503322527049

31. Ibbini M, Masadeh M. A fuzzy logic based closed-loop control system for blood glucose level regulation in diabetics. *J Med Eng Technol.* 2005;29(2):64-69. doi:10.1080/03091900410001709088

32. Kumar A, Pillai J. *Implantable Drug Delivery Systems: An Overview*. Elsevier Inc.; 2018. doi:10.1016/B978-0-12-813665-2.00013-2

33. Anhalt H, Bohannon NJ V. Insulin patch pumps: their development and future in closed-loop systems. *Diabetes Technol Ther*. 2010;12 Suppl 1:S51-S58. doi:10.1089/dia.2010.0016

34. Catargi B. Current status and future of implantable insulin pumps for the treatment of diabetes. *Expert Rev Med Devices*. 2004;1(2):181-185. doi:10.1586/17434440.1.2.181

35. Pickup J, Keen H. Continuous subcutaneous insulin infusion at 25 years: evidence base for the expanding use of insulin pump therapy in type 1 diabetes. *Diabetes Care*. 2002;25(3):593-598. http://www.ncbi.nlm.nih.gov/pubmed/11874953.

36. Renard E, Bouteleau S, Jacques-Apostol D, et al. Insulin underdelivery from implanted pumps using peritoneal route. Determinant role of insulin pump compatibility. *Diabetes Care*. 1996;19(8):812-817. http://www.ncbi.nlm.nih.gov/pubmed/8842596.

37. Burgman T. A Guideline for Smart Implant Systems Supporting Patients with Diabetes Type 1. http://www.scopus.com/inward/record.url?eid=2-s2.0-84934780860&partnerID=tZOtx3y1.

38. Renard E, Place J, Cantwell M, Chevassus H, Palerm CC. Closed-loop insulin delivery using a subcutaneous glucose sensor and intraperitoneal insulin delivery: feasibility study testing a new model for the artificial pancreas. *Diabetes Care*. 2010;33(1):121-127. doi:10.2337/dc09-1080

39. Renard E, Schaepelynck-Bélicar P. Implantable insulin pumps. A position statement about their clinical use. *Diabetes Metab*. 2007;33(2):158-166. doi:10.1016/j.diabet.2006.10.004

40. ROCHAT F, SCHOENEICH P, BONANI M, et al. DESIGN OF MAGNETIC SWITCHABLE DEVICE (MSD) AND APPLICATIONS IN CLIMBING ROBOT. In: *Emerging Trends in Mobile Robotics*. WORLD SCIENTIFIC; 2010:375-382.

doi:10.1142/9789814329927_0047

41. Gilpin K, Kotay K, Rus D, Vasilescu I. Miche: Modular Shape Formation by Self-Disassembly. *Int J Rob Res*. 2008;27(3-4):345-372. doi:10.1177/0278364907085557

42. Schempf H, Chemel B, Everett N. Neptune: above-ground storage tank inspection robot system. *IEEE Robot Autom Mag*. 1995;2(2):9-15. doi:10.1109/100.392414

43. Bratlie KM, York RL, Invernale MA, Langer R, Anderson DG. Materials for Diabetes Therapeutics. *Adv Healthc Mater*. 2012;1(3):267-284. doi:10.1002/adhm.201200037

44. Nielsen L, Khurana R, Coats A, et al. Effect of environmental factors on the kinetics of insulin fibril formation: elucidation of the molecular mechanism. *Biochemistry*. 2001;40(20):6036-6046. http://www.ncbi.nlm.nih.gov/pubmed/11352739.

45. Malik R, Roy I. Probing the mechanism of insulin aggregation during agitation. *Int J Pharm*. 2011;413(1-2):73-80. doi:10.1016/j.ijpharm.2011.04.024

46. Li S, Leblanc RM. Aggregation of Insulin at the Interface. *J Phys Chem B*. 2014;118(5):1181-1188. doi:10.1021/jp4101202

47. Liu W, Johnson S, Micic M, et al. Study of the Aggregation of Human Insulin Langmuir Monolayer. *Langmuir*. 2012;28(7):3369-3377. doi:10.1021/la204201w

48. Sluzky V, Tamada JA, Klibanov AM, Langer R. Kinetics of insulin aggregation in aqueous solutions upon agitation in the presence of hydrophobic surfaces. *Proc Natl Acad Sci U S A*. 1991;88(21):9377-9381. http://www.ncbi.nlm.nih.gov/pubmed/1946348.

49. Nayak A, Dutta AK, Belfort G. Surface-enhanced nucleation of insulin amyloid fibrillation. *Biochem Biophys Res Commun*. 2008;369(2):303-307.

doi:10.1016/j.bbrc.2008.01.159

50. Pandey LM, Le Denmat S, Delabouglise D, Bruckert F, Pattanayek SK, Weidenhaupt M. Surface chemistry at the nanometer scale influences insulin aggregation. *Colloids Surfaces B Biointerfaces*. 2012;100:69-76. doi:10.1016/j.colsurfb.2012.05.022

51. Gadelmawla ES, Koura MM, Maksoud TMA, Elewa IM, Soliman HH. Roughness parameters. *J Mater Process Technol*. 2002;123(1):133-145. doi:10.1016/S0924-0136(02)00060-2

52. Iacovacci V, Tamadon I, Rocchi M, Dario P, Menciassi A. Toward Dosing Precision and Insulin Stability in an Artificial Pancreas System. *J Med Device*. 2019;13(1):011008. doi:10.1115/1.4042459

53. Fu LM, Wang WT, Lee CY. Design and Fabrication of PDMS/PMMA-Based Rotary Micropump. *Appl Mech Mater*. 2016;829:29-34. doi:10.4028/www.scientific.net/AMM.829.29

54. I. J. Karassik, W. C. Krutzsch, W. H. Fraser and JPM. *Pump Handbook*. Vol 22.; 1976. doi:10.1002/aic.690220632

55. Matteucci M, Pérennès F, Marmiroli B, et al. Compact micropumping system based on LIGA fabricated microparts. *Microelectron Eng*. 2006;83(4-9):1288-1290. doi:10.1016/j.mee.2006.01.259

56. Kim ES, Gustenhoven E, Mescher MJ, et al. A microfluidic reciprocating intracochlear drug delivery system with reservoir and active dose control. *Lab Chip*. 2014;14(4):710-721. doi:10.1039/c3lc51105g

57. Lee SH, Lee Y Bin, Kim BH, et al. Implantable batteryless device for on-demand and pulsatile insulin administration. *Nat Commun*. 2017;8(May 2016):15032. doi:10.1038/ncomms15032

58. Lee I, Hong P, Cho C, Lee B, Chun K, Kim B. Four-electrode micropump with peristaltic motion. *Sensors Actuators, A Phys*. 2016;245:19-25. doi:10.1016/j.sna.2016.04.010

59.   Thoma F, Goldschmidtböing F, Woias P. A new concept of a drug delivery system with improved precision and patient safety features. *Micromachines*. 2015;6(1):80-95. doi:10.3390/mi6010080

60.   Kim H, Astle AA, Najafi K, Bernal LP, Washabaugh PD. An Integrated Electrostatic Peristaltic 18-Stage Gas Micropump With Active Microvalves. *J Microelectromechanical Syst*. 2015;24(1):192-206. doi:10.1109/JMEMS.2014.2327096

61.   Speed JS, Hyndman KA. In vivo organ specific drug delivery with implantable peristaltic pumps. *Sci Rep*. 2016;6:1-7. doi:10.1038/srep26251

62.   Dhumal SR, Kadam SS. Design and Development of Rotary Peristaltic Pump. *Int J Sci Adv Technol*. 2012;2(4):2221-8386. http://www.ijsat.com.

63.   Shen M, Dovat L, Gijs MAM. Magnetic active-valve micropump actuated by a rotating magnetic assembly. *Sensors Actuators, B Chem*. 2011;154(1):52-58. doi:10.1016/j.snb.2009.10.033

64.   Xiang J, Cai Z, Zhang Y, Wang W. A micro-cam actuated linear peristaltic pump for microfluidic applications. *Sensors Actuators, A Phys*. 2016;251:20-25. doi:10.1016/j.sna.2016.09.008

65.   Stork M, Mayer D. Peristaltic Pump with Magnetoelastic Drive. *IEEE Trans Magn*. 2018;54(5):1-4. doi:10.1109/TMAG.2018.2804331

5. Conclusion and future perspectives

The past decades witnessed great advancements in the field of minimally invasive surgery and in pharmacology domain. However, there is still lots of room to deliver effective treatment with minimized side effects. Capabilities derived from mechatronics can help in moving forward in this field by technologies and designs that is able to treat many pathologies in the human body, even in hard-to-reach areas. When dealing with therapeutic strategies, a proper balance among therapy efficiency and side effects on body should be pursued. This is the bottleneck of currently employed pharmacological therapeutic strategies. Two examples in our case study can be heart valve treatment in elderly and chemotherapy in cancer treatment.

The development of miniaturized systems, able to controllably reach a target location and to deliver therapy in a highly efficient fashion, may enable highly effective therapeutic strategies. Many research efforts have been devoted towards this objective but several limitations still hamper the reliable system for targeted therapy in the clinical practice. Among these issues; biocompatibility, actuators, safety and size can be pointed out.

In this Thesis, novel mechatronic solutions aiming to overcome some of these limitations were investigated. A main focus on solutions by mechanical (mechanisms) engineering approach was pursued. These solutions potentially allow to deliver drug for daily chronic diseases and one-time delivery for prosthesis. In addition, remote actuations (wirelessly or tele-surgery) enable to controllably actuate the systems when implanted device or surgery site is not simply accessible.

The Thesis first reviews the state of the art for two different robotic system (i.e manipulator for MIS and implantable drug delivery system) to provide unique characterization of each and negative aspects to improve. Chapter 2 presents the features that need to be added while available solutions might not reach the final goal.

After providing hints on robotic systems eligible for biomedical field, the design, developing and testing of two robotic systems for therapeutic delivery were reported. The first one was a flexible manipulator for aortic heart delivery, devised for MIS operation in right anterior minithoracotomy. The robotic manipulator is compatible with MIS approach and equipped with endoscopic visualization. Performance evaluation (*in vitro*) shows great functionality in precise positioning of Sorin prosthesis in aortic root based on patient anatomy. Endoscopic visions are very effective to fine the nadir points and novel mechanisms and available DoFs in the system make the delivery in safe, fast and effective way. Introducer with minimum disturbance in manipulator's pose and two stage valve expansion is a privilege of our design in compare with the robotic delivery in state of the art. Also, mathematical modelling of the manipulator for constant curvature kinematics are reported in Appendix I for controlling the manipulator and finding the tip's positon. Thus, tele-surgery by means of remote joysticks and camera visions on screen is also possible. Moreover, we introduced a simple cable tensioning strategy based on the leading tension concept, and we effectively achieved pose-preserving stiffening by considering a variety of starting poses. The maximum stiffening factor was in between 2 and 9, based on relevant margins from the initial pose to the workspace boundary, and on potential contributions by the structure itself. The robotic manipulator paves the way to future applications of these systems in the fields of surgical robotics.

The second one was an implantable insulin delivery device as substitution of pancreas for T1 diabetic patients. An advanced prototype of fully implantable artificial pancreas refillable by means of ingestible capsules was tested. The prototype was placed in intraperitoneal cavity and injecting insulin with resolution of 3µL on demand were performed. Also, successful refiling of the reservoir is performed by MSD and needle punching mechanisms. The proposed pumping mechanism resulted extremely efficient and led to drug release also in non-continuous fashion. Furthermore, the aspiration of insulin and variable volume reservoir makes the system to be filled very fast and keep the insulin far from bubbles or air. The proposed system may enable highly reliable targeted therapy in

locations that are not currently reachable be conventional means. The proposed device could potentially revolutionize diabetic treatment and the field of targeted therapy. In fact the possibility to refill the reservoir by capsules, paves the way to relax T1D patients from refiling and injections.

Despite the efficiency and reliability of the proposed systems, their dimensions and biocompatibility, may limit their application in future. So, further research/prototype might be necessary to enhance the materials and mechanisms.

The results reported in the literature till now, clearly demonstrate that a unique route towards this objective cannot be traced, yet. Each possible approach, ranging from nanomedicine efforts in developing smart nanoparticles, to macrorobotics attempts to develop highly controllable macrosystems suffers from severe limitations. Thus, only a multidisciplinary approach trying to merge the goals accomplished in the different fields and to develop multistage strategies, could pave the way towards novel and more efficient solutions.

To sum up, the combination of (*i*) mechanical controlling of both internal and external reactions, (*ii*) on board "intelligence" and constitutive materials, (*iii*) external control platforms and (*iv*) accurate mathematics and programming represents a paradigm to be pursued, towards the discovery of the holy grail of an efficient instrument for life-threatening pathologies.

Scientific production

Papers on ISI Journals

- V. Mamone, S. Condino, F. Cutolo, **I. Tamadon**, M. Murzi, A. Menciassi and V. Ferrari "Low Computational Cost Stitching Method in a Three-Eyed Endoscope" Journal of Healthcare Engineering, Augmented Reality in Healthcare, (Accepted)

- **Tamadon**, Y. Huan, A. G. de Groot, A. Menciassi and E. Sinibaldi "Smooth positioning and pose-preserving stiffening for an articulated/continuum manipulator for minimally invasive surgery" IEEE/ASME Transactions on Mechatronics, (Under review)

- V. Iacovacci#, **I. Tamadon**#, M. Rocchi, P. Dario, and A. Menciassi "Towards dosing precision and insulin stability in an artificial pancreas system" J. Med. Device., vol. 13, no. 1, p. 011008, Jan. 2019, (#equally contributing authors), **Doi:** 10.1115/1.4042459

Papers on International peer-reviewed Conferences

- **I. Tamadon**, V. Simoni, V. Iacovacci, F. Vistoli, L. Ricotti and A. Menciassi "Miniaturized peristaltic rotary pump for non-continuous drug dosing" 41th International conference of the IEEE Engineering in Medicine and Biology Society, (Accepted).

- **Tamadon,** G. Soldani, P. Dario, A. Menciassi "Novel Robotic Approach for Minimally Invasive Aortic Heart Valve Surgery" 40th International conference of the IEEE Engineering in Medicine and Biology Society, 17-21 Jul., 2018, Honolulu, USA. **DOI:** 10.1109/EMBC.2018.8513309

- V. Iacovacci, **I. Tamadon**, C. Perri, P. Dario, L. Ricotti, and A. Menciassi "Towards an autonomous fully-implantable artificial pancreas" 6th national congress of bioengineering, June 25th-27nd 2018, Milan, Italy.

- **I. Tamadon**, S. Tognarelli, C. Quaglia, et al. "Development of a robotic platform for minimally invasive aortic heart valve surgery" 29th Conference of the international Society for Medical Innovation and Technology, 9-10 Nov. 2017, Torino, Italy

- V. Iacovacci, L. Ricotti, **I. Tamadon**, et al. "Towards a fully implantable autonomous artificial pancreas" 44th ESAO (European Society for Artificial Organs) Congress, 6-9 Sep 2017 Vienna, Austria.

- G. Turini, S. Condino, S. Sinceri, **I. Tamadon** et al. "Patient Specific Virtual and Physical Simulation Platform for Surgical Robot Movability Evaluation in Single-Access Robot-Assisted Minimally-Invasive Cardiothoracic Surgery" AVR 2017: 4th International conference on Augmented Reality, Virtual Reality, and Computer Graphics, June 12-15, 2017, Lecce, Italy. **DOI:** 10.1007/978-3-319-60928-7_18

Patents

- **I. Tamadon**, A. Menciassi, G. Soldani, et al. "Flexible robotic platform for minimally invasive delivery of novel artificial heart valve under endoscopic guidance" Patent, Submitted in May, 2018.